# High Accuracy Evaluation of Heating Characteristics of Microwave Therapeutic Devices

January 2016

Yuta ENDO

Graduate School of Engineering

CHIBA UNIVERSITY

（千葉大学審査学位論文）

# High Accuracy Evaluation of Heating Characteristics of Microwave Therapeutic Devices

January 2016

Yuta ENDO

Graduate School of Engineering

CHIBA UNIVERSITY

# Table of contents

i

# Chapter 1

# Introduction

This thesis describes the studies on the medical application of microwave heating techniques.

In this chapter, the background of our studies are explained. First, basic knowledges about the medical applications of microwave are explained. Next, current situation and issues of the microwave treatments are mentioned. Finally, studies in this thesis are proposed.

## 1.1 Medical applications of microwave

Recently, microwave dielectric heating is applied in a wide range of medical treatments. In this section, basic knowledges about the medical applications of microwave (types of medial application using microwave and differences from the treatments using other energy sources such as radiofrecuency (RF) current and ultrasonic wave) are explained.

### 1.1.1 Treatments using microwave heating

By applying a microwave thermal effect to biological tissue, a wide range of diseases, including cancer are treated [1]-[3]. Treatments using the microwave are roughly categorized into the following according to the heating temperature and the heating duration: (1) the treatments in which the lesion tissue is heated over 60ºC in

several minutes; and (2) the treatments in which the lesion tissue is heated at 42ºC-60ºC for about an hour.

In the treatments (1), the lesion part such as tumor tissue is heat-coagulated and necrosed by the microwave thermal effect. Here, biological tissue is coagulated at the temperature over 60°C [4]-[6]. By the microwave heating, coagulation of the biological tissue completes in several minutes and treatments finishes in the short time.

The microwave coagulation therapy (MCT) for liver cancer has been practiced [7]-[10]. In the MCT, a needle-type microwave antenna is inserted into the tumor tissue under an ultrasonic image guide, and heats the tissue around the antenna including tumor by microwave, as shown in Fig. 1.1. Heated tissues are coagulated and undergo necrosis. MCT is the treatment with small physical burden on patient because of the short treatment time (within several minutes) and the little bleeding from the small incisional wound. The application of the MCT is limited for the treatment of the tumor with size ≤30 mm.

Other than the MCT, the microwave endometrial ablation (MEA) for the treatment of excessive menstruation has been practiced [11],[12]. The catheter ablation treatment for the rapid and irregular heartbeats using microwave energy is also studied [13],[14].

In the treatments (2), the lesion tissues are necrosed without tissue coagulation, employing low-temperature (below 60°C) and long time (about one hour) heating. The mechanisms of these treatments are different from the treatments which use necrosis due to tissue coagulation.

For example, in the high-temperature treatment for benign prostatic hypertrophy (BPH), enlarged prostate is heated to about 50°C for one hour by

microwave, protecting the urethra from thermal injury by using cooling water [15],[16].

Moreover, there is the cancer treatment called hyperthermia, in which tumor tissue is heated to the temperature between 42°C to 45°C [17]-[19]. At this temperature range, only tumor tissues suffer serious damage and undergo necrosis because they have higher thermosensitivity than normal tissues. The hyperthermia intensively kills tumor tissues conserving normal tissues. Therefore, the hyperthermia is applied in the case that the tumor exists in the vicinity of the important tissue such as a blood vessel, a lymph vessel, and a nerve tissue, etc. Figure 1.2 shows the hyperthermia for head and neck cancer.

In addition to the treatments (1) and (2), applications of the microwave heating technique in surgical operation, such as the hemostasis of a solid organ and the blood vessel sealing, have been studied [20]-[21]. Figure 1.3 shows examples of the surgical devices applying microwave thermal effect.

Detailed information about the principle of the microwave thermal effect and the influence of the biological tissue due to heating is described in Appendix.
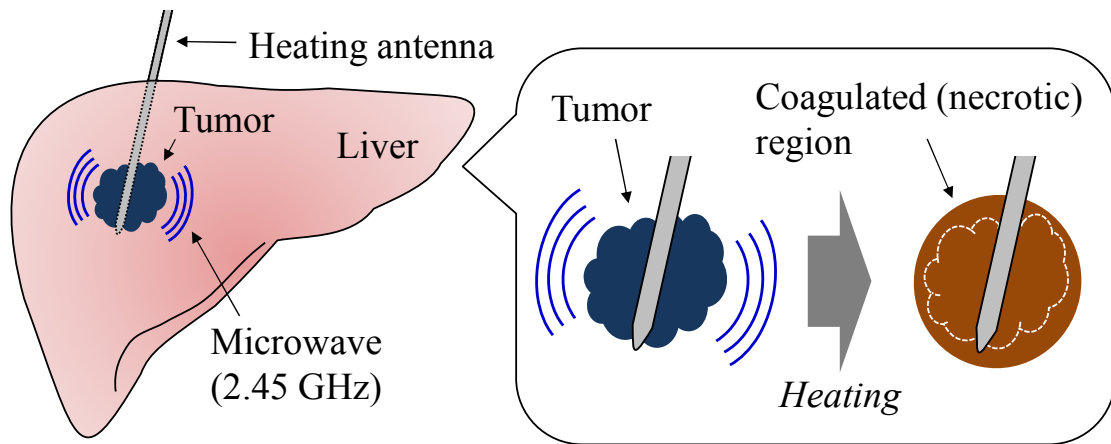
Fig. 1.1. Microwave coagulation therapy (MCT) for liver cancer.
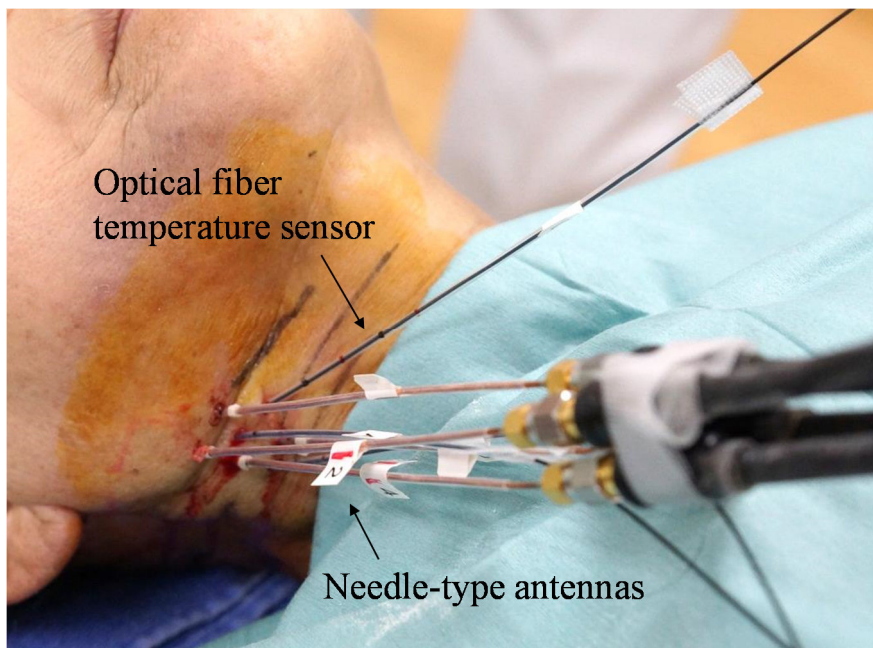


Fig. 1.2. Hyperthermia treatment of thyroid tumor.
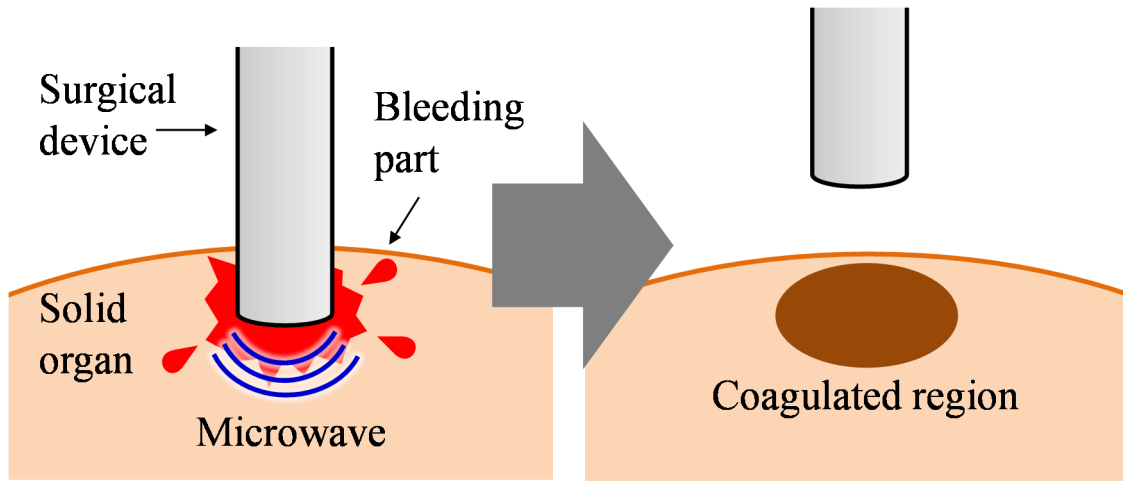
(a) Treatment of bleeding at a solid organ.
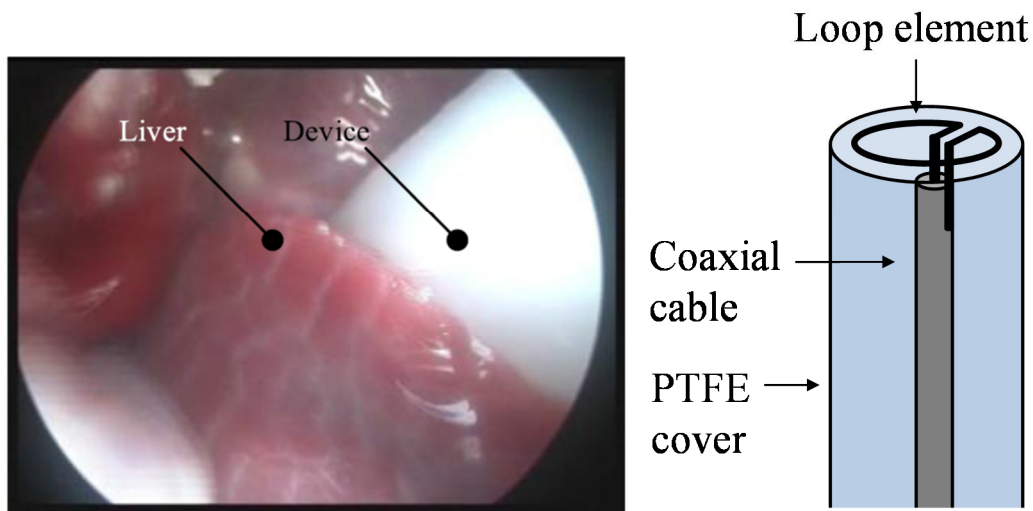


(b) Treatment of a swine liver with the surgical device having loop-based antenna [20].

Fig. 1.3. The surgical device applying microwave heating.

## 1.1.2 Comparison with other heating sources for medical use

Other energy sources which generate heat in the biological tissue, such as radiofrequency (RF) current and ultrasonic wave, are widely used in the medical field. In this subsection, differences of heating characteristics between the microwave and other energy sources are explained.

The joule heat generated in the biological tissue due to the radiofrequency (RF) current (several hundred kHz) are applied in medical treatments such as the RF ablation for liver cancer, the cardiac catheter ablation for irregular heartbeat and RF hyperthermia [22]-[24]. The electrical scalpel widely used in surgical operation is the medical device which use the arc discharge induced by the RF voltage for the tissue heating.

In the case of medical devices which use RF current, the biological tissue is arranged between an electrode pair and heated by the joule heat caused by the RF current, considering the tissue as the resistance element, as shown in Fig. 1.4. Here, the electrode pair is composed of an active electrode which heats surrounding tissue and a return electrode whose size is larger than or equal to the size of the active electrode. Strong heating effect occurs around the small-sized active electrode because joule heat is strong at the part of the high current density. In the case that the return electrode is larger than the active electrode, heating effect hardly occur around it because of the low current density.

Moreover, the current path concentrates in the tissue with low electrical resistance, avoiding the tissue with high resistance. Generally, tissues with low water content ratio such as fat and bone have high electrical resistance. Moreover,

the decrease of the water content ratio of the tissue caused by heating leads the increase of the electrical resistance. This implies that current distribution in the tissue changes in the middle of heating. In the case that thick blood vessel exists near the cancer in RF ablation, the current concentrates on the blood with low electrical resistance. This leads insufficient heating of the target part (tumor tissue). Thus, current path is strongly influenced by the structure of the tissue around the electrodes.

In the case of the RF ablation for liver cancer and the cardiac ablation, the large-sized return electrode is attached to patient's skin. If the setting of the return electrode to the skin is inadequate, the joule heat increases around the return electrode and causes thermal injury on the skin.

The ultrasonically activated scalpel is the surgical device which uses ultrasonic vibration at several MHz for heating and dissection of the tissue. The mechanical vibration of the active blade causes some troubles in a surgical operation, as shown in Fig. 1.5. For example, the tissue in contact with a vibrating active blade scatters around. In the case of a laparoscopic surgery, scattered tissue adheres to the lens of the laparoscope and obstructs a visual field. Moreover, if cancer cells are included in the scattered tissue, tumor metastasis is caused. The tip of the active blade causes strong mechanical damage to the biological tissue. If this part touches the unexpected part of a patient's body, serious problem will be caused.

In the case of microwave heating, the distribution of the electromagnetic field around a heating antenna is not susceptible to the surrounding tissue. There is no need to use pair of electrodes which is potential cause of thermal injury. Moreover, serious troubles caused by the mechanical vibration of the device are not generated.
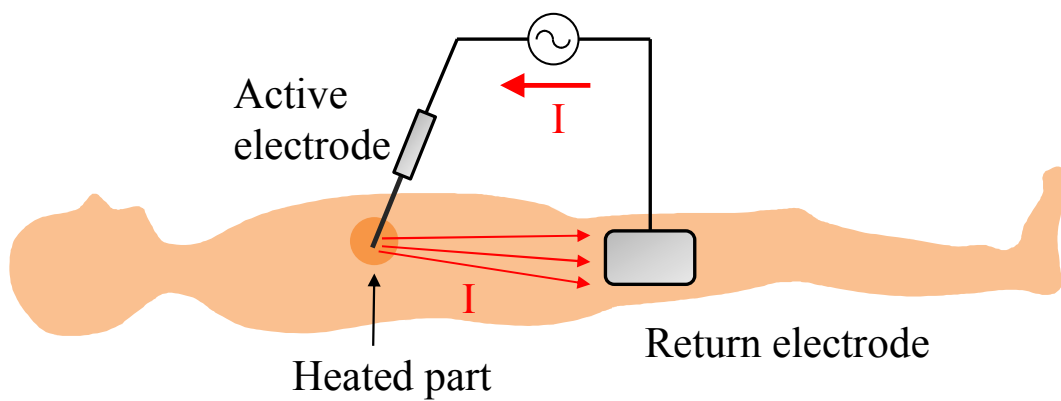
(a) Radiofrequency ablation (RFA).
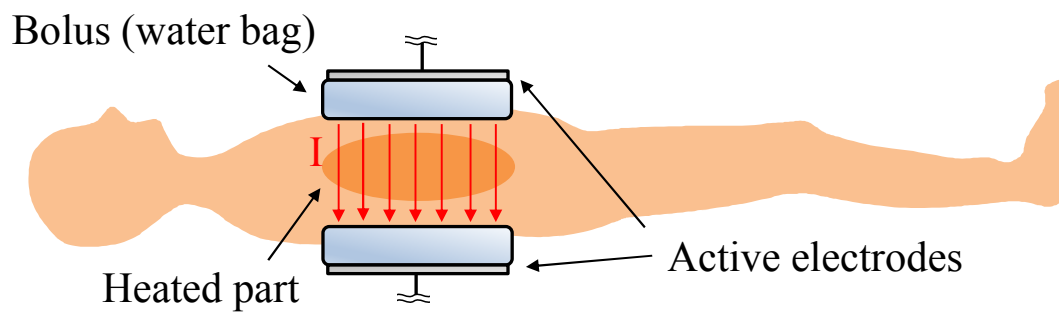


(b) Hyperthermia treatment using RF current.

Fig. 1.4. Heating system by RF current.
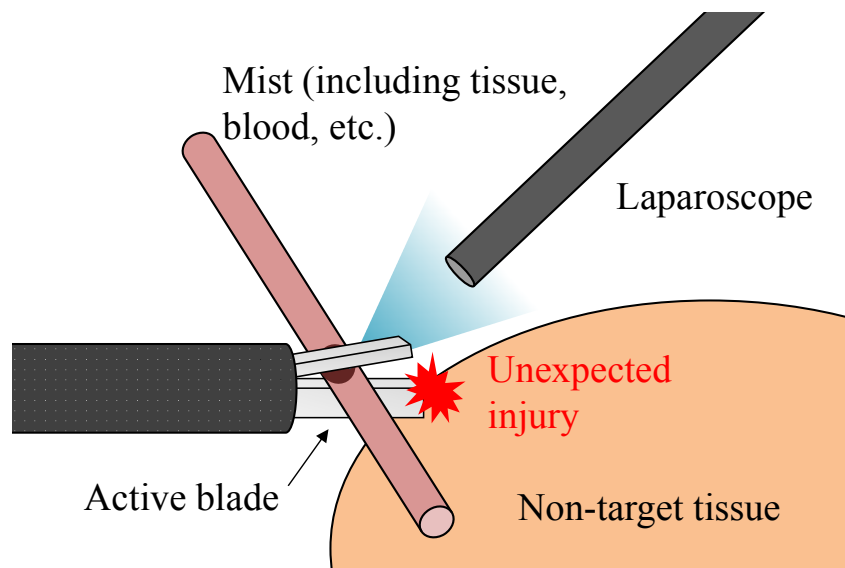
Fig. 1.5. Troubles in treatments applying ultrasound vibration.

# 1.2 Current situation and issues of the medical application of microwave heating

This section subscribes the current situation and issues of the medical treatments applying microwave heating.

In the treatments such as MCT and MEA, small-diameter antennas suitable to the insertion into solid organs and lumen tissues have been used. Many previous studies proposed various types of antennas for these purposes [14],[25],[26]. The structures of the antennas are based on coaxial cable to transmit microwave power to a target part, as shown in Fig. 1.6.

On the other hand, there are not enough studies about the design of an antenna mounted on the surgical device for the blood vessel sealing and the treatment of the bleeding from the organ surface. Therefore, the types of the devices available for these purposes are insufficient and the spread of the surgical treatments applying microwave heating are stagnated. In order to promote the spread of the surgical treatments applying microwave heating which have excellent safety compared with other heating sources such as radiofrequency (RF) current and ultrasonic wave, the increase in the types of the devices are required.

A numerical simulation of the tissue temperature provides valuable information for the treatments using microwave heating [27]-[29]. For example, simulation results contributes to the setting of an appropriate heating condition and the estimating the size of the coagulated region, in preoperative planning. A coagulated region is estimated by the obtained temperature distribution from the numerical simulation, because biological tissues are coagulated at about 60°C. Moreover, the

numerical simulation will be useful for development of therapeutic devices.

However, the numerical simulator which can obtain accurate temperature distributions in tissues have not been developed. This is because of the difficulties in simulating the changes of the physical properties of tissue which is caused by heating.
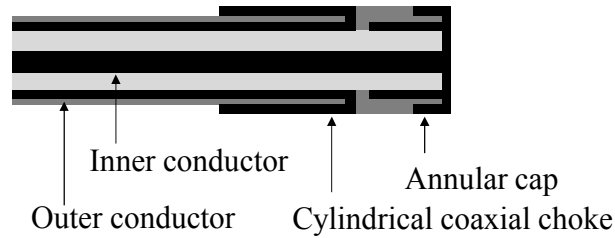
(a) Cap-choke catheter antenna for microwave cardiac ablation [14].
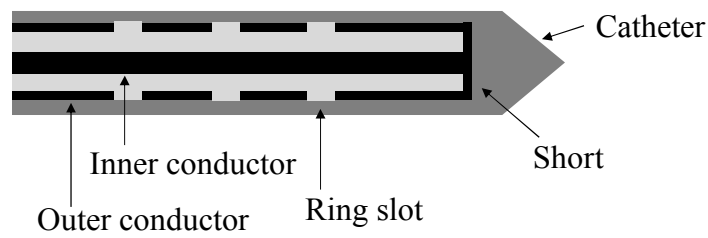


(b) Ring-slot applicator for interstitial microwave hyperthermia [25].
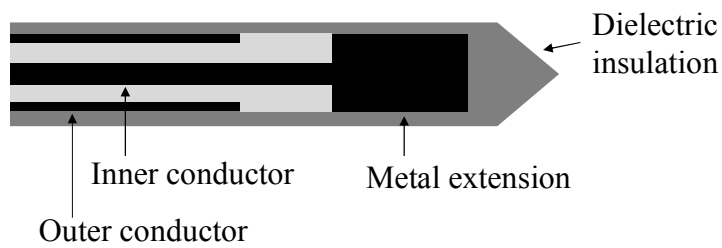


(c) Coaxial-fed dipole antenna for treatment of hepatic tumor [26].

Fig. 1.6. Heating antennas based on coaxial cable.

# 1.3 Studies in this thesis

Based on the situations mentioned in the former section, we worked on two issues: (1) development of the numerical simulator to calculate the accurate temperature of the biological tissue under microwave heating; and (2) development of the forceps-type surgical device applying microwave heating.

To obtain the temperature distribution in the biological tissue under the microwave heating, the electromagnetic field around the heating antenna is need to be calculated first. Next, the temperature of the tissue is calculated by using the dielectric loss in the tissue as the heating source, which is calculated from the electric field. In the numerical simulation of the electromagnetic field and the temperature, numerical models of the biological tissues which have accurate dielectric and thermal constants of them are necessary to obtain the realistic calculation results. Here, changes in the dielectric and thermal constants of biological tissues due to the heating should be considered.

In this study, the numerical model of biological tissue which recreate the changes in the dielectric and thermal constants due to the heating was developed, and this model was mounted on the numerical simulator.

Developing the forceps-type surgical device applying microwave heating for the various treatments such as blood vessel sealing, it is necessary to mount the tissue cutting mechanism on the proposed device, as well as the heating mechanism by the microwave antenna. In the case of existing forceps-type devices for blood vessel sealing applying joule heat by the RF current such as LigaSure and EnSeal, the tissue after sealing is mechanically cut by using the blade. The proposed device was also designed to have both the microwave antenna and the cutting blade.

In the chapter 2, study on the numerical modeling of the heated liver tissue for the numerical simulation of the MCT is described. Changes in the dielectric and thermal constants of the tissue due to the heating are numerically modeled, based on the empirically measured data.

In the chapter 3, development of the numerical simulator to calculate the electromagnetic field and the temperature in the tissue under microwave heating is described. The numerical model of the liver tissue proposed in the chapter 2 is employed for the simulation of the MCT.

In the chapter 4, development of the forceps-type surgical device applying microwave heating is described. The outline and the structure of the proposed device, the evaluation of the heating characteristics of the proposed device by numerical analyses with the simulator proposed in chapter 3, and the heating experiment using prototype of the proposed device are given in each section.

Chapter 5 summarizes this thesis.

# References

[1]     A. Rosen, M. A. Stuchly, and A. Vander Vorst, "Applications of RF/microwaves in medicine," IEEE Trans. Microw. Theory and Tech., vol.50, no. 3, pp. 963-974, Mar. 2002.

[2]     F. Sterzer, "Microwave medical devices," IEEE Microwave Mag., vol. 3, no. 1, pp. 65-70, Mar. 2002.

[3]     C. P. Hancock, et al., "A New Wave in Electrosurgery : A Review of Existing and Introduction to New Radio-Frequency and Microwave Therapeutic Systems," IEEE Microwave Mag., vol. 16, no. 2, pp. 14-30, Mar. 2015.

[4]     S. J. Graham, L. Chen, M. Leitch, R. D. Peters, M. J. Bronskill, F. S. Foster, R. M. Henkelman, and D. B. Plewes, "Quantifying tissue damage due to focused ultrasound heating observed by MRI," Magn. Reson. Med., vol. 41, no. 2, pp. 321-328, Feb. 1999.

[5]     R. D. Peters, E. Chan, J. Trachtenberg, S. Jothy, L. Kapusta, W. Kucharczyk, and R. M. Henkelman, "Magnetic resonance thermometry for predicting thermal damage: An application of interstitial laser coagulation in an *in vivo* canine prostate model," Magn. Reson. Med., vol. 44, no. 6, pp. 873-883, Dec. 2000.

[6]     N. J. McDannold, R. L. King, F. A. Jolesz, and K. H. Hynynen, "Usefulness of MR Imaging-Derived Thermometry and Dosimetry in Determining the Threshold for Tissue Damage Induced by Thermal Surgery in Rabbits," Radiology, vol. 216, no. 2, pp. 517-523, 2000.

[7]     T. Seki, M. Wakabayashi, T. Nakagawa, T. Itoh, T. Shiro, K. Kunieda, M. Sato, S. Uchiyama, and K. Inoue, "Ultrasonically guided percutaneous microwave

coagulation therapy for small carcinoma," Cancer, vol. 74, no. 3, pp. 817-825, Aug. 1994.

[8]   P. Liang, B. Dong, X. Yu, D. Yu, Z. Cheng, L. Su, J. Peng, Q. Nan, and H. Wang, "Computer-aided dynamic simulation of microwave-induced thermal distribution in coagulation of liver cancer," IEEE Trans. Biomed. Eng., vol. 48, no. 7, pp. 821-829, July 2001.

[9]   C. L. Brace, P. F. Laeseke, D. W. van der Weide, and F. T. Lee, "Microwave ablation with a triaxial antenna: results in *ex vivo* bovine liver," IEEE Trans. Microwave Theory Techn., vol. 53, no. 1, pp. 215-220, Jan. 2005.

[10]  J. M. Bertram, D. Yang, M. C. Converse, J. M. Webster, and D. M. Mahvi, "A review of coaxial-based interstitial antennas for hepatic microwave ablation," Critical Reviews™ in Biomedical Engineering, vol. 34, no. 3, pp. 187-213, Feb. 2006.

[11]  S. A. Jack and K. G. Cooper, "Microwave endometrial ablation: an overview," Reviews in Gynaecological Practice, vol. 5, no. 1, pp. 32-38, Mar. 2005.

[12]  K. G. Cooper, et al., "Comparison of microwave endometrial ablation and transcervical resection of the endometrium for treatment of heavy menstrual loss: a randomised trial," The Lancet, vol. 354, no. 9193, pp. 1859-1863, Nov. 1999.

[13]  J. G. Whayne, S. Nath, and D. E. Haines, "Microwave catheter ablation of myocardium in vitro. Assessment of the characteristics of tissue heating and injury," Circulation., vol. 89, no. 5, pp. 2390-2395, May 1994.

[14]  P. Bernardi, M. Cavagnaro, J. C. Lin, S. Pisa, and E. Piuzzi, "Distribution of SAR and temperature elevation induced in a phantom by a microwave cardiac ablation catheter," IEEE Trans. Microwave Theory Techn., vol. 52, no. 8, pp.

1978-1986, Aug. 2004.

[15] D. Despretz, J. C. Camart, C. Michel, J. J. Fabre, B. Prevost, J. P. Sozanski, and M. Chivé, "Microwave prostatic hyperthermia: interest of urethral and rectal applicators combination − Theoretical study and animal experimental results," IEEE Trans. Microwave Theory Techn., vol. 44, no. 10, pp. 1762-1768, Oct. 1996.

[16] P. S. Debicki and M. Okoniewski, et al., "Cooled microwave transrectal applicator with adjustable directional beam for prostate treatment", Int. J. Hyperthermia, vol. 11, no. 1, pp.95 -108 1995

[17] M. Converse, E. J. Bond, S. C. Hagness, and B. D. Van Veen, "Ultra wide band microwave space-time beam-forming for hyperthermia treatment of breast cancer: a computational feasibility study," IEEE Trans. Microwave Theory Techn., vol. 52, no. 8, pp. 1876-1889, Aug. 2004.

[18] A. Winter, J. Laing, R. Paglione, and F. Sterzer, "Microwave hyperthermia for brain tumors," Neurosurgery, vol 17, no. 3, pp. 387-399, Sep. 1985.

[19] R. U, K. T. Noell, K. T. Woodward, B. T. Worde, R. I. Fishburn, and L. S. Miller, "Microwave-induced local hyperthermia in combination with radiotherapy of human malignant tumors," Cancer, vol. 45, no. 4, pp. 638-646, Feb. 1980.

[20] M. Inoue, K. Saito, M. Takahashi, and K. Ito, "Development of Coagulation Device for Biological Tissue using Microwave Energy," IEICE Transactions on Communications C, vol. J97-C, no. 5, pp. 218-224, May 2014 (in Japanese).

[21] Y. Tezuka, K. Saito, M. Takahashi, and K. Ito, "Development of surgical device for tissue coagulation by microwave energy," in Proc. 2013 Asia-Pacific Radio Science Conf., Taipei, Taiwan, p.55, Sep. 2013.

[22] H. Rhim and G. D. Dodd, "Radiofrequency thermal ablation of liver tumors,"

Journal of Clinical Ultrasound, vol. 27, no. 5, pp. 221-229, June 1999.

[23] S. Nath, J. P. DiMarco, and D. E. Haines, "Basic Aspects of Radiofrequency Catheter Ablation," Journal of Cardiovascular Electrophysiology, vol. 5, no. 10, pp. 863-876, Oct. 1994.

[24] M. Hiraoka, S. Jo, Y. Dodo, K. Ono, M. Takahashi, H. Nishida, and M. Abe, "Clinical results of radiofrequency hyperthermia combined with radiation in the treatment of radioresistant cancers," Cancer, vol. 54, no. 12, pp. 2898-2904, Dec. 1984.

[25] K. Ito, M. Hyodo, M. Shimura, and H. Kasai, "Thin applicator having coaxial ring slots for interstitial microwave hyperthermia," in IEEEAP-S Antennas Propagation Soc. Int. Symp. Dig., pp.1233-1236, vol. 3, May 1990.

[26] P. Wang, C. L. Brace, M. C. Converse, and J. G. Webster, "Tumor boundary estimation through time-domain peaks monitoring: numerical predictions and experimental results in tissue-mimicking phantoms," IEEE Transactions on Biomedical Engineering, vol. 56, no. 11, pp. 2634-2641, Nov. 2009.

[27] Z. Ji, and C. L. Brace, "Expanded modeling of temperature-dependent dielectric properties for microwave thermal ablation." Physics in medicine and biology, vol. 56, no.16, pp. 5249-5264, July 2011.

[28] D. Yang, M. C. Converse, D. M. Mahvi, and J. G. Webster, "Expanding the bioheat equation to include tissue internal water evaporation during heating," IEEE Trans. Biomed. Eng., vol.54, no.8, pp.1382-1388, Aug. 2007.

[29] K. Saito, Y. Hayashi, H. Yoshimura, and K. Ito, "Heating characteristics of array applicator composed of two coaxial-slot antennas for microwave coagulation therapy," IEEE Trans. Microwave Theory Techn., vol.48, no.11, pp.1800-1806, Nov. 2000.

# Chapter 2

# Physical properties of heated biological tissue

## 2.1 Introduction

In the case of MCT for liver cancer and other medical treatments applying microwave heating, numerical analyses of the electromagnetic field and the temperature around the antenna inserted in the tissue provide useful information for evaluating the therapeutic effect of the treatment [1]-[3]. In numerical analyses of the electromagnetic field and temperature, the finite difference time domain (FDTD) method or the finite element method are employed. In these analyses, biological tissues are modeled as sets of voxels or as elements with physical components, such as dielectric and thermal properties. The numerical modeling of the physical properties of biological tissues in such analyses must be highly accurate to obtain accurate analytical results.

Generally, biological tissues contain large amount of water in them. The dielectric constants (relative permittivity and conductivity) of the biological tissues depend on the water content ratio [wt%] of them [4]. In MCT, the water content ratio of the tissue around the heating antenna decreases along with heat-induced coagulation and evaporation [5]. At boiling temperature (100°C under atmospheric pressure), water contained in the tissue evaporates by absorbing the evaporated latent heat (2,257 kJ/kg), and the temperature of the water does not rise until the

evaporation finishes as in Fig. 2.1. This suggests that the reproduction of the behavior of the water content ratio along the heating and the modeling of the physical properties of the biological tissue depending on water content ratios are necessary for high accuracy analyses of the electromagnetic field and the temperature around the antenna.

There are insufficient numbers of models of the influence of the water content ratio on liver tissue treated with MCT. In a previous study [1], the dielectric constants of heated tissues were expressed as functions of the temperature. In this method, dehydration-induced changes in the dielectric constants were not distinguished from heat-induced changes. In the case that heated and dehydrated tissue once cooled, such as the intermittent heating, irreversibility in dielectric constants of the tissue is not sufficiently modeled. In another study [5], the water content ratio of dehydrated tissues were approximated as a function of the temperature. However, the relationship between the water content ratio and other physical properties (dielectric and thermal constants) were not investigated.

In this chapter, the water content ratios and dielectric and thermal constants of liver tissues heated under various conditions were measured, in order to evaluate the relationship between them. Moreover, they were numerically modeled for coupled analysis for electromagnetic field and temperature, as shown in Fig. 2.2. In this analysis, the dielectric and thermal constants of the biological tissues were expressed as functions of the water content ratio. The distribution of the specific absorption rate (SAR) in the liver was calculated by an electromagnetic field analysis employing the FDTD method. The obtained SARs were used as heating sources in the temperature analysis by the finite-difference method (FDM). In the temperature analysis, based on the temperatures and absorbed heat quantities of the tissues, the

water content ratios of the tissues were updated. These series of procedures were repeated until the total heating duration.

In section 2.2, measurement of water content ratio, dielectric and thermal constants of heated liver tissue are discussed. Section 2.3 presents the numerical modeling of the liver tissue based on the measured results. Section 2.4 summarizes the investigations.



Fig. 2.1. Evaporation of water.

```
┌─────────────────────────────────────┐
│   Analysis for electromagnetic field │◄──┐
│          (FDTD method)               │   │
└─────────────────────────────────────┘   │
                │                          │
                ▼                          │
┌─────────────────────────────────────┐   │
│   Calculation of specific absorption │   │
│     rate (SAR) (heating source)      │   │
└─────────────────────────────────────┘   │
                │                          │
                ▼                          │
┌─────────────────────────────────────┐   │
│      Analysis for temperature        │   │
│      (Finite Difference Method)      │   │
└─────────────────────────────────────┘   │
                │                          │
                ▼                          │
┌─────────────────────────────────────┐   │
│      Update of water content ratio   │───┘
└─────────────────────────────────────┘
```
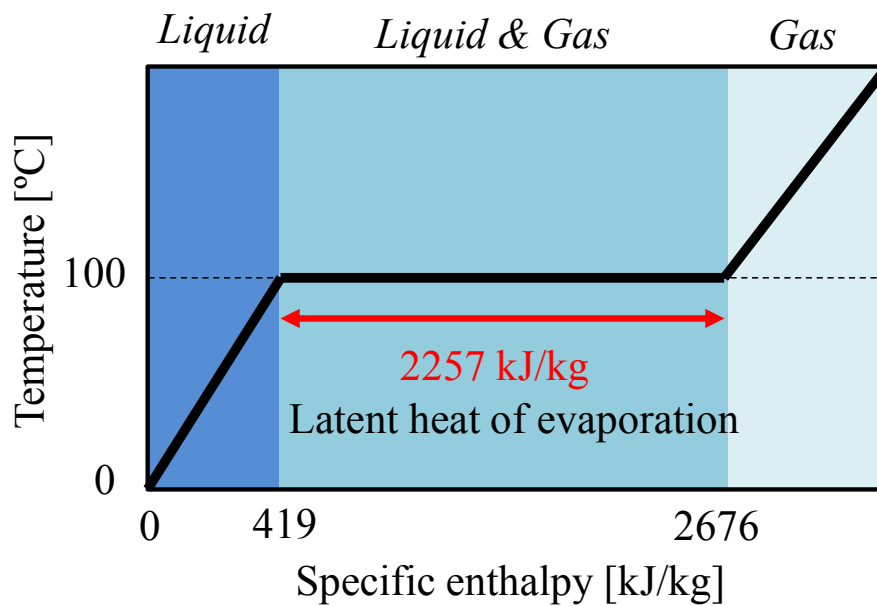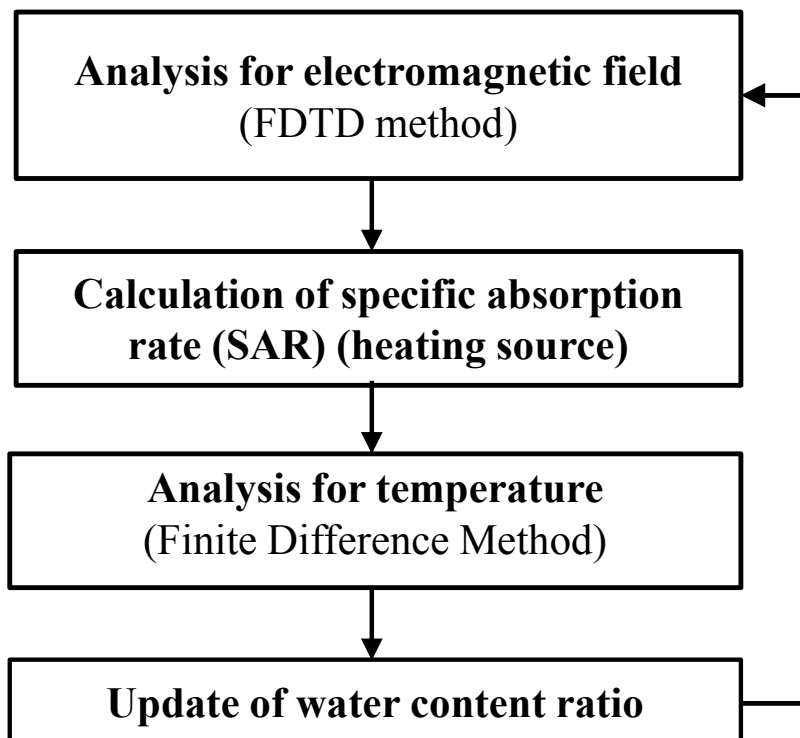
Fig. 2.2. Schematic diagram of proposed numerical simulator.

## 2.2 Measurement of water content ratio, dielectric and thermal constants of heated liver tissue

In this study, the dielectric and thermal constants are modeled as functions of a variable (i.e., the water content ratio of the tissue). The water content ratio of biological tissue heated at less than 100°C is expressed as a function of the temperature to simulate dehydration due to heat coagulation. When the tissue temperature reaches 100°C, the evaporation-induced decrease in the water content ratio caused by the absorption of the microwave energy is also modeled.

These functions were based on empirically measured values of swine liver tissues heated and dehydrated under various conditions. In this study, the swine liver tissues were heated in one of two ways: heating with a water bath at 50–100°C to induce tissue dehydration by coagulation or microwave heating to induce tissue dehydration by evaporation.

### 2.2.1 Preparation of the measurement samples

In this study, swine liver tissue was employed because its dielectric properties and thermal properties are very similar to those of human liver tissue [3].

In our previous study of the dielectric constants and water content ratios of swine liver tissues heated in a water bath at 60–100°C, the minimum value of the water content ratio of the tissue after heating was approximately 57 wt% [4]. This value is likely the lower limit in heating-induced dehydration below 100°C. The average value of the water content ratio of the tissue before heating was about 73

wt%. A water content ratio lower than 57 wt% is needed in numerical modeling of evaporation-induced tissue dehydration. Therefore, to decrease the water content ratio further, microwave heating was employed for dehydration of the swine liver tissues, in addition to heating in a water bath.

Figure 2.3 shows images about preparation of measurement samples. In the case of the heating using a water bath, pieces of swine liver tissue (mass: about 3 g, thickness: about 5 mm) were heated in water at 50–100°C. The water temperature was controlled by an induction heating (IH) device. The tissue pieces were wrapped in cling film to prevent water absorption. The heating duration was set to 600 s, which was sufficient time to dehydrate the tissue at the target temperature [4]. At each heat setting, five samples were prepared.

In the case of the microwave heating, the tissue pieces were heated using a household microwave oven. The output power of the microwave oven was set to 100 W, which is the minimum output power of the used oven. The heating times were different for each sample (5–20 min) to prepare samples with various values of water content ratios. For the microwave heating, 60 samples were prepared.
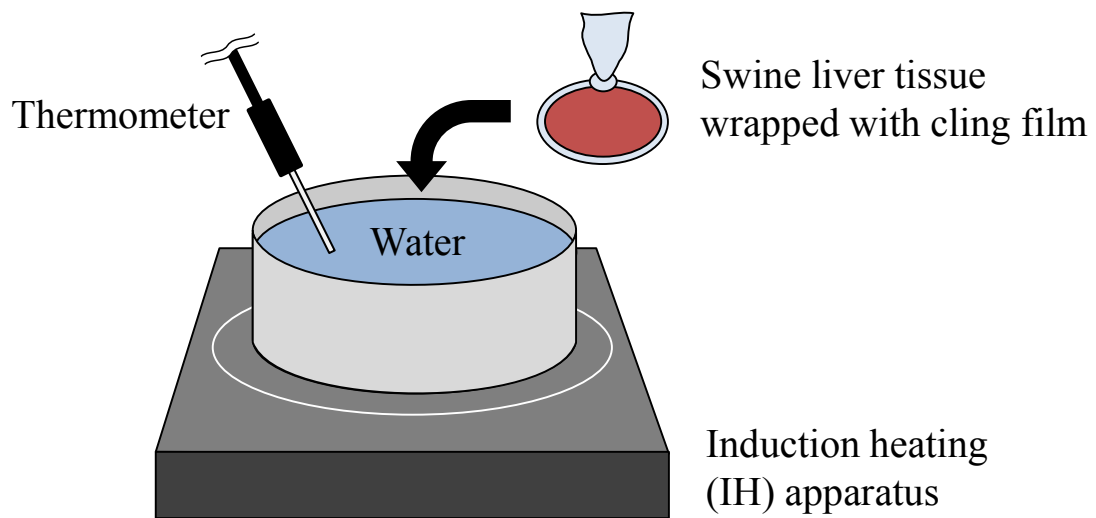
(a) Heating with water bath.
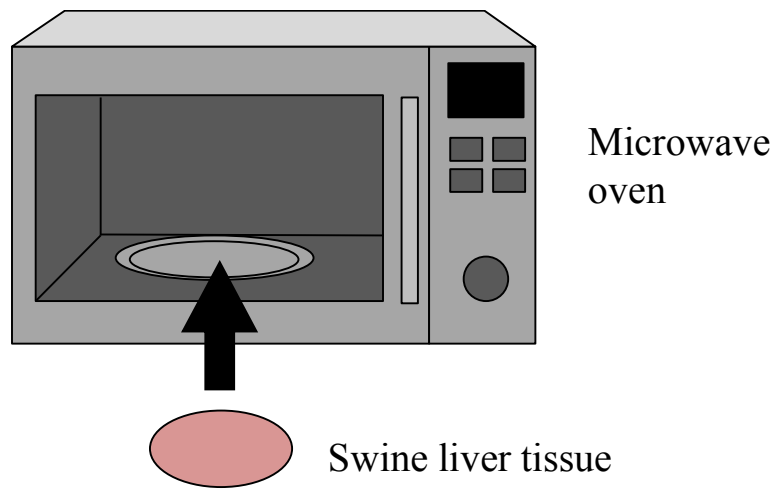


(b) Heating with microwave oven.

Fig. 2.3. Preparation of measurement samples.

## 2.2.2 Measurement method

The dielectric constants of the prepared samples were measured using an open-ended coaxial probe. A Keysight 85070E Dielectric Probe Kit (Keysight Technologies, Santa Rosa, CA, USA) was used for this purpose.

Before measuring the dielectric constant, water remaining on the tissue surface was wiped off with paper. The samples were cooled to room temperature (about 20°C) to evaluate the relationship between the water content ratio and dielectric constant. The dielectric properties of biological tissue are temperature dependent. In the case of liver tissue at 2.45 GHz, the temperature rise leads the decrease of the relative permittivity and the increase of conductivity. However, variations of them are sufficiently smaller than those with decrease of the water content ratio. In [6], the ratios of the change in relative permittivity and conductivity between 30 and 50°C were ≤0.1/°C and ≤0.005 (S/m)/°C, respectively. In contrast, in the case of the water content ratio, the variations were 0.67/wt% and 0.03 (S/m)/wt%, respectively [4].

The water content ratio [wt%] of the prepared samples was measured by the loss on drying method [7]. Using this method, the water content ratio of the sample is obtained by comparing the mass of the sample before and after drying. In this study, microwave heating in a microwave oven was used to remove the water from the sample, the same one that was used for the preparation of the dielectric and thermal constant samples (Fig. 2.4). Microwave power is mainly used to heat water in samples, and heated water evaporates at 100°C. Therefore, the temperature of the sample does not greatly exceed 100°C. An excessive temperature rise leads to carbonization of the sample, and carbonization causes measurement errors.

The mean values of the dielectric constants and water content ratio of the raw

tissue without heating measured under the above conditions were $\varepsilon_r= 45.0$, $\sigma= 1.78$ S/m, and 73.2 wt%, respectively. These values approximately match those reported in the literature [4], [8].

The measurements of the thermal constants were carried out at the Agne Gijutsu Center Inc., Tokyo, Japan. The specific heat and thermal conductivity of the samples were measured using the adiabatic method and the hot wire method, respectively, at room temperature (20°C). In these measurements, two types of samples were employed: (1) tissue heated in a water bath at 100°C for 600 s (water content ratio: approximately 57 wt%) and (2) tissue completely dried by microwave heating (water content ratio: 0 wt%).
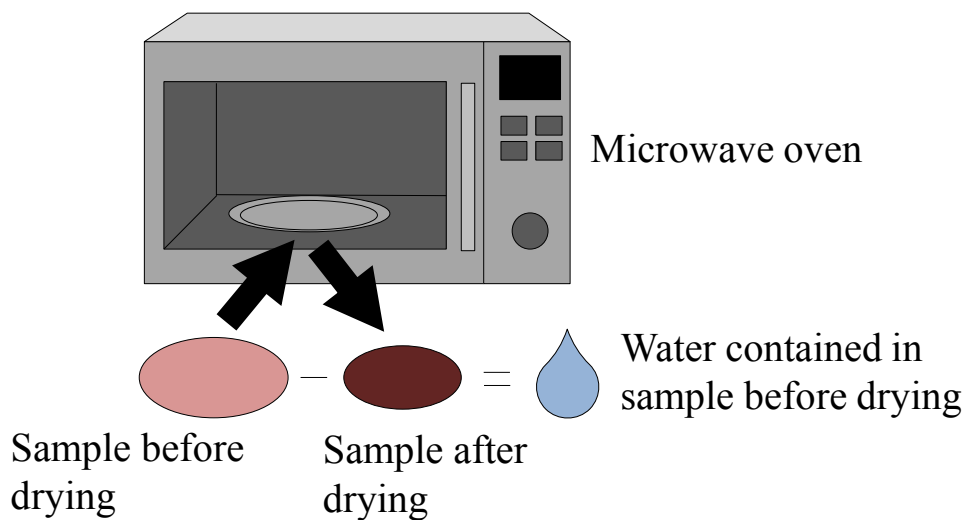


Fig. 2.4. Measurement of water content ratio.

## 2.2.3 Measured results

Figure 2.5 shows the relationship between the heating temperatures and water content ratios of the tissues heated using the water bath. Under each heating condition, the water content ratio values obtained from five samples were averaged. The results indicate that the water content ratios varied according to the heating temperature. The relationship between the water content ratio and the temperature was expressed as an approximate straight line by a least-squares method.

Figure 2.6 shows the relationship between the water content ratios and dielectric constants of the dehydrated tissues with various water content ratios: heated in the water bath for 30 s, 120 s, and 600 s and heated in the microwave oven. In these figures, variations in the measured values can be observed at a low water content ratios below 60 wt%. These are caused by the nonuniform distribution of the water in the microwave-heated tissue. These figures indicate that the water content ratio affects both the relative permittivity and the conductivity. The relative permittivity gradually decreased along with a decrease in the water content ratio and converged at the minimum value. With regard to the conductivity, the value suddenly decreased when the water content ratio was around 40 wt%. Approximation curves of the relative permittivity and conductivity were obtained using the sigmoidal function (Gompertz function). The coefficients of determination $R^2$ for approximation curves were 0.99 for relative permittivity and 0.96 for conductivity. These values indicate measured values were properly approximated.

Figure 2.7 shows the measured thermal constants of the two samples. In these graphs, the literature values of the raw tissue, with the water content ratio approximated as 73.2 wt%, are also plotted [9]. These graphs indicate that the

28

specific heat and thermal conductivity also depended on the water content ratio. These relationships were approximated using sigmoidal function (Gompertz function).
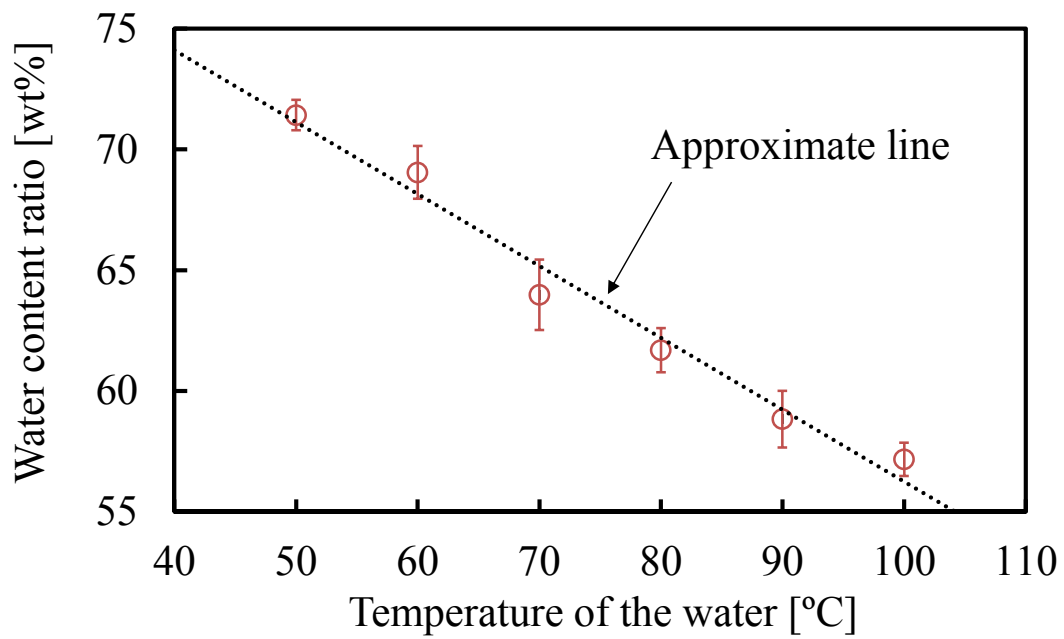


Fig. 2.5. Water content ratio vs. temperature.
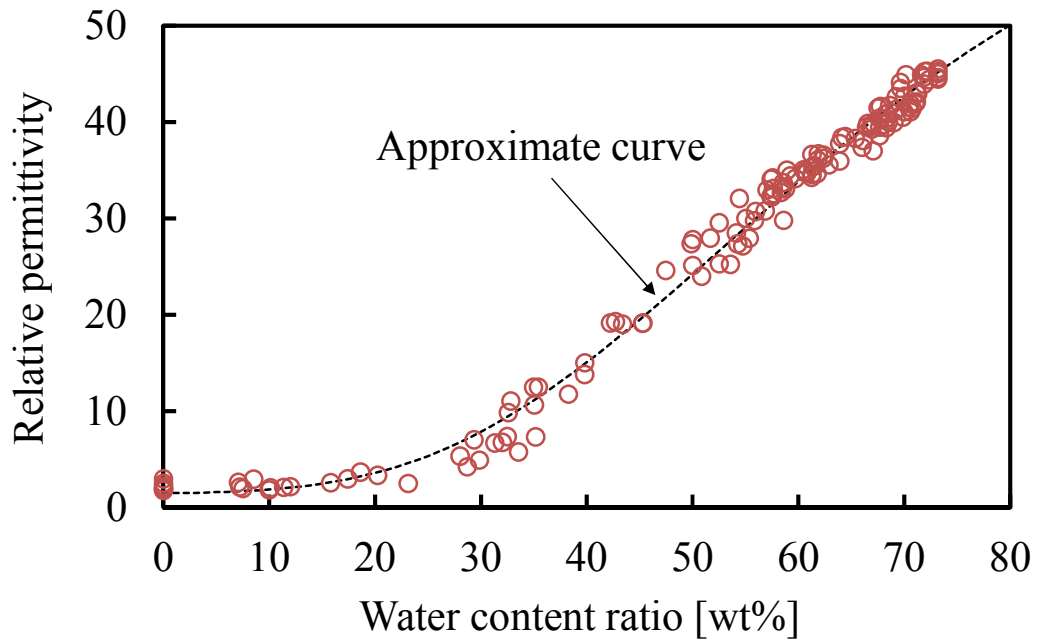
(a) Relative permittivity.
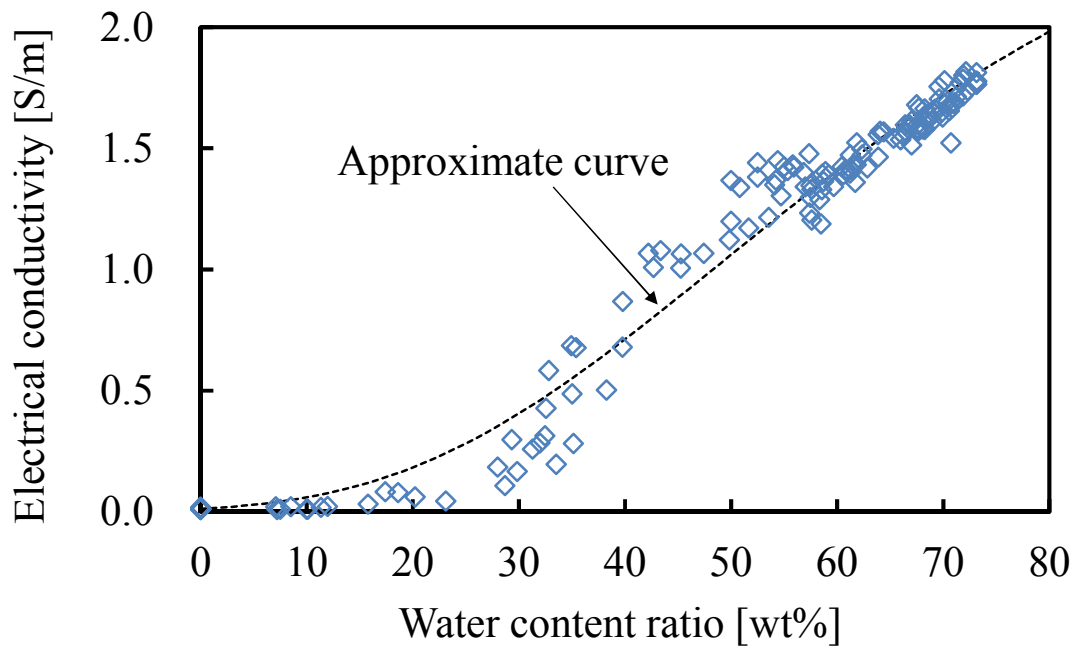


(b) Electrical conductivity.

Fig. 2.6. Dielectric constants vs. water content ratio.
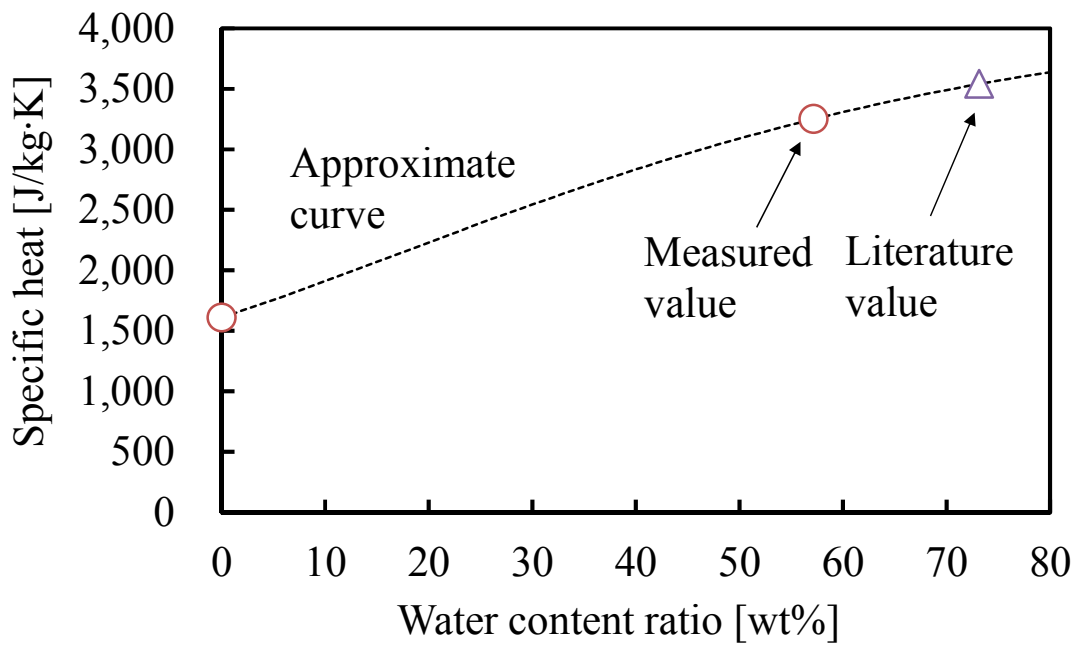
(a) Specific heat.
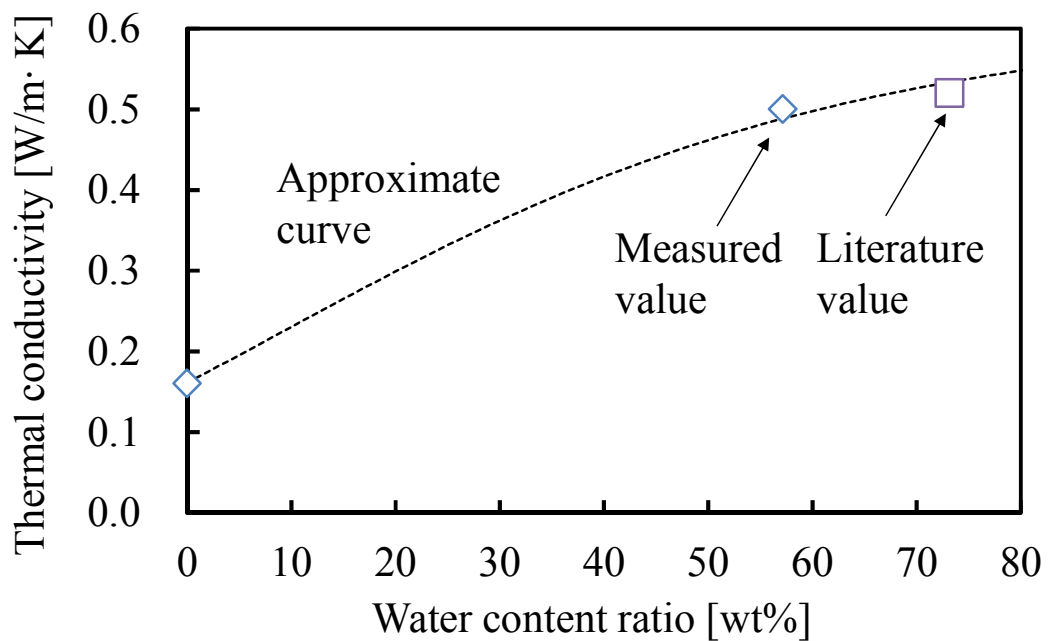


(b) Thermal conductivity.

Fig. 2.7. Thermal constants vs. water content ratio.

# 2.3 Numerical modeling

Based on the measured data, numerical models of the water content ratio, dielectric and thermal constants of the heated liver tissue were prepared for the analyses by the FDTD method and the FDM.

The numerical modeling of the water content ratio was conducted as follows: First, the water content of the heated tissue was considered to change, as shown in Figure 2.8. At temperatures below 100°C without evaporation, the water content ratio of the tissue was expressed as the function of the temperature variable. This function was obtained using the approximate straight line of the measured water content ratio $R_w$ [wt%] in Fig. 2.5, as follows:

$$R_w(T) = -0.298T + 86.0 \quad \text{(2.1)}$$

where $T$ denotes the temperature of the tissue [°C]. In Eq. 2.1, $R_w$ takes a value of 73.2 wt% (the mean value of the water content ratio of liver tissue without heating) when $T$ is 43.0°C. To avoid $R_w$ having a value over 73.2 wt%, $R_w$ was set to 73.2 wt% only when $T$ was below 43.0°C.

The water content ratio of evaporation-induced dehydrated tissue at 100°C was numerically modeled. The mass of the water contained in a certain tissue voxel in the FDTD calculation $M_w$ [kg] was expressed as follows:

$$M_w = V \times \rho \times R_w \times 10^{-2} \quad \text{(2.2)}$$

where $V$ and $\rho$ denote the mean volume [m³] and the mass density [kg/m³] of the voxel, respectively. Generally, water at 100°C evaporates by absorbing heat, with

2,257 kJ/kg the latent heat at which the evaporation of water occurs. Therefore, the amount of heat required to evaporate all the water contained in the voxel $Q_{eva}$ [J] was expressed as follows:

$$Q_{eva} = M_w \times 2,257 \times 10^3 \quad (2.3)$$

When the temperature of the voxel reached 100°C, the water content ratio of the voxel was 56.2 wt% according to Eq. 2.1. Based on the assumption that the water content ratio linearly decreased, the amount of heat required to reduce 1 wt% of the water content ratio of the voxel at 100°C $\Delta Q_{eva}$ [J/wt%] was expressed as in Eq. 2.4:

$$\Delta Q_{eva} = Q_{eva}/56.2 \quad (2.4)$$

The amount of the decrease in the water content ratio $\Delta R_w$ [wt%] per one time step $\Delta t$ [s] in the temperature analysis was expressed as follows:

$$\Delta R_w = \Delta Q_{obt}/\Delta Q_{eva} \quad (2.5)$$

where $\Delta Q_{obt}$ denotes the amount of heat of the voxel in the time step. $\Delta Q_{obt}$ includes the heat transferred from neighboring voxels and the heat obtained from the electrical field. In this model, the amount of heat of the voxel at 100°C was only used for the evaporation of the water contained in the voxel and not for the elevation of the temperature.

The relative permittivity, $\varepsilon_r$, and electrical conductivity, $\sigma$ [S/m], of the dehydrated tissues were numerically modeled as functions using the water content ratio as a variable. These functions were obtained from the approximation curves shown in Fig. 2.6, as below:

$$\varepsilon_r\left(R_w\right) = 69.58 \times 0.0006^{\exp(-0.0379 \times R_w)} + 1.42 \quad (2.6)$$

$$\sigma(R_w) = 2.8 \times 0.0044^{\exp(-0.0344 \times R_w)} \quad (2.7)$$

The convergence values of these two functions were set to be the values of the relative permittivity and the electrical conductivity of a saline solution at room temperature at 2.45 GHz ($\varepsilon_r = 71.0$ and $\sigma = 2.8$ S/m).

The specific heat, $c$ [J/kg·K], and the thermal conductivity, $\kappa$ [W/m·K], of the dehydrated tissues were also modeled in a similar way. These functions were also obtained as below from the approximation curves in Fig. 2.7:

$$c(R_w) = 3231 \times 0.21^{\exp(-0.0269 \times R_w)} + 946 \quad (2.8)$$

$$\kappa(R_w) = 0.61 \times 0.26^{\exp(-0.0311 \times R_w)} \quad (2.9)$$

The convergence values were set to be the values of the specific heat and thermal conductivity of the water at room temperature ($c = 4,177$ J/kg·K and $\kappa = 0.61$ W/m·K).

As above, the water content ratio, dielectric constants, and thermal constants of the dehydrated tissues were numerically modeled.
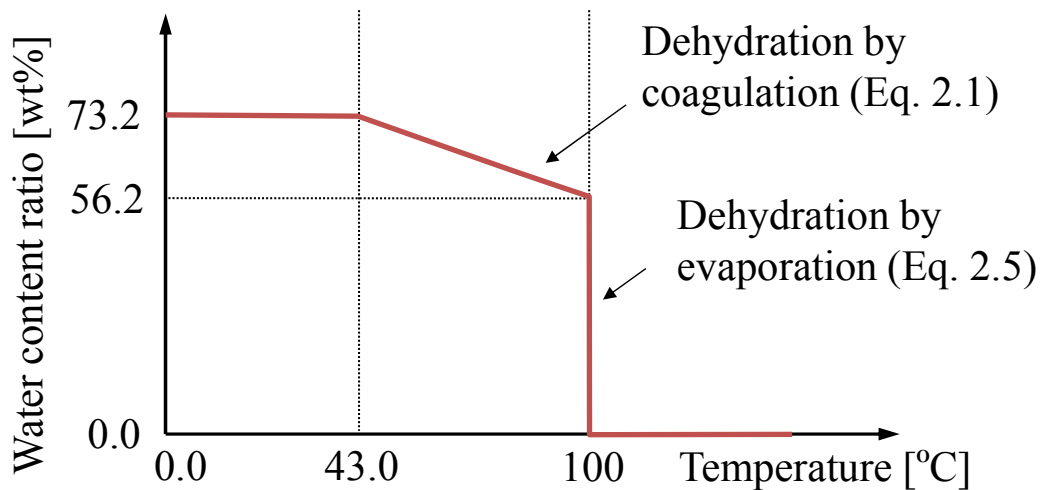


Fig. 2.8. Change in the water content ratio of the heated tissue.

# 2.4 Conclusion

In this study, water content ratios, dielectric and thermal constants of liver tissues heated under various conditions were measured, in order to evaluate the relationship between them. Measured results show the water content ratio of the liver tissue was decreased linearly with respect to the heating temperature. Moreover, dependencies of the dielectric and thermal constants on the water content ratio were observed.

Based on the measured results, the water content ratio and dielectric and thermal constants of heated liver tissues were numerically modeled for the coupled analysis of the electromagnetic field and temperature. The water content ratio was expressed as the function of the temperature in the case that the tissue temperature is below 100°C. The decrease of the water content ratio by evaporation at 100°C was also modeled. Moreover, the dielectric and thermal constants of the liver tissue were expressed as the functions of the water content ratio of the tissue.

For numerical analyses of other medical treatments applying microwave heating, similar studies will be necessary for other biological tissues such as the cardiac tissue in the case of the catheter ablation [10],[11].

Moreover, detailed relationships between porous structures formed in the tissue dehydrated by microwave heating and physical constants of the tissue (dielectric and thermal constants) should be investigated.

# References

[1]     Z. Ji, and C. L. Brace, "Expanded modeling of temperature-dependent dielectric properties for microwave thermal ablation." Physics in medicine and biology, vol. 56, no.16, pp. 5249-5264, July 2011.

[2]     D. Yang, M. C. Converse, D. M. Mahvi, J. G. Webster, "Expanding the bioheat equation to include tissue internal water evaporation during heating," IEEE Trans. Biomed. Eng., vol.54, no.8, pp.1382-1388, Aug. 2007.

[3]     K. Saito, Y. Hayashi, H. Yoshimura, K. Ito, "Heating characteristics of array applicator composed of two coaxial-slot antennas for microwave coagulation therapy," IEEE Trans. Microwave Theory Techn., vol.48, no.11, pp.1800-1806, Nov. 2000.

[4]     Y. Endo, Y. Tezuka, K. Saito, and K. Ito, "Dielectric properties and water contents of coagulated biological tissue by microwave heating," IEICE Communications Express, vol.4, no.4 pp.105-110, Apr. 2015.

[5]     D. Yang, M. C. Converse, D. M. Mahvi, J. G. Webster, "Measurement and analysis of tissue temperature during microwave liver ablation," IEEE Trans. Biomed. Eng., vol.54, no.1, pp.150-155, Jan. 2007.

[6]     M. Lazebnik, M. C. Converse, J. H. Booske and S. C. Hagness, "Ultrawideband temperature-dependent dielectric properties of animal liver tissue in the microwave frequency range," Phys. Med. Biol., vol. 51, pp. 1941-1955, 2006.

[7]     J. K. Towns, "Moisture content in proteins: its effect and measurement," Journal of Chromatography A, vol. 705, pp. 115-127, 1995.

[8]     C. Gabriel, "Compilation of the dielectric properties of body tissues at RF microwave frequencies," Brooks Air Force Technical Report AL/OE-TR-1996-

0037, 1996.

[9]     P. A. Hasgall, E. Neufeld, M. C. Gosselin, A. Klingenböck, and N. Kuster, "IT'IS Database for thermal and electromagnetic parameters of biological tissues," Version 2.4, July 2013.

[10]    J. G. Whayne, S. Nath, and D. E. Haines, "Microwave catheter ablation of myocardium in vitro. Assessment of the characteristics of tissue heating and injury," Circulation., vol. 89, no. 5, pp. 2390-2395, May 1994.

[11]    P. Bernardi, M. Cavagnaro, J. C. Lin, S. Pisa, and E. Piuzzi, "Distribution of SAR and temperature elevation induced in a phantom by a microwave cardiac ablation catheter," IEEE Trans. Microwave Theory Techn., vol. 52, no. 8, pp. 1978-1986, Aug. 2004.

# Chapter 3

# Development of the numerical simulator to calculate the tissue temperature under microwave heating

## 3.1 Introduction

In this chapter, the coupled numerical simulator for electromagnetic field and temperature in the liver tissue under the microwave heating is developed. In these analyses, the numerical models of liver tissue, whose dielectric constants and thermal constants are changed with the decrease of water content ratio, proposed in chapter 2 are employed.

In section 3.2, simulations of microwave coagulation therapy (MCT) for liver cancer are described. Here, the simulation employing the liver tissue model which ignores variations of dielectric and thermal constants due to heating (modeled as fixed values) are also conducted, for comparison.

Section 3.3 presents the *ex vivo* experiment for the evaluation of the validity of the simulated results by the proposed numerical simulator. Section 3.4 summarizes this chapter.

# 3.2 Analysis of MCT

Figure 3.1 shows a flowchart of the numerical analyses using the liver tissue model proposed in chapter 2. First, the distribution of the electrical field that radiated from the coaxial-slot antenna was calculated, with the dielectric constants defined by the initial water content ratios using the FDTD method. $\varepsilon_r(R_w)$ and $\sigma(R_w)$ are the water content ratio-dependent relative permittivity and electrical conductivity, respectively.

Next, the values of the SAR [W/kg] of the biological tissue were obtained from the electrical field using the following formula:

$$\text{SAR} = \frac{\sigma(R_w)}{\rho} E^2 \quad (3.1)$$

where $\rho$ and $E$ are the mass density [kg/m³] and root-mean-square electrical field [V/m], respectively. The SAR is the value of the heat generated in the biological tissue exposed to the electrical field.

Using the SAR data and the initial water content ratio, the tissue temperature was analyzed by the following bioheat transfer equation [1]:

$$\rho c(R_w)\frac{\partial T}{\partial t} = \kappa(R_w)\nabla^2 T - \rho\rho_b c_b F(T - T_b) + \rho \cdot \text{SAR} \quad (3.2)$$

where $c(R_w)$ and $\kappa(R_w)$ are the water content ratio-dependent specific heat [J/kg·K] and thermal conductivity [W/m·K], respectively. In Eq. 3.2, $T$ is the temperature [°C], $t$ is the time [s], $\rho$ is the density [kg/m³], $\rho_b$ is the density of the blood [kg/m³], $c_b$ is the specific heat of the blood [J/kg·K], $T_b$ is the temperature of the blood [°C], and $F$ is the blood flow rate [m³/kg·s]. The first and second terms in the right-hand side of

Eq. 3.2 denote the heat transfer between neighboring tissues and the heat transfer between the tissues and the blood flowing in the tissues, respectively. The heat generation in tissues by the absorption of the electrical field is denoted in the third term. In this analysis, the FDM was employed in the numerical calculation. The finite-difference approximation was based on [2].

In the temperature analysis, the values of the water content ratio $R_w$ of the tissue voxels were updated at every time step $\Delta t$ [s]. After the temperature analysis, the electromagnetic field analysis was repeated using the updated water content ratios. In this study, three different values (0.5 s, 1 s and 6 s) were set to the duration of each temperature analysis $t_e$ [s] to evaluate the influence of the $t_e$ on the analytical results. The above processes were repeated until a predetermined heating duration $t_h$ [s] had elapsed.

In this study, all the numerical calculations were executed by self-written codes.

**Start**

**Initial values**

$$T = T_0, R_w = R_{w0}$$

$T$: temperature [°C]
$T_0$: initial temperature [°C]
$R_w$: water content ratio [wt%]
$R_{w0}$: initial water content ratio [wt%]

$t = 0$
$t$: total duration [s]

**Analysis of the electromagnetic field**
(FDTD method)

$\varepsilon_r(R_w)$: relative permittivity (Eq. 2.6)
$\sigma(R_w)$: electrical conductivity [S/m] (Eq. 2.7)

$$\text{SAR} = \frac{\sigma(R_w)}{\rho} E^2 \quad [\text{W/kg}]$$

**Analysis of the temperature**
(Finite Difference Method)

$c(R_w)$: specific heat [J/kg·K] (Eq. 2.8)
$\kappa(R_w)$: thermal conductivity [W/m·K] (Eq. 2.9)

**Update of $R_w$**
Eq. 2.1 ($T<100$)
Eq. 2.5 ($T=100$)

$R_w$ (updated)

$t = t + t_e$

$t_e$: duration of each temperature analysis [s]

Y

$t < t_h$

$t_h$: heating duration [s]

N

**End**

Fig. 3.1. Detailed flowchart of the numerical analyses.

41

## 3.2.1 Analytical model

Figure 3.2 shows the analytical model for the electromagnetic field and the temperature. A coaxial-slot antenna, which radiates 2.45 GHz microwaves, was employed as a heating antenna [3]. A coaxial-slot antenna has been employed previously for interstitial heating in MCT and hyperthermia [2],[4]. The coaxial-slot antenna was composed of a semi-rigid coaxial cable with a diameter of 1.6 mm. A ring slot was cut on the outer conductor, and the tip of the cable was short circuited. The electric field was strong near the slot, heating the surrounding tissue. The antenna was covered with a catheter formed of polytetrafluoroethylene (PTFE) to prevent adhesion of the coagulated tissue.

In the analyses, we employed nonuniform grids and used small-sized grids only for the antenna. The same grids were employed in both analyses.

Table 3.1 lists the physical property values of the liver tissue used in the numerical analyses, including the values of the proposed model and those of the non-heated tissue. In the temperature analysis, the physical properties of the PTFE were set to the metallic part of the coaxial-slot antenna to reduce the calculation time.

The numerical analyses were conducted under the following two conditions: (1) both the dielectric and thermal constants of the tissue depended on the water content ratio (proposed model) and (2) both the dielectric and thermal constants were fixed. In both conditions, the mass density $\rho$ [kg/m$^3$] was the same as the mass density of nonheated tissue. The heat transfer by blood flow was ignored, and the blood flow rate $F$ was set as 0 because the main aim of this study was to evaluate the effects of the changes in dielectric and thermal properties on the temperature.

Table 3.2 lists the analytical conditions for the electromagnetic field and the

temperature. The maximum input power to the antenna, frequency, and total heating duration $t_h$ were set to 40 W, 2.45 GHz, and 60 s, respectively. The net-input power to the antenna was changed, as well as the reflection coefficient at the feeding point.

Table 3.1. Physical properties.

| Dielectric constants | | | |
|---|---|---|---|
| Liver | $\varepsilon_r$ | Cond. 1 | Eq. 2.6 |
| | | Cond. 2 | 43.03 [5] |
| | $\sigma$ [S/m] | Cond. 1 | Eq. 2.7 |
| | | Cond. 2 | 1.69 [5] |
| PTFE | $\varepsilon_r$ | Cond. 1, 2 | 2.1 [6] |
| | $\sigma$ [S/m] | Cond. 1, 2 | 0 [6] |
| Thermal constants | | | |
| Liver | $c$ [J/kg·K] | Cond. 1 | Eq. 2.8 |
| | | Cond. 2 | 3,540 [7] |
| | $\kappa$ [W/m·K] | Cond. 1 | Eq. 2.9 |
| | | Cond. 2 | 0.52 [7] |
| | $\rho$ [kg/m$^3$] | Cond. 1, 2 | 1,080 [7] |
| | $F$ [m$^3$/kg·s] | Cond. 1, 2 | 0 |
| PTFE | $c$ [J/kg·K] | Cond. 1, 2 | 1,046 [6] |
| | $\kappa$ [W/m·K] | Cond. 1, 2 | 0.25 [6] |
| | $\rho$ [kg/m$^3$] | Cond. 1, 2 | 2,200 [6] |

Table 3.2. Analytical conditions.

| Parameters for FDTD calculation | |
|---|---|
| Cell size [mm] (minimum) | 0.1 |
| Cell size [mm] (maximum) | 1.0 |
| Time step [ps] | 0.235 |
| Absorbing boundary condition | Mur (1st order) |
| Parameters for FDM calculation | |
| Cell size [mm] (minimum) | 0.1 |
| Cell size [mm] (maximum) | 1.0 |
| Time step [s] | 0.001 |
| Temperature of boundary [$^{o}$C] | 37.0 |
| Initial temperature [$^{o}$C] | 37.0 |
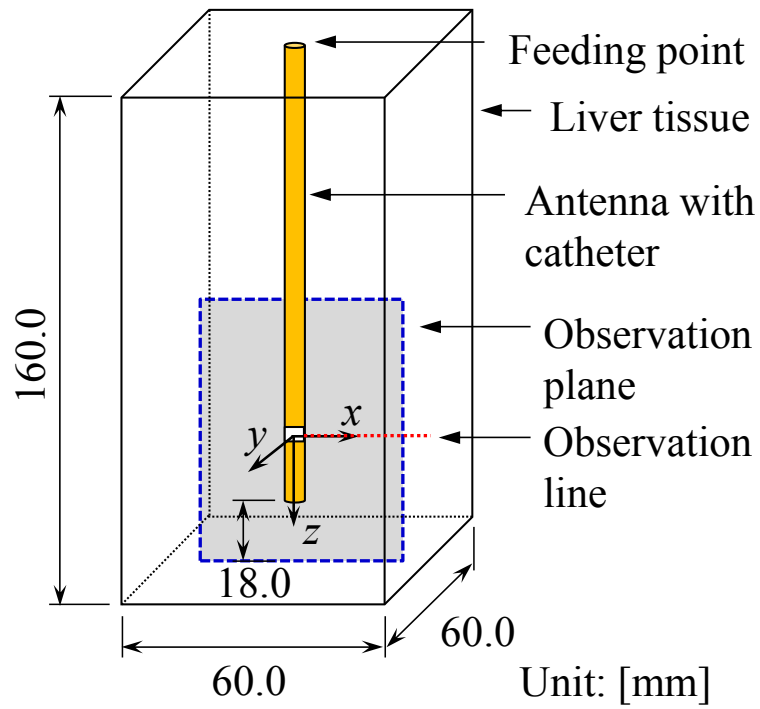
(a) FDTD model.
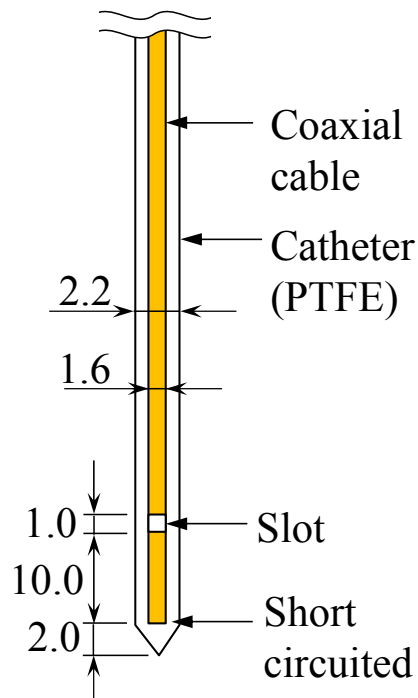


(b) Specific heat.

Fig. 3.2. Analytical model of MCT.

45

## 3.2.2 Analytical results

Figure 3.3 shows the SAR distributions on the observation plane in the case of condition 1. At the start of the heating ($t$= 0 s), a high-SAR region formed around the slot. At the end of the heating ($t$= 60 s), the high-SAR region remained proximal to the slot, but the SAR around the slot significantly decreased. This change was caused by the decrease in electrical conductivity associated with tissue dehydration.

Figure 3.4 shows the distributions of the water content ratio on the observation plane after 60 s of heating under condition 1. This figure indicates the water content ratios significantly decreased in the vicinity of the slot where strong electrical field distributes. Along this, the dielectric constants and the thermal constants of the tissues also decreased, which give effect on the electromagnetic field and the temperature distribution.

Figure 3.5 shows the distributions of the temperature on the observation plane after 60 s of heating. As indicated in the figure, the size of the region over 60°C seemed to be about the same under both conditions. At temperatures over 60°C, tumor tissues will be coagulated and undergo complete necrosis. Figure 3.6 shows the time variations in the volume of the coagulated tissue. Here, the region where the temperature became over 60°C was regarded as the coagulated region. This figure also indicates the size of the coagulated region was mostly not influenced by the differences in the analytical conditions, as with the Fig. 3.5.

Figure 3.7 shows the profiles of the temperature and water content ratio on the observation line which is set on the observation plane to include the slot of the antenna. This figure shows almost no difference in calculated results depending on the values of $t_e$. In condition 1, the tissue temperature slightly exceeded 100°C in the

region where the water content ratio was 0 wt%. An excessively high temperature (over 180°C) was observed near the antenna in condition 2.

Figure 38 shows the time variation in the temperature and the water content ratio at the point 0 mm in Fig. 3.7. In condition 1, a gentle temperature rise was observed over 100°C when the water content ratio was 0 wt%. In the case of $t_e$= 6 s, the water content ratio decreased to 0 wt% in shorter time than the case of $t_e$= 0.5 s. Moreover, in the case of $t_e$= 6s, a sharp increase of the temperature was observed just after the time when the water content ratio decreased to 0 wt%. However, almost no difference in the temperature and water content ratio was shown at the end of the heating ($t$= 60 s) by the difference of $t_e$ setting.

Figure 3.9 shows the reflection coefficient at the feeding point of the antenna in condition 1. This figure indicates that the reflected power slightly increased over time under every condition of $t_e$. This can be explained by the reduction in the water content ratio of the tissue around the slot decreasing the power consumption in that region.

In the proposed numerical analysis, SARs (heating sources in the temperature analysis) are calculated every $t_e$. Here, the calculated SARs are the values expressing decease of water content ratios and the SARs are used in the next temperature analysis for $t_e$. At the strong-electric-field region where water content ratio drastically decreases by high SARs, the temperatures and the water content ratios are sensitively affected by the $t_e$ setting. However, almost no changes in the temperatures and the water content ratios are caused by the differences in $t_e$, after the time when the water content ratio decreased to 0 wt% at the strong-electric-field region.
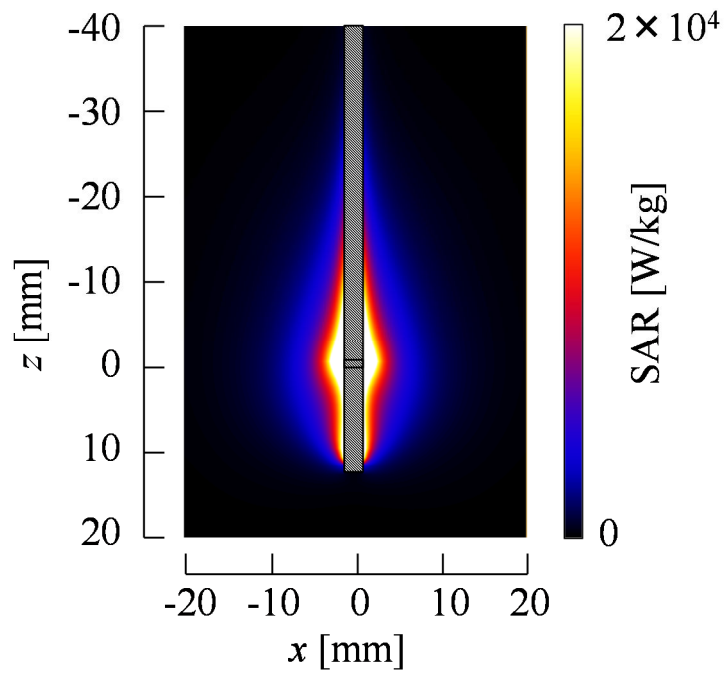
(a) $t = 0$ s.
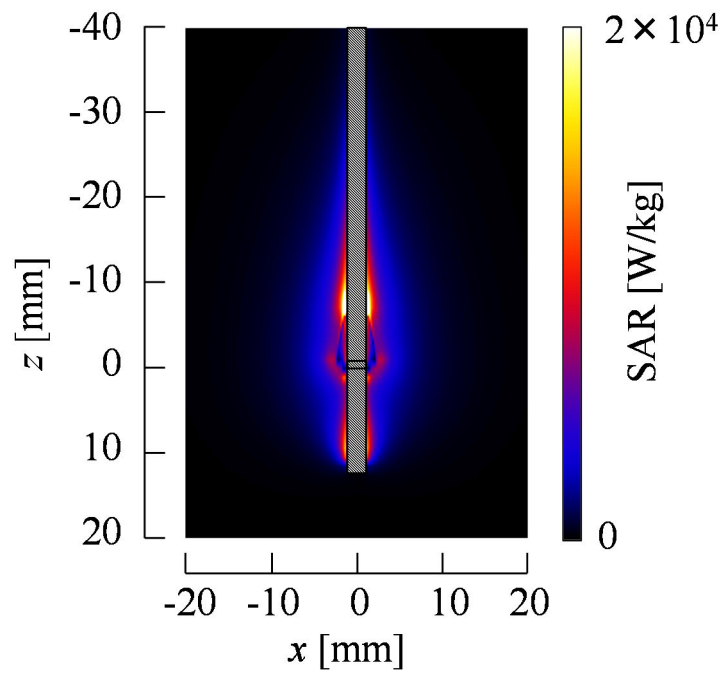


(b) $t = 60$ s.

Fig. 3.3. SAR distributions on the observation plane in condition 1 ($t_e = 0.5$ s).
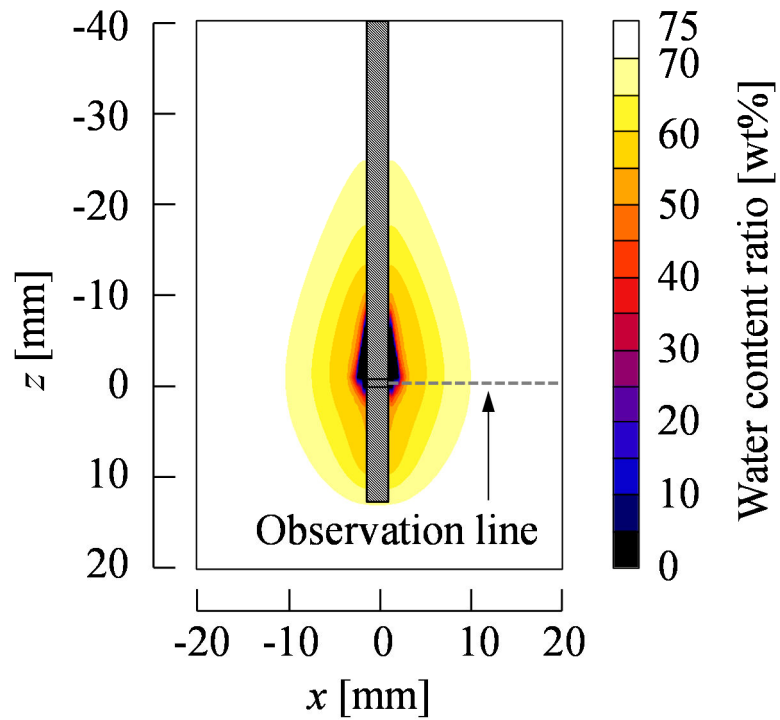
Fig. 3.4. Distributions of the water content ratio after heating for 60 s in condition 1. The observation line is for Figure 3.7 ($t_e$= 0.5 s).
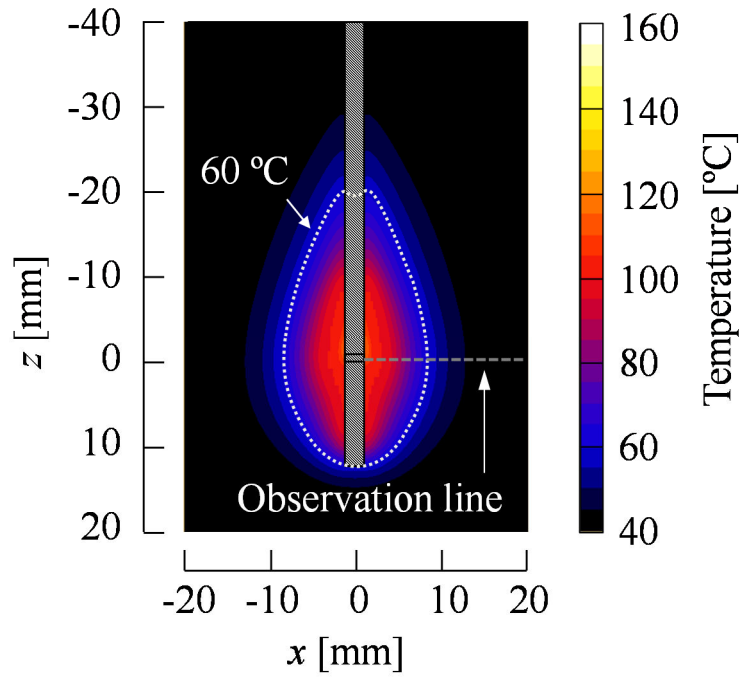
(a) Condition 1.
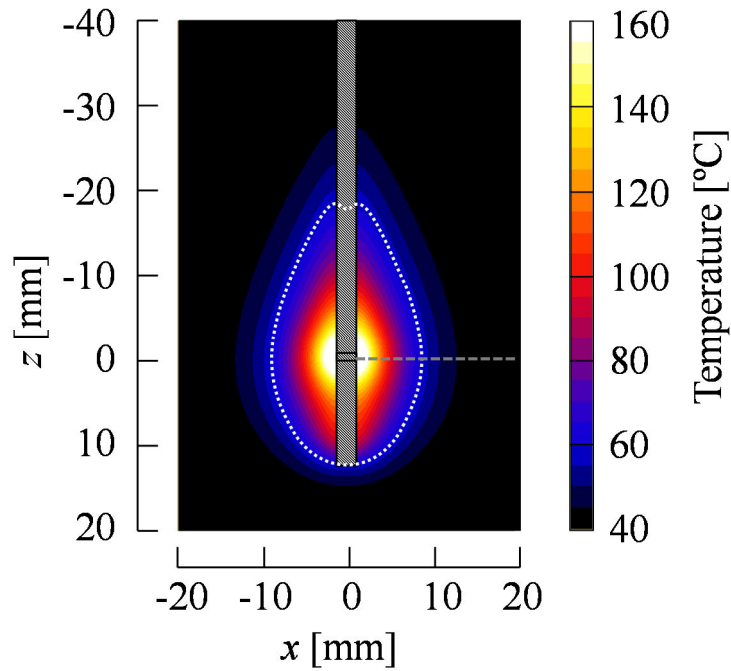


(b) Condition 2.

Fig. 3.5. Temperature distributions on the observation plane after heating for 60 s. The observation line is for Fig. 3.7 ($t_e$= 0.5 s).
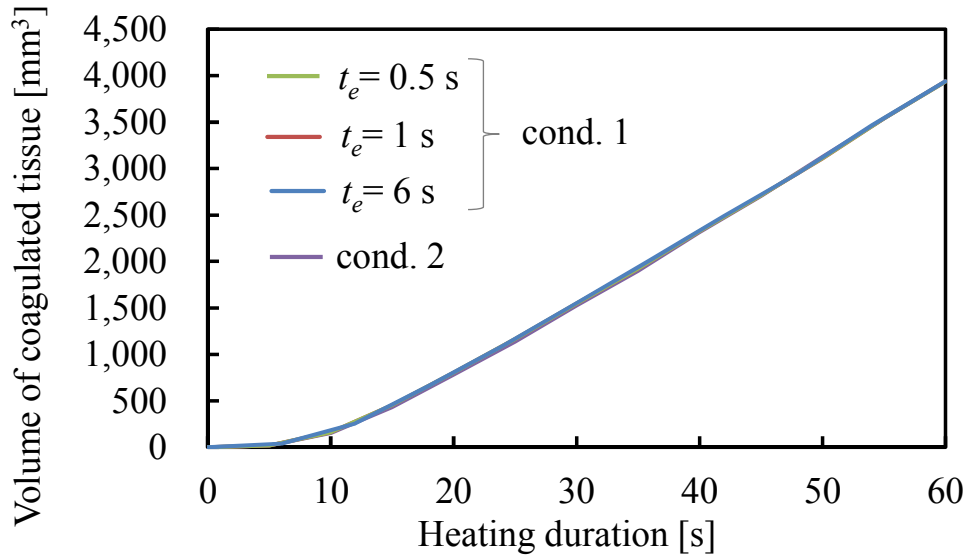
Fig. 3.6. Time variation in the volume of coagulated tissue.
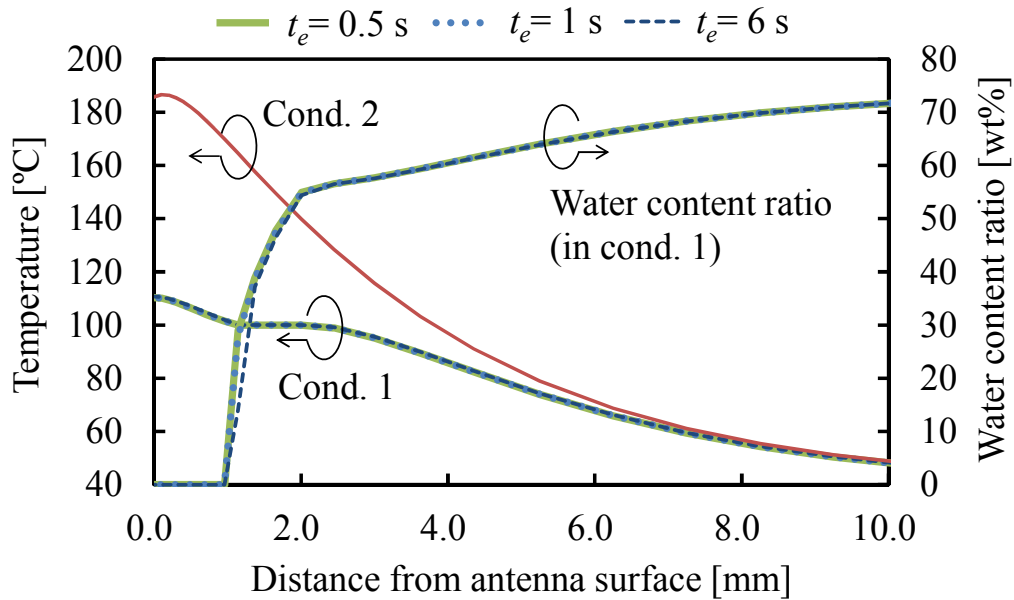


Fig. 3.7. Temperature and water content ratio on the observation line.
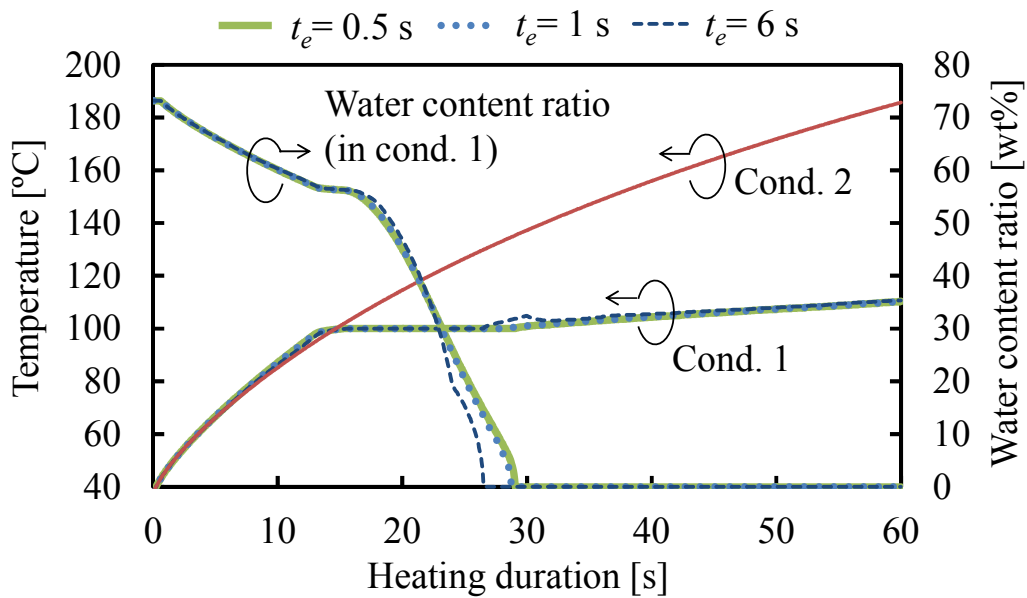
Fig. 3.8. Time variation in temperature and water content ratio at 0.0 mm in Fig. 3.7.
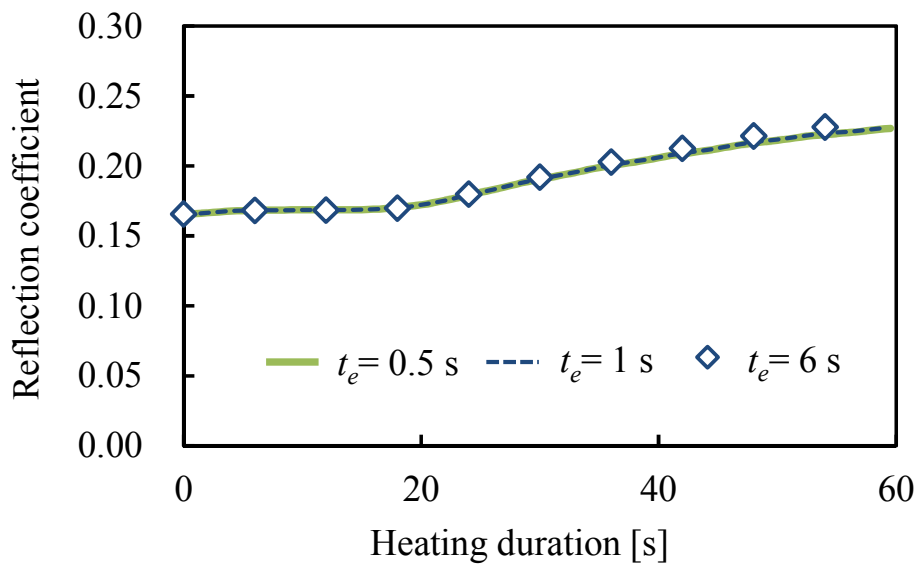


Fig. 3.9. Time variation in the reflection coefficient in condition 1.

## 3.3 *Ex vivo* experiment

In order to evaluate the validity of the developed numerical simulator, calculated temperatures were compared with the measured temperatures in the *ex vivo* experiment. The *ex vivo* experiment with the extracted swine liver was performed under the same conditions used in the numerical analysis.

Figure 3.10 shows the time variation in the temperature at the observation point (0 mm in Fig. 3.7). In the figure, the measured temperatures in the *ex vivo* experiment and calculated temperatures are plotted. The temperatures were measured with an AM-8051E thermometer and an SF-E-200-AMP thermocouple (Anritsu Meter, Tokyo, Japan). The temperature values 2 s after the end of the microwave irradiation were measured to avoid interference. Therefore, the actual temperature was approximately 10°C higher than the measured value at maximum.

Figure indicates that the measured values were similar to those obtained in condition 1, taking into account potential measurement errors. These results imply that the obtained temperature distributions under condition 1 were closer to actual values than those under condition 2, which ignored the change in the water content ratio.
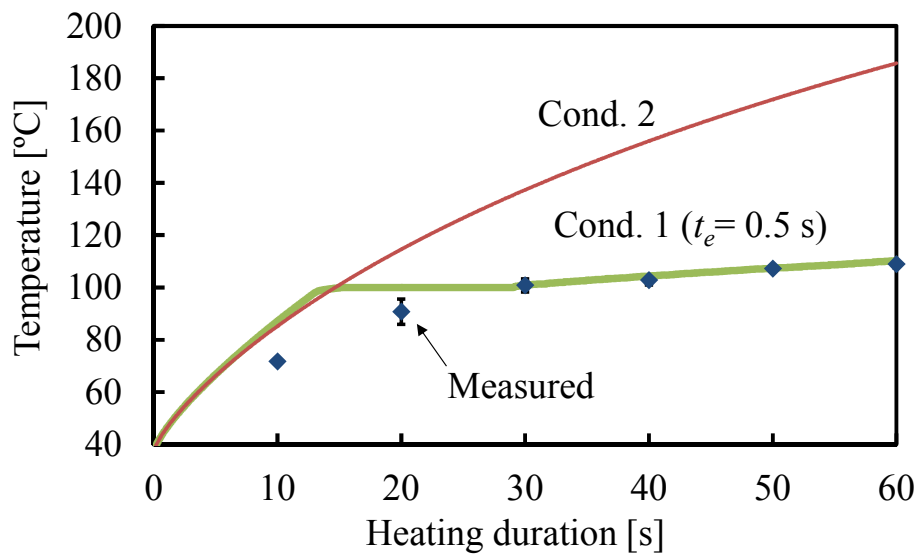
Fig. 3.10. Time variation in temperature at 0.0 mm in Fig. 3.7.

# 3.4 Conclusion

Numerical analyses of the electromagnetic field and tissue temperature at the time of the MCT were conducted, employing the numerical model of the liver tissue proposed in chapter 2. For a comparison, numerical analyses using the values of liver tissue at room temperature (fixed values) were performed.

After 60 s of heating, the water content ratios of the tissue in the vicinity of the antenna significantly decreased, and the heating effects also decreased in these regions compared to the non-heated tissue. The size of the necrosis region (over 60°C) was successfully evaluated under two conditions, but the temperature over 100°C was not accurately calculated in condition 2 (i.e., both the dielectric and thermal constants were fixed).

A previous study reported similar findings for tissue temperature [4]. However, in the method in [4], the decrease in the water content ratio was only reflected in the temperature analysis and not in the electromagnetic field analysis. Therefore, accurate distributions of the electric field (heating source) cannot be obtained, particularly in the vicinity of the heating antenna where tissue dehydration is prevalent.

To evaluate the risk of MCT-related problems, such as charring, which may cause bleeding if the charred part is cast off, and the generation of surgical smoke, which contains toxic substances [8],[9], it is important to perform studies at temperatures over 100°C.

The results of the present study imply that more accurate analyses of the electromagnetic field and the temperature in heated tissue can be obtained by examine the effects of changes in the water content ratio of tissue. The findings of

this study can also help to improve the safety of MCT.

Using the method proposed in this study, the temperature of biological tissue heated over 100°C can be analyzed accurately, even with treatments other than MCT, such as radiofrequency ablation using an electric current at several hundred kHz as the heating source [10],[11] and hemostasis with microwave energy in surgical operations [6].

To obtain more accurate numerical analyses in MCT, heating-induced changes in the mass density and blood flow rate of tissue should be numerically modeled.

# References

[1]    H. H. Pennes, "Analysis of tissue and arterial blood temperatures in the resting human forearm," J. AppL. Phys., vol. 1, no. 11, pp. 93-122, 1948.

[2]    K. Saito, Y. Hayashi, H. Yoshimura, K. Ito, "Heating characteristics of array applicator composed of two coaxial-slot antennas for microwave coagulation therapy," IEEE Trans. Microwave Theory Techn., vol.48, no.11, pp.1800-1806, Nov. 2000.

[3]    K. Ito, K. Ueno, M. Hyodo, and H. Kasai, "Interstitial applicator composed of coaxial ring slots for microwave hyperthermia," Proc. of International Symposium on Antennas and Propagation, pp. 253-256, 1989.

[4]    D. Yang, M. C. Converse, D. M. Mahvi, J. G. Webster, "Expanding the bioheat equation to include tissue internal water evaporation during heating," IEEE Trans. Biomed. Eng., vol.54, no.8, pp.1382-1388, Aug. 2007.

[5]    C. Gabriel, "Compilation of the dielectric properties of body tissues at RF microwave frequencies," Brooks Air Force Technical Report AL/OE-TR-1996-0037, 1996.

[6]    Y. Endo, K. Saito, and K. Ito, "The development of forceps-type microwave tissue coagulator for surgical operation," IEEE Trans. Microwave Theory Techn., vol. 63, no. 6 pp.2041-2049, June 2015.

[7]    P. A. Hasgall, E. Neufeld, M. C. Gosselin, A. Klingenböck, and N. Kuster, "IT'IS Database for thermal and electromagnetic parameters of biological tissues," Version 2.4, July 2013.

[8]    W. L. Barrett and S. M. Garber, "Surgical smoke: a review of the literature. Is this just a lot of hot air?," Surgical Endoscopy, vol. 17, no. 6, pp. 979-987, June

2003.

[9]     L. Bigony, "Risks associated with exposure to surgical smoke plume: a review of the literature," AORN Journal, vol. 86, no. 6, pp. 1013-1024, Dec. 2007.

[10]    D. Panescu, J. G. Whayne, S. D. Fleischman, M. S. Mirotznik, D. K. Swanson, and J. G. Webster, "Three-dimensional finite element analysis of current density and temperature distributions during radio-frequency ablation," IEEE Trans. Biomed. Eng., vol. 42, no. 9, pp. 879-890, Sept. 1995.

[11]    S. Labonte, "Numerical model for radio-frequency ablation of the endocardium and its experimental validation," IEEE Trans. Biomed. Eng., vol. 41, no. 2, pp. 108-115, Feb. 1994.

# Chapter 4

# Development of the forceps-type surgical device applying microwave heating

In surgical operations, hemostasis is one of the most important treatments because an excessive loss of blood puts the patient at great risk.

Surgical devices using radiofrequency (RF) (from several hundred kHz to several MHz) current or ultrasonic vibration have been widely used for cutting and coagulation of biological tissues. These devices enable simple and quick surgical procedures, such as the resection of biological tissue, without bleeding. They have many advantages and disadvantages based on the characteristics of the energy source employed.

Microwaves only have a heating effect on the biological tissues, and this effect is not as excessive in comparison with that of the arc discharge due to the RF current and ultrasonic vibration. Therefore, coagulation devices using microwave energy can safely heat biological tissues without carbonization and mechanical damage. Moreover, adhesion of the coagulated tissue to the device can be prevented by coating the microwave radiator with a material such as polytetrafluoroethylene (PTFE).

In previous studies, we have developed stick-shaped microwave tissue coagulators for the hemostasis of solid organs, such as the liver [1],[2]. These devices have a heating antennas on the distal ends. To stop bleeding, the distal ends of the

devices are pushed to the bleeding sites, radiating microwave energy from the antennas. However, these devices are not suitable for the hemostasis of thin tissues such as blood vessel and other lumen tissues, whose position is unstable in treatments.

Therefore, in this study, a forceps-type surgical device for the hemostasis of thin biological tissues, such as blood vessels is proposed. Fig. 4.1 is an image of the introduced device, which has an upper jaw equipped with a heating antenna and a lower jaw equipped with a cutting blade. The biological tissue is grasped between the two jaws and heated by the heating antenna. Then, the coagulated tissue is cut with the blade. We have designed a heating antenna and evaluated the primary coagulating capability of the proposed device [3]-[5].

In this work, more detailed coagulating characteristics of the proposed device were investigated through numerical analyses and an *ex vivo* experiment with swine liver tissues. The validity of the device was evaluated through an *in vivo* experiment with swine. In the numerical analysis, the temperature of the biological tissue grasped with the device was calculated using the numerical simulator developed in chapter 3.
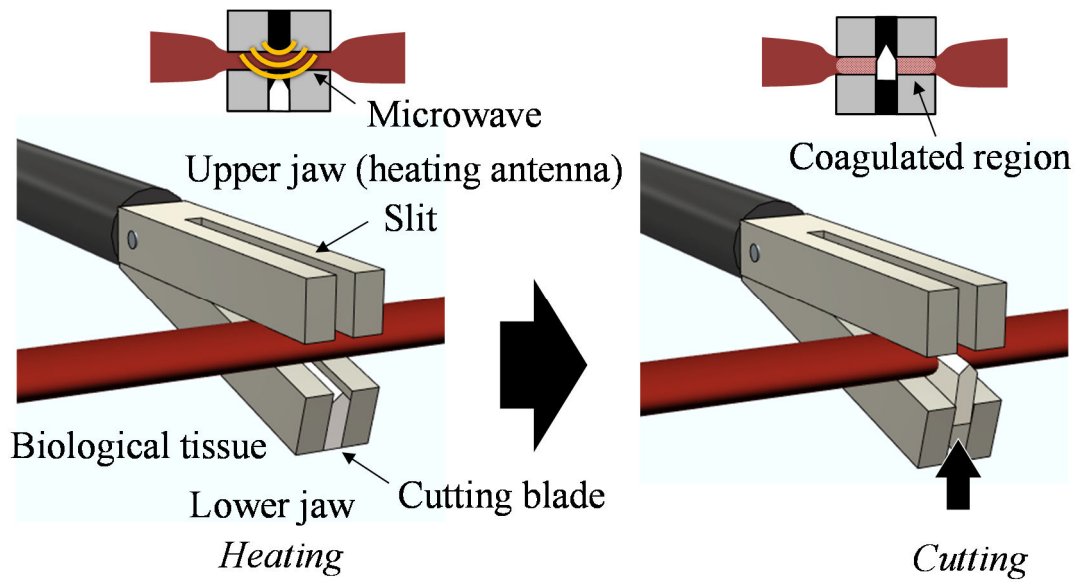
Fig. 4.1. Illustration of proposed device. Copyright ©
2015, IEEE.

# 4.1 Structure of proposed device

The proposed device was assumed to be used in various types of surgical operations including water-filled laparoendoscopic surgery (WaFLES) [6]. WaFLES is one of novel laparoscopic surgeries, saline solution rather than carbon dioxide gas is employed for the swelling of the abdomen for various advantageous reasons. Therefore, the device was designed to effectively heat grasped tissue in saline solution.

Figure 4.2 shows a simplified model of the proposed device. The mechanical parts for the opening/closing operation of the jaws were ignored because the main purpose was to evaluate the coagulation characteristics. In the numerical calculation, the distance between the two jaws changed according to the thickness of the tissue, and the overall height of the device was also changed. The thickness of the blade was set to be 1.0 mm (the blade enters the 1.0-mm-width slit at the tip of the upper jaw when cutting the grasped tissue).

The heating antenna comprises a forked loop element at the tip of a semi-rigid coaxial cable for feeding. The antenna element is connected to the inner conductor of the coaxial cable through the center wire and to the side of the outer conductor at two points. Each narrow loop works as a short-circuited parallel line which transmits microwave power to the distal end of the antenna. The electrical field concentrates on the 1.0-mm slit between the two loops where the blade enters, creating a strong heating effect in the grasped biological tissue, near this part. The length of the grasping part $l_g$ [mm] was determined to induce a high intensity electrical field on the region where grasped tissue would exist, and to make impedance matching the coaxial cable in saline solution at 2.45 GHz, the operating frequency of the heating

antenna, one of the industrial, scientific, and medical (ISM) bands in Japan.

The size of the device when the jaws are closed is smaller than the inner diameter of a trocar (= 12 mm). Trocars are surgical apparatus those are placed in the abdominal wall during laparoscopic surgery and work as ports for the subsequent placement of other surgical instruments, shown in Fig. 4.3.

The proposed device mainly consists of polytetrafluoroethylene (PTFE), which is an excellent material for heat resistance, chemical resistance, electrical property (low loss), and biocompatibility. Moreover, PTFE prevents adherence of the coagulated tissue on the device.

Coaxial cable ($\phi$ 2.2)

Slit for cutting blade

*Upper jaw*

PTFE

Heating antenna

3.0

Cutting blade

1.0

Thickness of tissue

2.0

$l_g$ (length of grasping part)

5.0

Unit: mm

*Lower jaw*

(a) General view.

5.0

1.0

$l_g$ (length of grasping part)

0.5

1.0

Connected to inner conductor

3.0

2.0

Coaxial cable

Connected to outer conductor
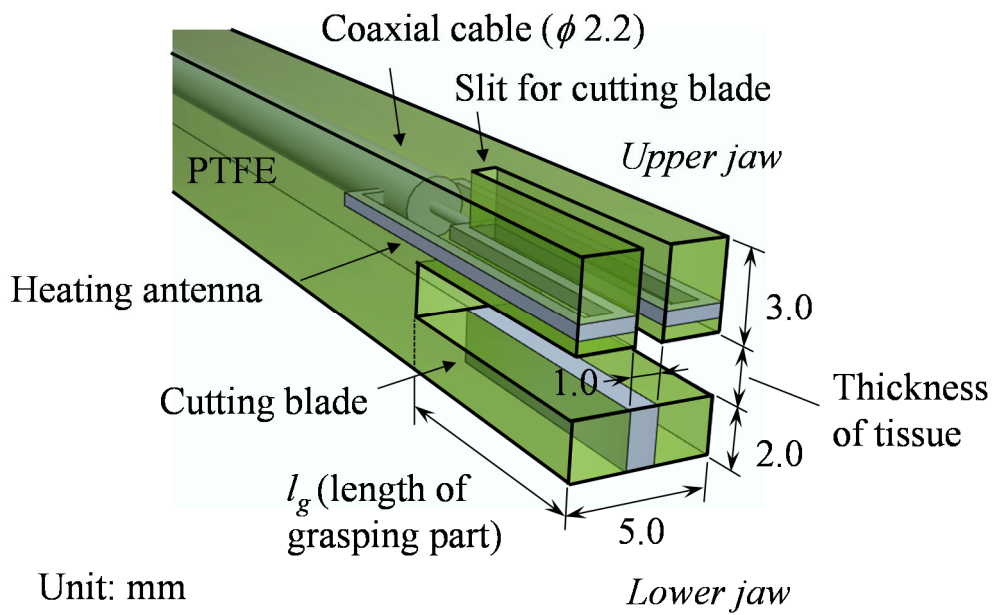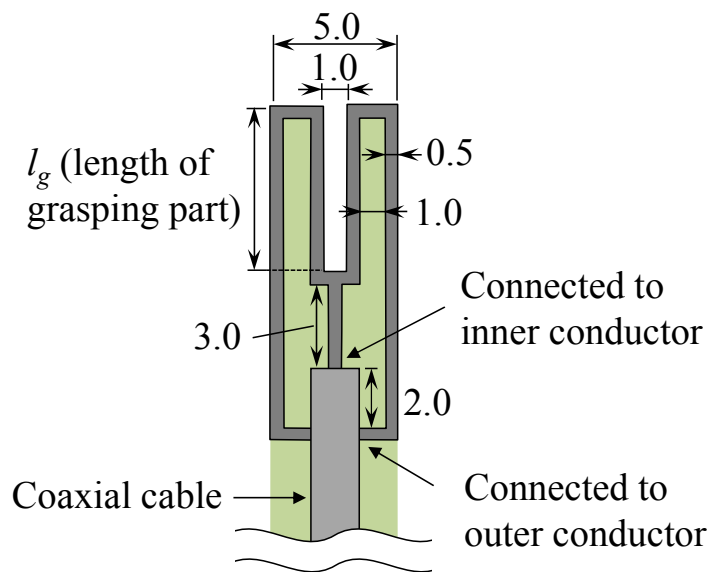
(b) Heating antenna.

Fig. 4.2. Structure of proposed device. Copyright © 2015, IEEE.
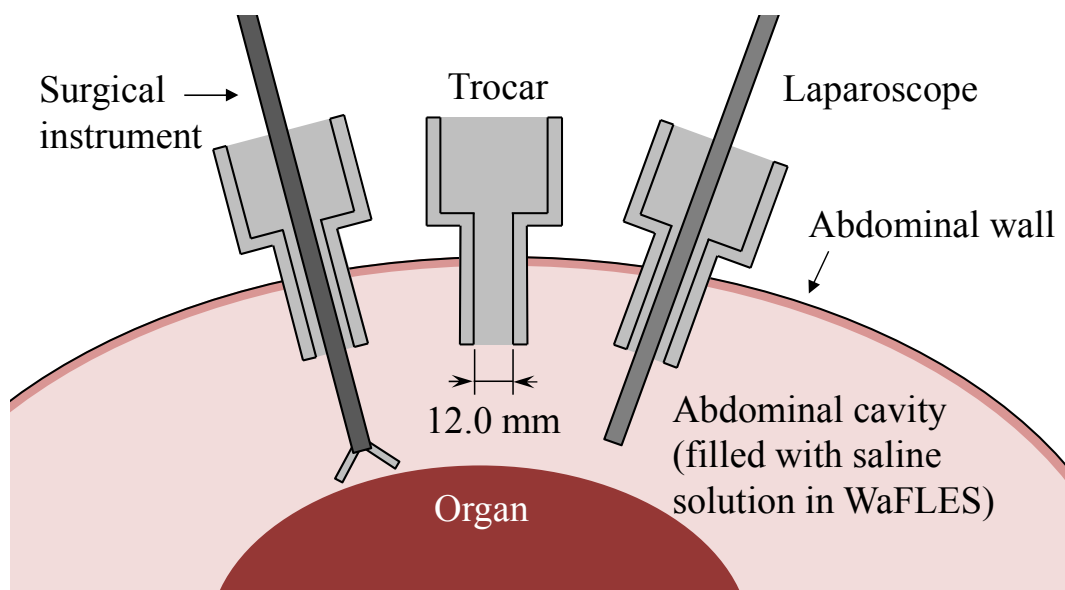
Fig. 4.3. Image of laparoscopic surgery. Copyright © 2015, IEEE.

# 4.2 Numerical analyses

In this section, the numerical analyses for the evaluation of the tissue-coagulation characteristics of the proposed device is described. The coagulated region of the tissue caused by the microwave heating, was estimated based on the calculated tissue temperatures. For the numerical analyses, the numerical simulator proposed in chapter 3 was used.

## 4.2.1 Analytical model

Figure 4.4 illustrates the numerical model. A thin biological tissue is grasped with the proposed device in a saline solution (37°C), simulating the situation of WaFLES. Here, the region grasped between the two jaws is defined as "the grasped region". The thickness of the grasped tissue changed from 0.5 to 2.0 mm and the width was set to 6.0 mm in all conditions. These sizes were determined assuming a situation in which the columnar-shaped tissue with a diameter of about 4–5 mm is grasped between the jaws.

Table 4.1 lists the physical property values of the objects used in the numerical analyses. In this analysis, physical properties of a liver is set to the numerical model of the grasped tissue. The blood flow rate $F$ of the tissue was set to $8.33 \times 10^{-6}$ m$^3$/kg·s. However, at the grasped region between the two jaws of the device, $F$ was set to 0 considering the compression of the jaws. The physical properties of the PTFE were set to the metallic part of the proposed device to reduce the calculation time. The relative permittivity and the electrical conductivity of the saline solution (37°C) were measured by using an Agilent 85070E Dielectric Probe (Agilent Technologies, Santa

Clara, CA, USA).

Table 4.2 lists the analytical conditions for the electromagnetic field and the temperature. In the numerical analyses, the non-uniform grid is employed to construct the analysis area, and small-size grids are employed to constitute the small structures such as the antenna element. We employed the same grids in the both analyses. In the temperature analysis, the time step was determined to satisfy a stable condition [9]. The temperature of the blood $T_b$ and the initial temperature of the biological tissue were set to 37.0°C. The saline solution was modeled as the object with constant temperature (37.0°C), assuming irrigation.

The maximum input power to the heating antenna was set to 70 W, approximate maximum net input power of the microwave oscillator used in the experiment described in section 4.3. In the numerical analysis, the net-input power to the antenna was determined by subtracting the reflection power at the feeding point from 70 W. The total heating duration $t_h$ was set to 10 s.

In this study, two different values (0.5 s and 1 s) were set to the duration of each temperature analysis $t_e$ [s].
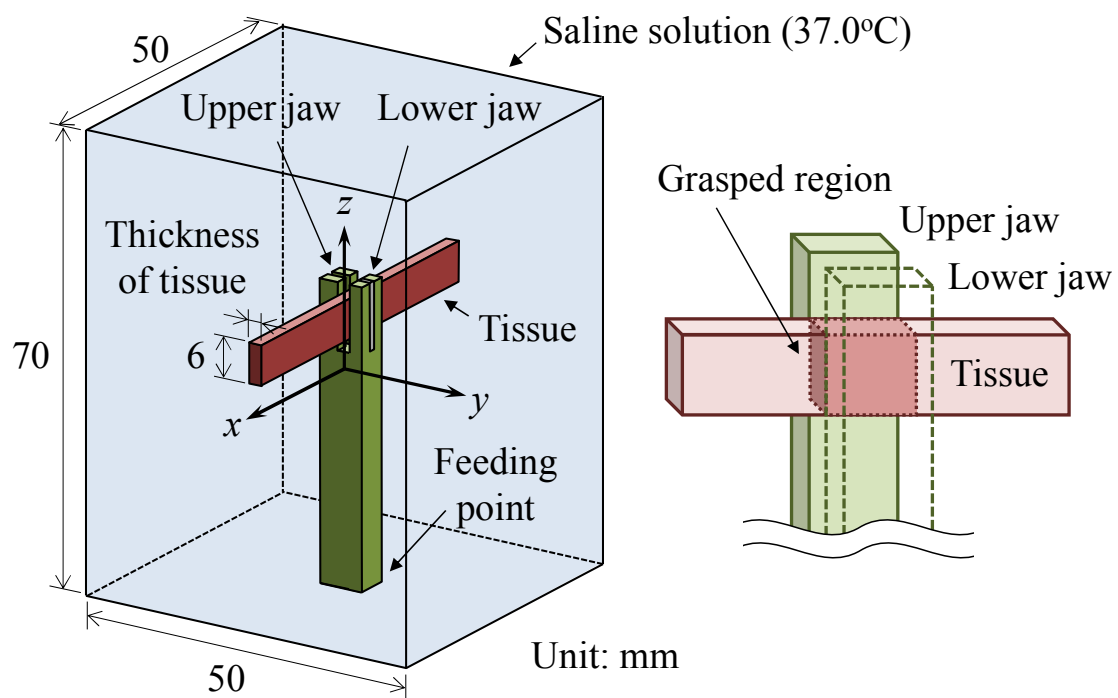
Fig. 4.4. FDTD analytical model. Copyright © 2015, IEEE.

Table 4.1. Physical properties. Copyright © 2015, IEEE.

| Dielectric constants | | |
|---|---|---|
| Liver | $\varepsilon_r$ | Eq. 2.6 |
| | $\sigma$ [S/m] | Eq. 2.7 |
| PTFE | $\varepsilon_r$ | 2.1 |
| | $\sigma$ [S/m] | 0 |
| Saline solution (0.9 w/v%) | $\varepsilon_r$ | 71.00 |
| | $\sigma$ [S/m] | 2.80 |
| Thermal constants | | |
| Liver | $c$ [J/kg·K] | Eq. 2.8 |
| | $\kappa$ [W/m·K] | Eq. 2.9 |
| | $\rho$ [kg/m³] | 1,080 [7] |
| | $F$ [m³/kg·s] | 8.33×10⁻⁶ [8] |
| PTFE | $c$ [J/kg·K] | 1,046 |
| | $\kappa$ [W/m·K] | 0.25 |
| | $\rho$ [kg/m³] | 2,200 |
| Blood | $c_b$ [J/kg·K] | 3,960 [8] |
| | $\rho_b$ [kg/m³] | 1,060 [8] |

Table 4.2. Analytical conditions. Copyright © 2015, IEEE.

| Parameters for FDTD calculation | |
|---|---|
| Cell size [mm] (minimum) | 0.1 |
| Cell size [mm] (maximum) | 1.0 |
| Time step [ps] | 0.192 |
| Absorbing boundary condition | Mur (1st order) |
| Parameters for FDM calculation | |
| Cell size [mm] (minimum) | 0.1 |
| Cell size [mm] (maximum) | 1.0 |
| Time step [s] | 0.001 |
| Temperature of boundary [$^o$C] | 37.0 |
| Temperature of blood [$^o$C] | 37.0 |
| Initial temperature [$^o$C] | 37.0 |

## 4.2.2 Analytical results

Figure 4.5 shows the reflection coefficients at the feeding point of the device at $t= 0$ s, under the conditions of $l_g= 5$ mm, 10 mm, and 15 mm. This figure indicates that the device work efficiently at 2.45 GHz in the case of $l_g= 10$ mm. In this case, the length from the distal end of the antenna element to the coaxial cable assumed to be approximately 1/4 wavelength, under the situation in which the antenna element is surrounded by the various types of media, in particular, the saline solution which have high relative permittivity and makes strong wavelength shortening effect. This means that the frequency characteristics of the input characteristics were strongly affected by the saline solution, instead of the grasped tissue.

As a result, the length of the grasping part $l_g$ which makes the device operate efficiently at 2.45 GHz was determined as 10 mm. Therefore, following numerical analyses were performed with the device in the case of $l_g= 10$ mm.

Figure 4.6 presents the distributions of the electrical field induced by the heating antenna (tissue thickness: 2.0 mm) at the start of the heating ($t= 0$ s) and the end of the heating ($t= 10$ s). Figure 4.6 (a) and (b) show that strong electrical field is generated around the slit of the antenna. Figure 4.6 (c) and (d) show a relatively strong electrical field induced along the cutting blade of the lower jaw. Figure 4.6 (e) and (f) show that the strong electric field distributes in the region including the grasped tissue. Moreover, these figures show decreases of the electrical field inside the tissue due to 10 s of heating.

Figure 4.7 shows the SAR distributions of the grasped region (tissue thickness: 2.0 mm). At the start of the heating ($t= 0$), a high-SAR region formed around the slit

of the heating antenna. At the end of the heating ($t$=10 s), the SARs around the slit significantly decreased. This change was caused by the decrease in electrical conductivity associated with tissue dehydration.

Figure 4.8 shows the distributions of the water content ratio on the observation plane after 10 s of heating. This figure indicates the water content ratios significantly decreased in the vicinity of the slit where strong electrical field distributes. Along this, the dielectric constants and the thermal constants of the tissues also decreased, which give effect on the electromagnetic field and the temperature distribution.

Figure 4.9 shows the distributions of the temperature on the observation plane after 10 s of heating. These figures indicate that the part of the tissue that contacts with the saline solution strongly receives the cooling effect due to the saline solution. In Fig. 4.9 (c), the area surrounded by a dotted line means the region heated to over 60°C (the coagulation temperature of biological tissues). This means that the grasped tissue except the region where strong cooling effect due to the saline solution works is extensively coagulated. Similar temperature distributions were observed even in the numerical analyses with other tissue thicknesses than 2.0 mm.

Figure 4.10 shows the time variations in the temperature and the water content ratio at observation point. The observation point was set at the center of the grasped tissue in every thickness of the tissue as in the Fig. 4.7 (g). These figures show that the temperatures at the observation points rose to around 100°C for about one second under every analytical condition. In Fig. 4.10 (a) and (b), the sharp temperature rise was observed at the time when the water content ratio decreased to 0 wt% under both $t_e$ conditions. These are the analysis errors caused by the process that the SARs are updated every $t_e$. In the case that extremely high SARs are used for heating sources, smaller $t_e$ is required to suppress the error.

Figure 4.11 presents the ratio of the coagulated-tissue volume in the grasped region. The coagulated-tissue region was defined as the region whose water content ratio was less than the value at 60°C. This figure indicates that the 10 s of heating made the volume exceeding 70% of the grasped region coagulated, under every analyzed situations. As shown in Fig. 4.9, the non-coagulated region concentrates on the surface part of the grasped region. In order to stop the blood flow in the grasped tissue, it is necessary to coagulate the inner part of the tissue rather than the surface. These results showed the sufficient tissue-coagulating capability of the proposed device for the surgical procedures such as hemostasis and blood vessel sealing. Moreover, there were almost no changes in values at 10 s regardless of the $t_e$ conditions, in each thickness.

Figure 4.12 shows the time variations in the reflection coefficient at the feeding point of the antenna. This figure indicates that there were almost no changes in the reflected power through the 10 s of heating under every analytical condition. Regarding every tissue thickness condition, the reflection coefficient under the condition of $t_e$= 1 s were a little higher than that under the condition of $t_e$= 0.5 s. This was because that the water content ratios of the tissues near the antenna decreased and the dielectric properties also decreased in the case of $t_e$= 1 s more than the case of $t_e$= 0.5 s.
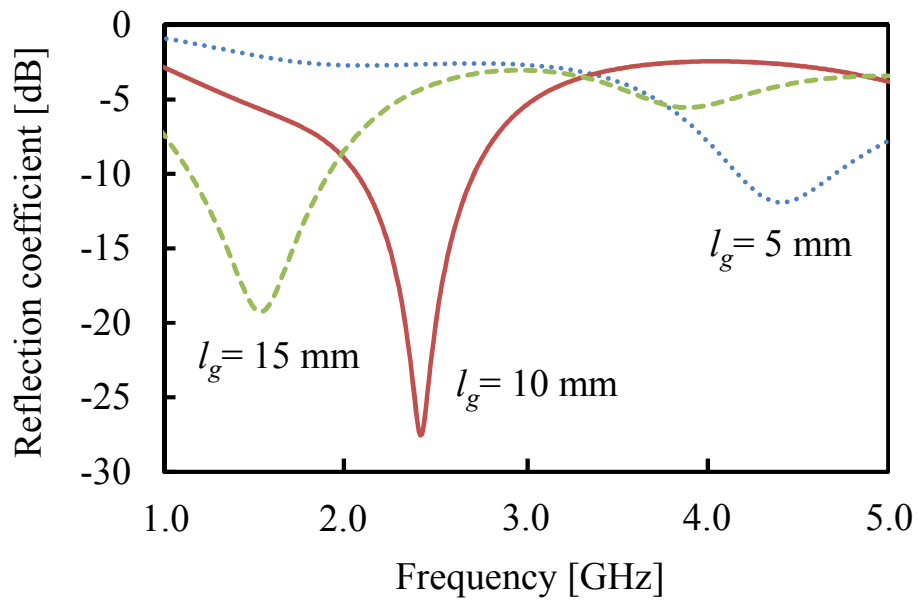
Fig. 4.5. Reflection coefficient at feeding point at $t= 0$ s.
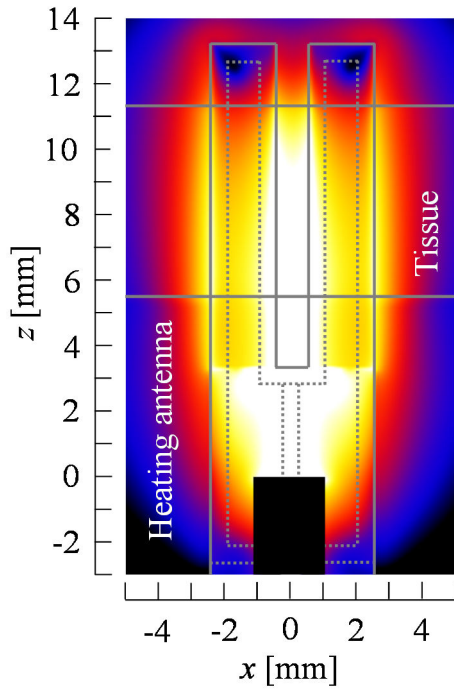
(a) Plane in contact with upper jaw (*t*= 0 s).
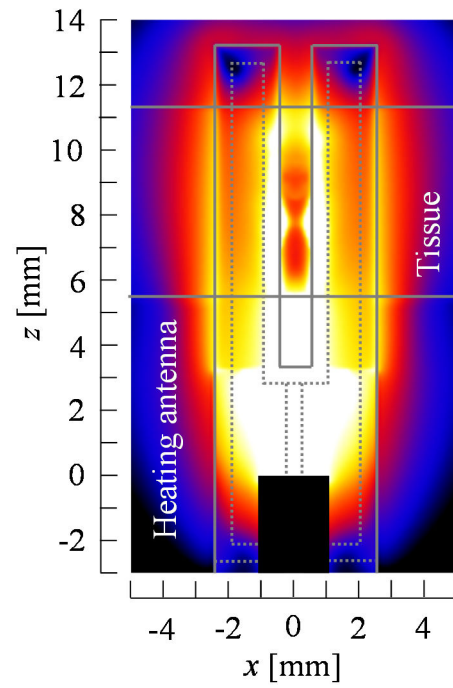
(b) Plane in contact with upper jaw (*t*= 10 s).
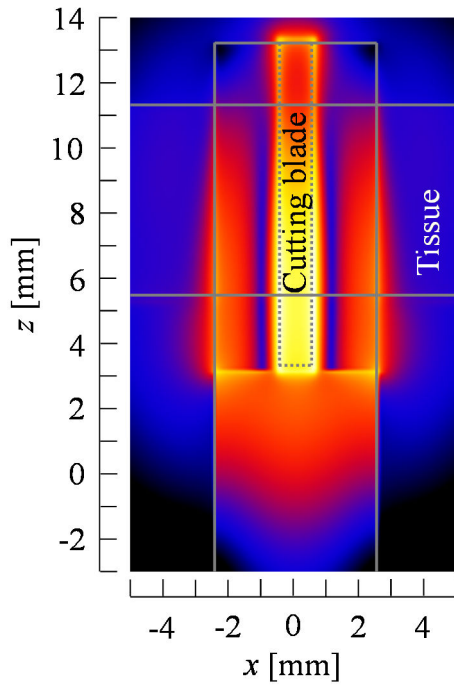
(c) Plane in contact with lower jaw (*t*= 0 s).
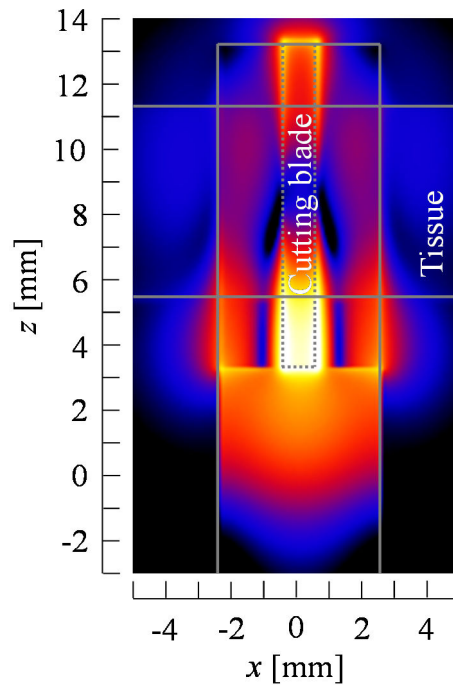
(c) Plane in contact with lower jaw (*t*= 10 s).
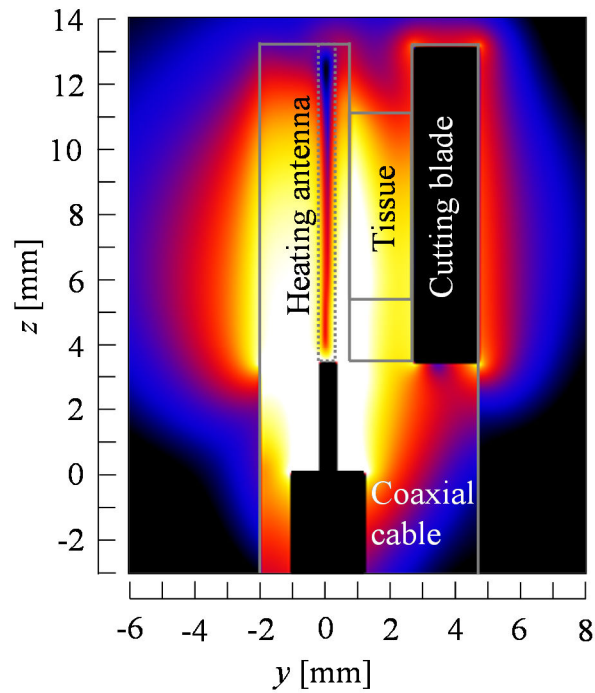
(e) Cross section including center point of device ($t= 0$ s).
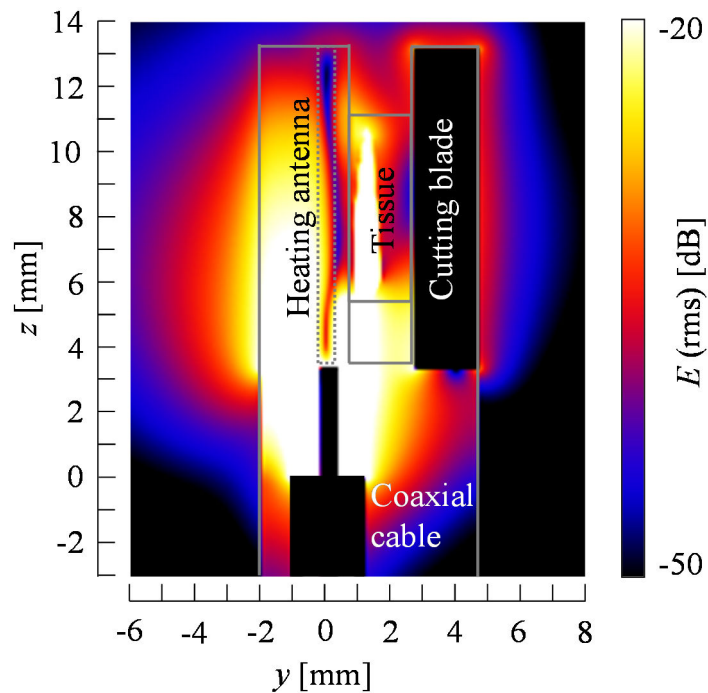


(f) Cross section including center point of device ($t= 10$ s).

Fig. 4.6. Distributions of electrical field ($t_e= 1$ s). Copyright © 2015, IEEE.
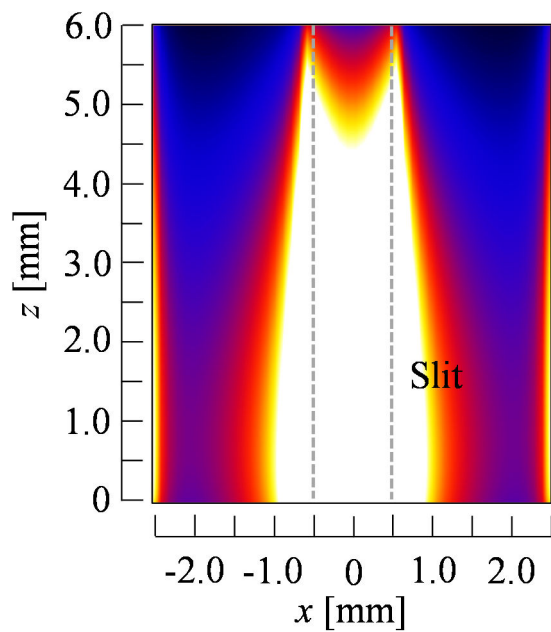
(a) Surface in contact with upper jaw (*t*= 0 s).
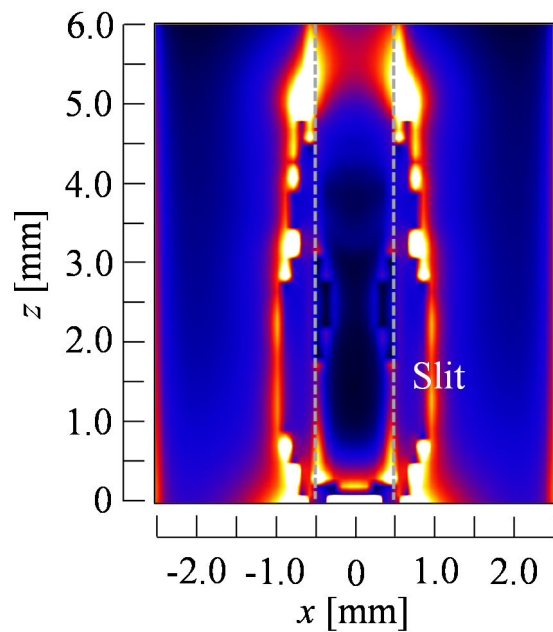
(b) Surface in contact with upper jaw (*t*= 10 s).
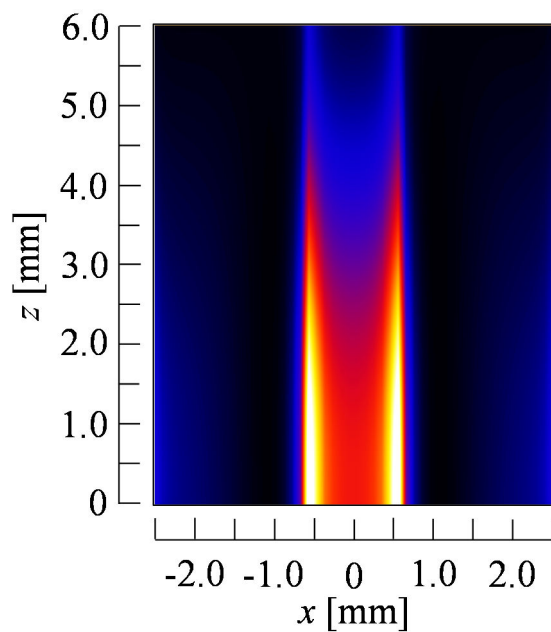
(c) Surface in contact with lower jaw (*t*= 0 s).
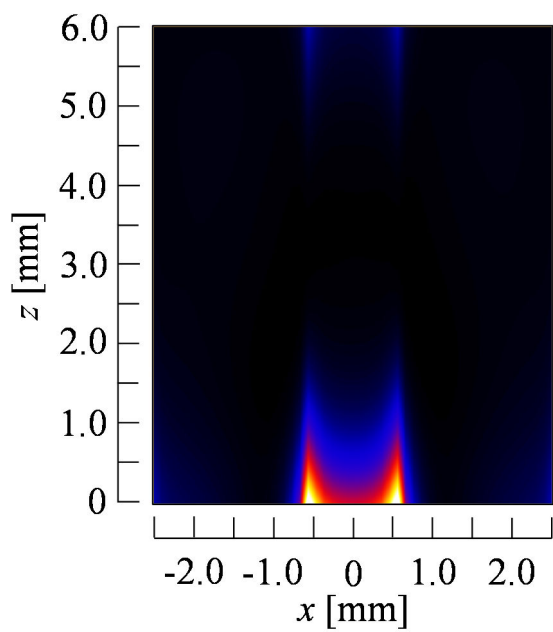
(d) Surface in contact with lower jaw (*t*= 10 s).
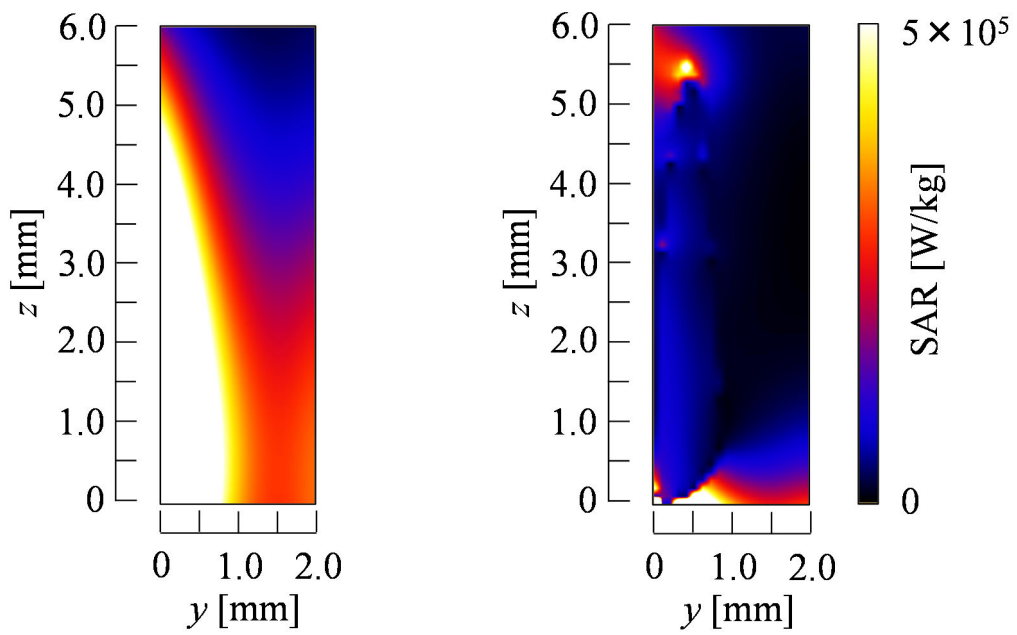
(e) Cross section ($t$= 0 s).  (f) Cross section ($t$= 10 s).

Observation plane

✕ Observation point in Fig. 4.10



Upper/Lower jaw
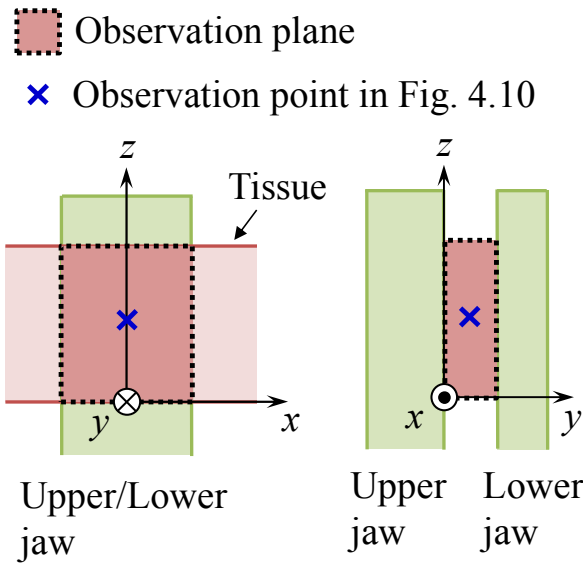
Upper jaw  Lower jaw

(g) Observation planes.

Fig. 4.7. SAR distributions of grasped region ($t_e$= 1 s)
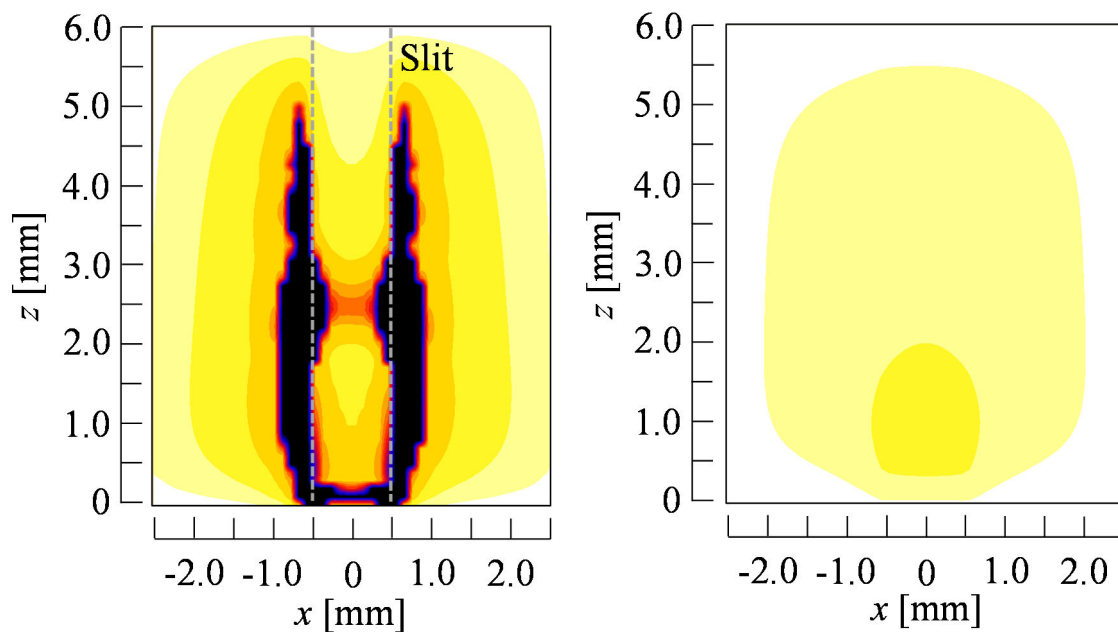
(a) Surface in contact with upper jaw.

(b) Surface in contact with lower jaw
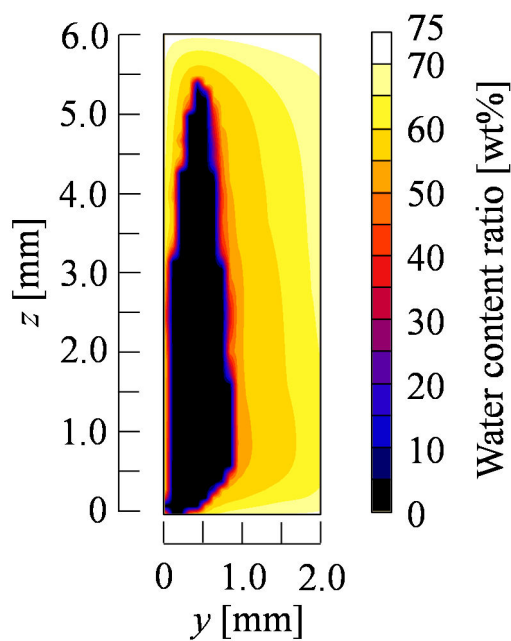
(c) Cross section.

Fig. 4.8. Water content ratio distributions of grasped region after heating ($t= 10$, $t_e= 1$ s).
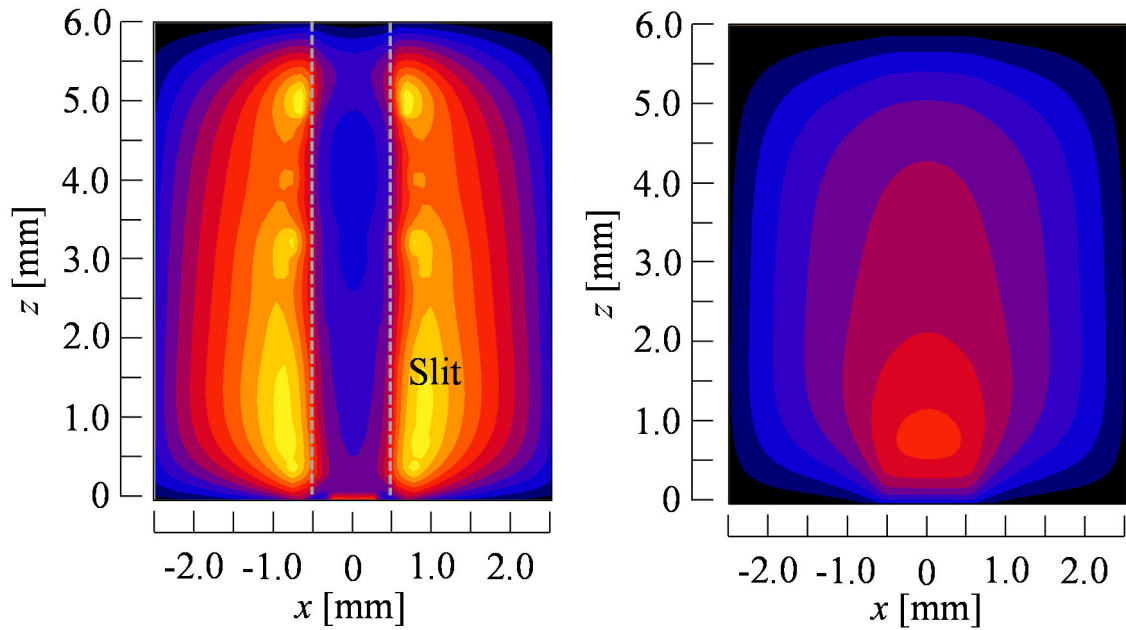
(a) Surface in contact with upper jaw.

(b) Surface in contact with lower jaw
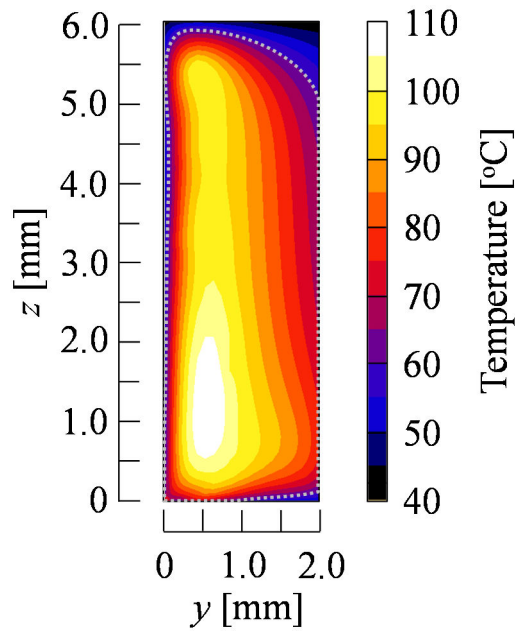
(c) Cross section.

Fig. 4.9. Temperature distributions of grasped region ($t=$ 10 s, $t_e=$ 1 s). Copyright © 2015, IEEE.
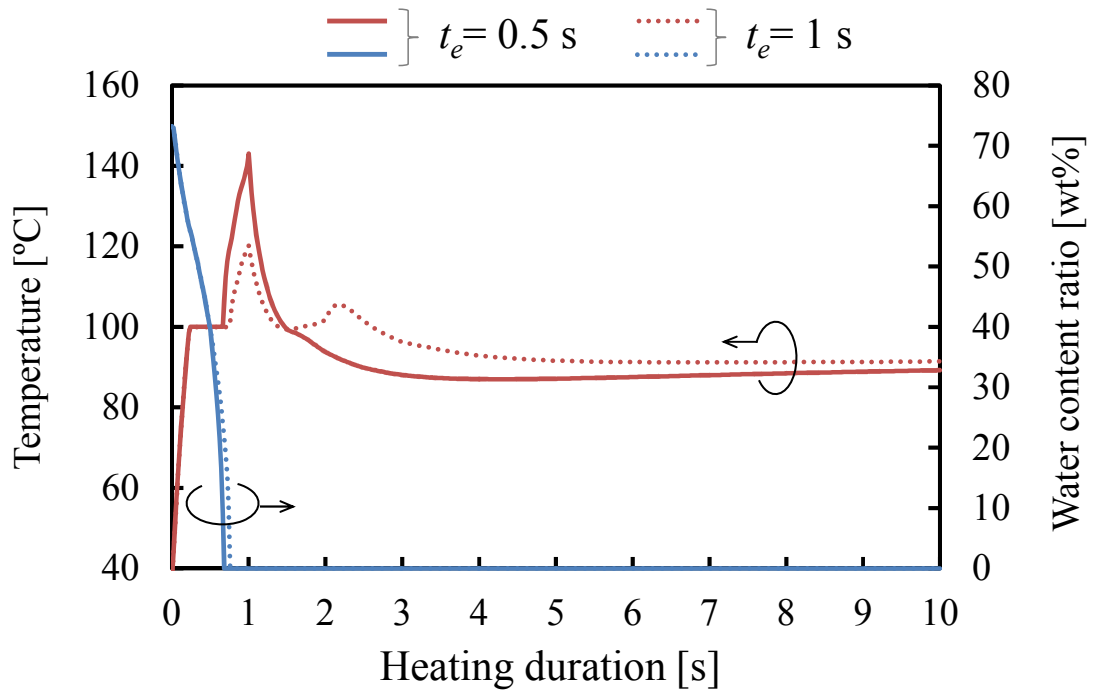
(a) Thickness of tissue = 0.5 mm.
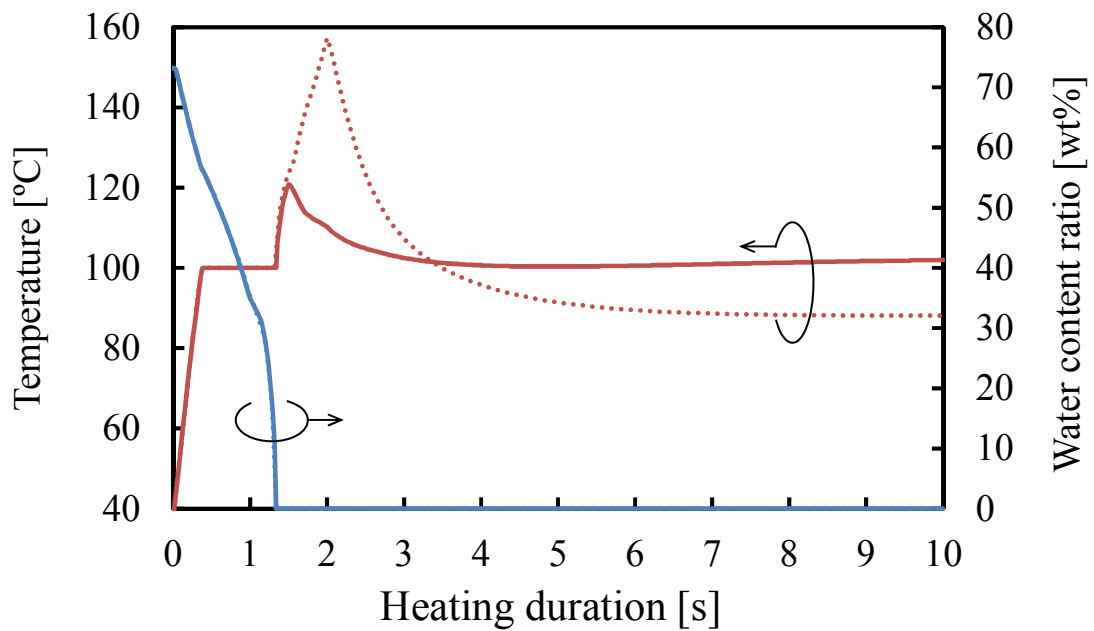


(b) Thickness of tissue = 1.0 mm.
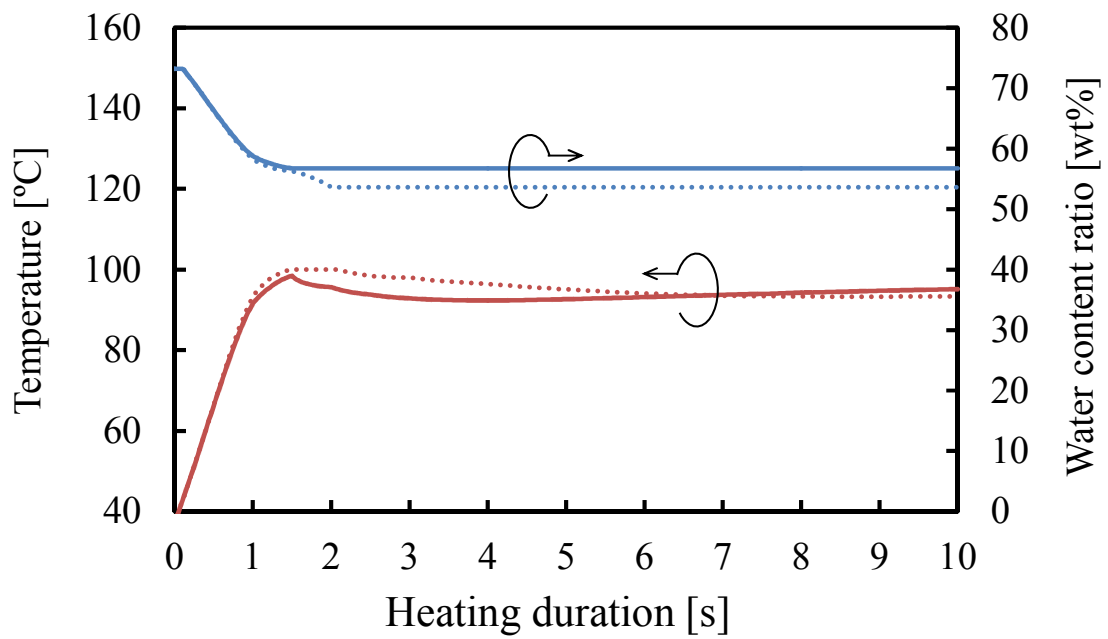
(b) Thickness of tissue = 2.0 mm.

Fig. 4.10. Time variation in temperature and water content ratio at observation point.
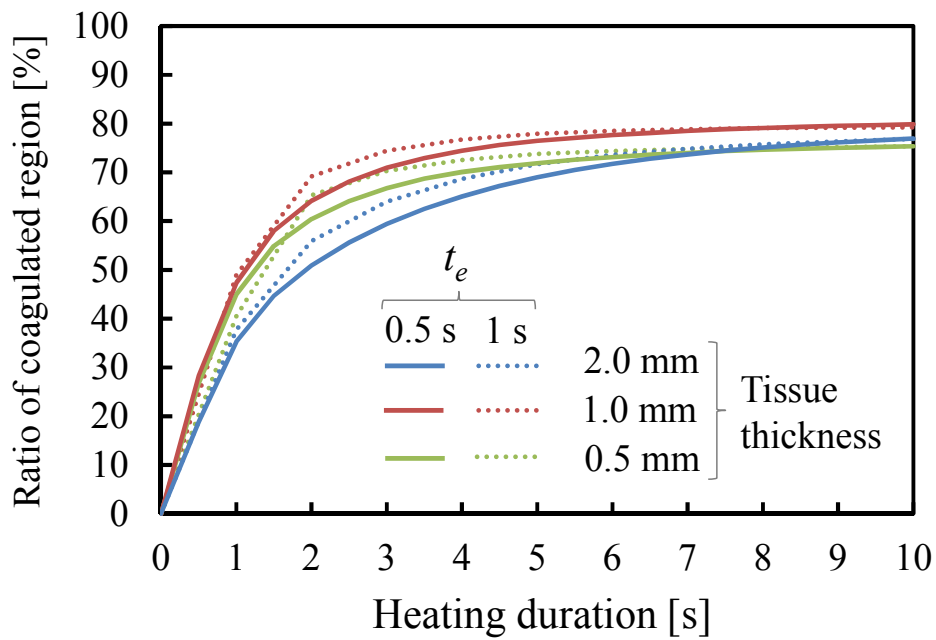
Fig. 4.11. Time variation in the ratio of coagulated tissue in grasped region.
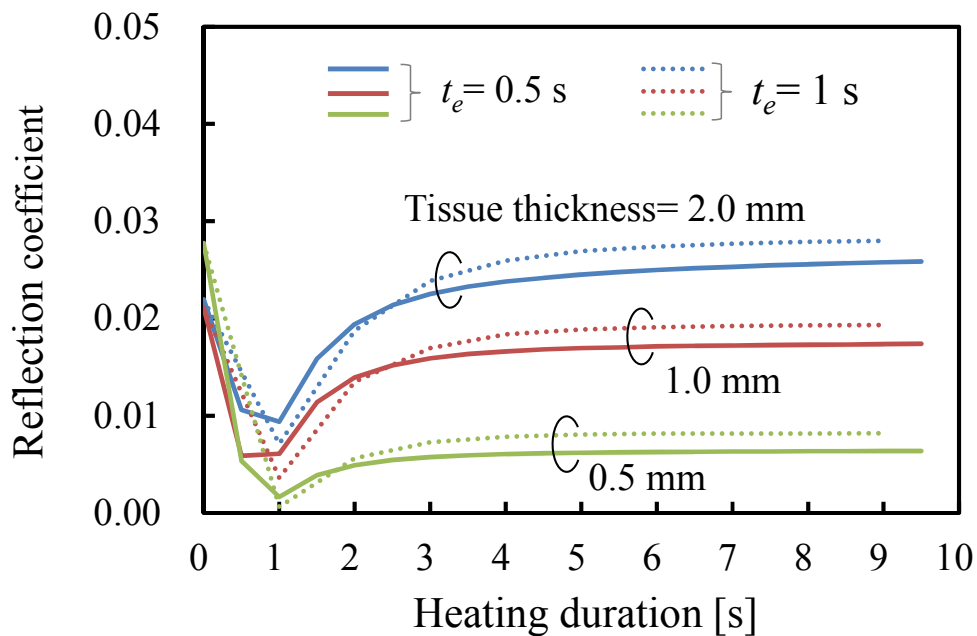


Fig. 4.12. Time variation in the reflection coefficient.

# 4.3 *Ex vivo* experiment

In the preceding section, the tissue-coagulation capability of the proposed device was confirmed by the numerical analysis. This section describes the *ex vivo* experiment to evaluate the validity of the proposed device. In this experiment, a simplified prototype of the proposed device which has only heating mechanism was employed for evaluation of tissue-coagulation capability. This prototype has a heating antenna, and an aluminum plate without cutting capability, imitating the cutting blade.

In this investigation, a thinly sliced swine liver tissue simulating a human blood vessel was employed. A swine liver has dielectric and thermal properties equivalent to those of human's liver [9]. Moreover, differences between the physical properties of a liver tissue and a blood vessel tissue, the main target of the proposed device, are small [7], [10].

## 4.3.1 Experimental system

Fig. 4.13 shows the simplified prototype of the proposed device. The upper jaw is composed of a heating antenna coated with epoxy resin, and the lower jaw consists of acrylic resin with an aluminum plate. The sizes of the jaws, important part for the tissue heating, follow those of Fig. 4.2. Figure 4.14 shows the experimental system. A thinly sliced swine liver tissue was grasped and heated with the prototype in saline solution whose temperature was kept at approximately 30°C. The size of the liver tissue was 6 mm in width and 2 mm in thickness, in the state of being grasped between the jaws. Figure 4.15 expresses the reflection coefficient at the feeding point

of the prototype during tissue heating in saline solution. This figure indicates that the prototype operates excellently at 2.45 GHz as well as the numerical model.

The net input power to the proposed device during the heating was monitored with R&S®RNT Power Reflection Meter and the NRT-Z44 Power Sensor (Rohde & Schwarz, Munich, Germany). In this experiment, the net input power was calculated by subtracting the reflected power from the forward power and controlled to 70 W. The duration of the tissue heating was set to 10 s.
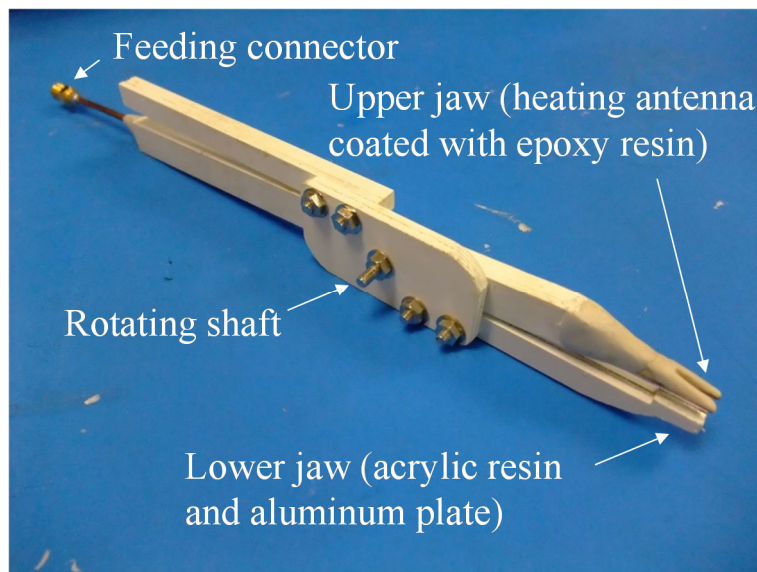


Fig. 4.13. Prototype of proposed device. Copyright © 2015, IEEE.
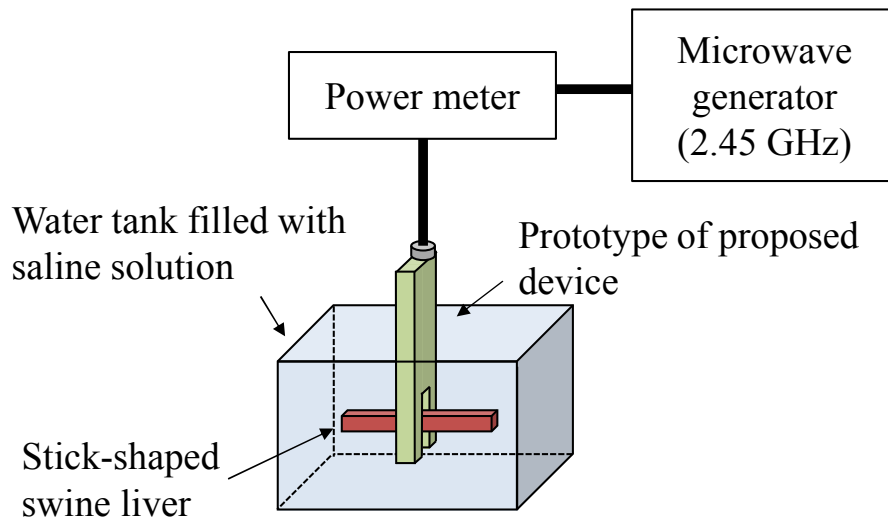
(a) Experiment system.
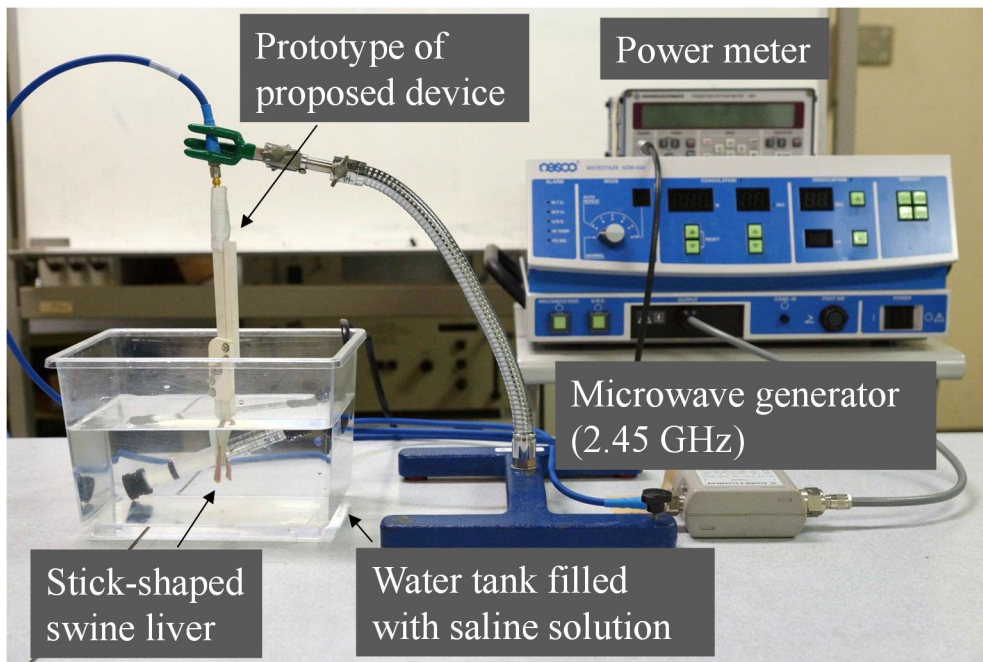


(b) Photograph of setup.

Fig. 4.14. Setup of *ex vivo* experiment. Copyright © 2015, IEEE.
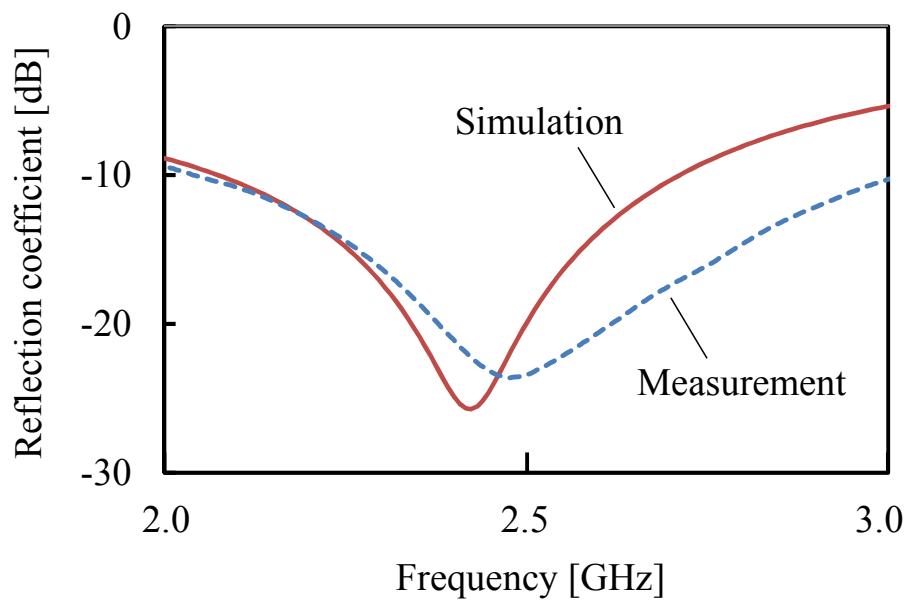
Fig. 4.15. Reflection coefficient at feeding point of device grasping tissue in saline solution. Copyright © 2015, IEEE.

## 4.3.2 Experimental results

Figure 4.16 shows the state of the tissue heated with the prototype. Here, the observation planes are the same as those of Fig. 4.9. In each figure, the discolored area of the tissue is the region where liver tissue was coagulated. The grasped region is expressed by the broken line. These pictures indicate that the coagulated region is almost identical to or a little larger than the grasped region. On the other hand, the numerically calculated temperature was widely lower than the coagulating temperature (60°C) on the surface of the tissue. However, in the almost all volume of the grasped region, the temperature exceeded 60°C. This temperature distribution was caused by the overestimation of the cooling effect at the tissue surface by the saline solution, in the numerical analysis. Taking into account this inadequacy, the experimental results indicate the validity of the analytical results.

The experimental results showed the sufficient tissue coagulating capability of the prototype of the proposed device. Moreover, these results indicated the validity of the proposed device for the tissue coagulation.
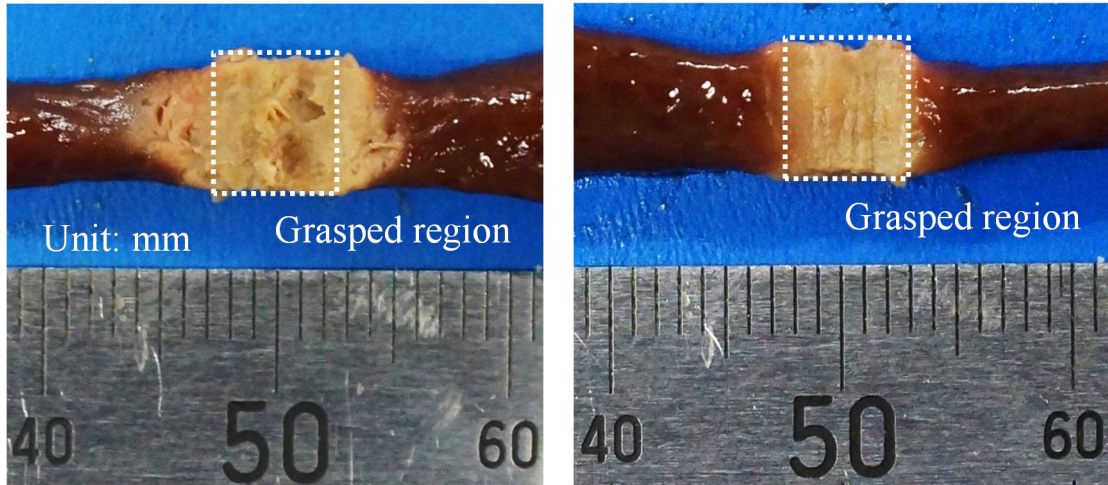
(a) Surface in contact with upper jaw.

(b) Surface in contact with lower jaw.



(c) Cross section.

Fig. 4.16. State of tissue after heating. Copyright © 2015, IEEE.

## 4.4 *In vivo* experiment

The studies in the section 4.2 and 4.3 confirmed the validity of the proposed device for tissue coagulation. In this section, to evaluate the effectiveness of the proposed device for the actual surgical procedure, an *in vivo* experiment with a living swine was conducted. The experimental protocol was conducted in accordance with the guidelines of the Committee on the Ethics of Animal Experiments of Chiba University.

Figure 4.17 illustrates the experimental system. Simulating the conditions of WaFLES, the abdominal cavity of a swine under general anesthetic was filled with the saline solution (37°C). The surgical procedure was performed through an incision on the abdominal wall without using a trocar. In this experiment, the procedure was performed by a surgeon using the proposed device. The prototype of the proposed device was employed to stop the blood flow of the vein while removing the prostate. The net input power and the heating duration were set to 60 W and 10 s, respectively. Here, the reflection coefficient at the feeding point of the device which was estimated using the power reflection meter was less than -10.0 dB at 2.45 GHz. Figure 4.18 shows the photograph around the incision site.

Figure 4.19 shows the laparoscopic images of the surgical site. Fig. 4.19 (a) indicates the bleeding from the small wound. This is typical venous bleeding generated in a surgical site, according to the subjective evaluation of the surgeon. As in Fig. 4.19 (b), this bleeding site was treated with the prototype. Fig. 4.19 (c) indicates that the heating with the prototype stopped the bleeding.

The results of the *in vivo* experiment confirmed some effectiveness of the proposed device for the actual surgical procedure.
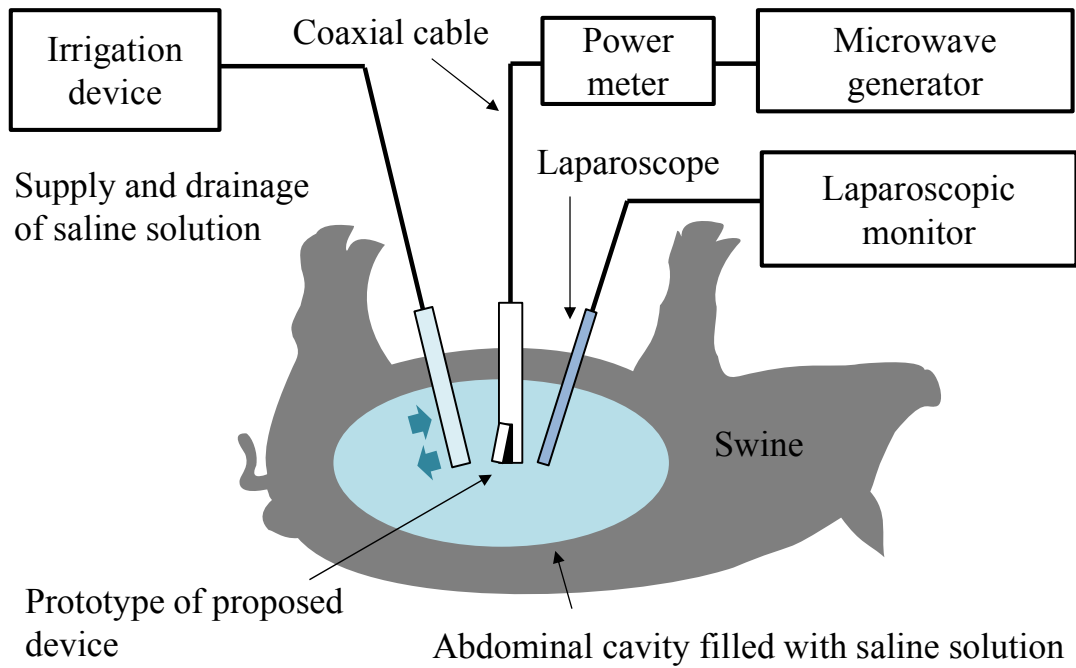
Fig. 4.17. System of *in vivo* experiment. Copyright ©
2015, IEEE.
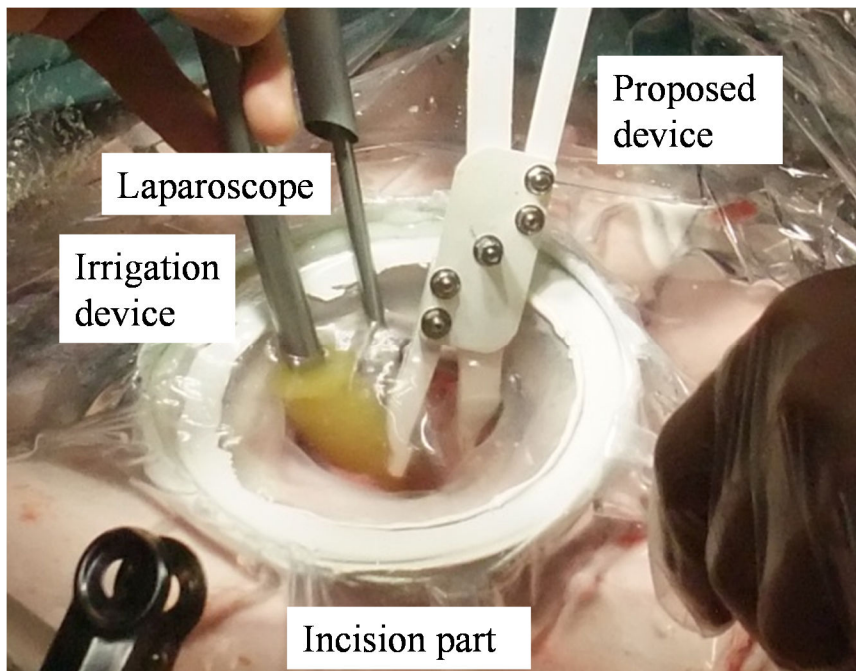


Fig. 4.18. Photograph around incision part. Copyright ©
2015, IEEE.
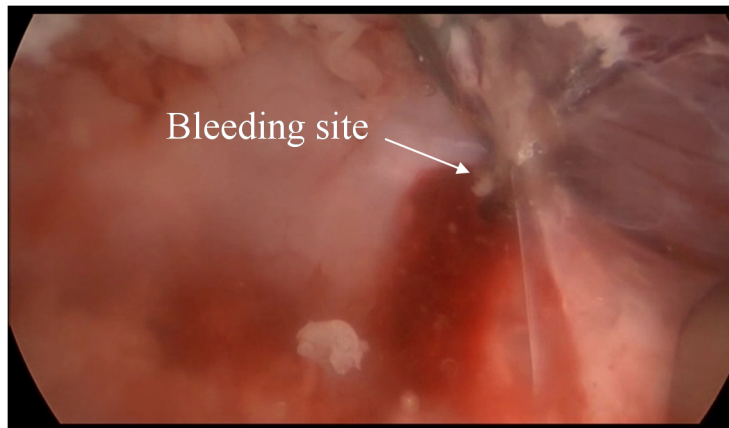
(a) Before heating.
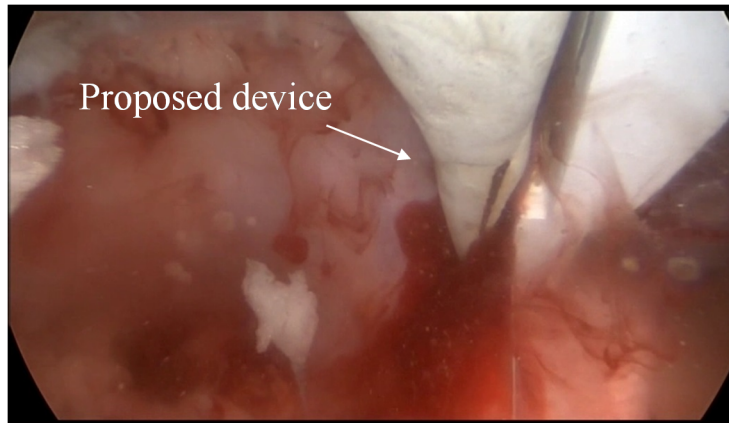


(b) Beginning of heating.
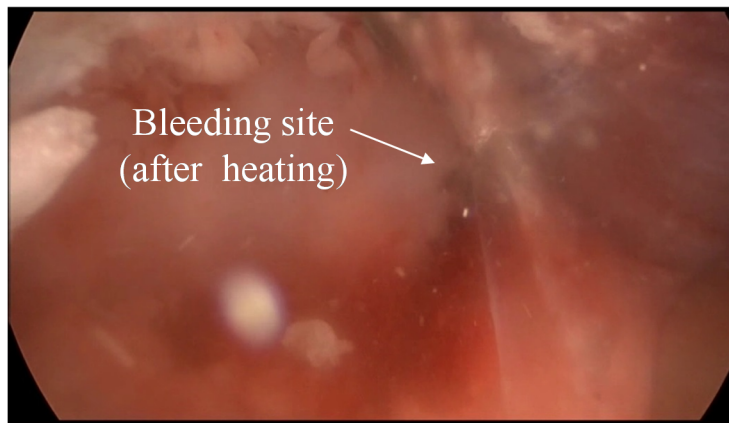


(c) After heating.

Fig. 4.19. Laparoscopic image of surgical site. Copyright © 2015, IEEE.

# 4.5 Conclusion

In this chapter, a forceps-type surgical device employing microwave heating for the hemostasis and the sealing of the thin biological tissues, such as blood vessel and other lumen tissues, was proposed.

The tissue-coagulation capability of the proposed device was confirmed by a numerical analysis and an *ex vivo* experiment. In the numerical analysis, the tissue-coagulating capability of the proposed device was estimated by the temperatures and water content ratios. These values were analyzed by using the numerical simulator proposed in chapter 3. In the *ex vivo* experiment, the simplified prototype of the proposed device was employed. In these studies, the numerical model and the experimental system simulating the condition of WaFLES were employed. The results of these investigations indicated the effectiveness of the proposed device for the coagulation of tissue.

Moreover, to evaluate the effectiveness of the proposed device for actual surgical procedures, an *in vivo* experiment with living swine was conducted. In this experiment, the prototype of the proposed device was used for the treatment of a venous hemorrhage, in the situation simulating WaFLES. As a result, some effectiveness of the proposed device for the actual surgical procedures was confirmed.

In order to realize the practical use of the proposed device in surgical operations, further studies are required. An *in vivo* experiment to evaluate the effectiveness of the arterial hemostasis should be performed. Moreover, the function to detect coagulation and hemostasis of the grasped tissue should be equipped to the proposed device, to prevent excessive heating.

# References

[1]  M. Inoue, K. Saito, M. Takahashi, and K. Ito, "Evaluation on heating characteristics of the microwave antenna for tissue coagulation device," Program and Abstracts of the 11th Int. Congress of Hyperthermic Oncology and the 29th Japanese Congress of Thermal Medicine, p.173, Aug. 2012.

[2]  Y. Tezuka, K. Saito, M. Takahashi, and K. Ito, "Development of surgical device for tissue coagulation by microwave energy," in Proc. 2013 Asia-Pacific Radio Science Conf., Taipei, Taiwan, p.55, Sep. 2013.

[3]  Y. Endo, Y. Tezuka, K. Saito, and K. Ito, "Development of Biological Tissue Coagulation Device by Microwave Energy," in Proc. 8th European Conf. on Ant. and Prop. (EuCAP), pp.367-368, The Hague, The Netherlands, Apr. 2014.

[4]  Y. Endo, K. Suzuki, Y. Tezuka, K. Saito, M. Takahashi, and K. Ito, "Development of forceps type device for biological tissue coagulation by microwave energy," in Proc. 31st URSI General Assembly and Scientific Symposium, Beijing, China, Aug. 2014.

[5]  Y. Endo, Y. Tezuka, K. Suzuki, K. Saito, and K. Ito, "Numerical evaluation on heating characteristics of microwave forceps with cutting blade," in Proc. The 6th Asian Congress of Hyperthermic Oncology (ACHO) & The 31st Japanese Congress of Thermal Medicine (JCTM), pp.164, Fukui, Japan, Sep. 2014.

[6]  T. Igarashi, Y. Shimoyama, T. Yamaguchi, H. Kawahira, H. makino, W. Yu, and Y. Naya, "Water-Filled Laparoendoscopic Surgery (WAFLES): Feasibility Study in Porcine Model," Journal of Laparoscopic & Advanced Surgical Techiques, vol. 22, no. 1, pp. 70-75, 2012.

[7]  P. A. Hasgall, E. Neufeld, M. C. Gosselin, A. Klingenböck, and N. Kuster,

"IT'IS Database for thermal and electromagnetic parameters of biological tissues," Version 2.4, July 30th, 2013.

[8]    P. M. Van den Berg, A. T. De Hoop, A. Segal, and N. Praagman, "A computational model of the electromagnetic heating of biological tissue with application to hyperthermic cancer therapy," IEEE Trans. Biomed. Eng., vol. 30, no. 12, pp. 797-805, 1983.

[9]    K. Saito, Y. Hayashi, H. Yoshimura, and K. Ito, "Heating characteristics of array applicator composed of two coaxial-slot antennas for microwave coagulation therapy," IEEE Trans. Microwave Theory Techn., vol. 48, no. 11, pp. 1800-1806, Nov. 2000.

[10]   C. Gabriel, "Compilation of the dielectric properties of body tissues at RF microwave frequencies," Brooks Air Force Technical Report AL/OE-TR-1996-0037, 1996.

# Chapter 5

# Conclusion and future tasks

This thesis describes two kinds of studies relating to the medical application of the microwave heating to the biological tissue. The first one is the development of the numerical simulator for the medical treatment applying microwave heating such as MCT. The second one is the development of the forceps type surgical device for the blood vessel sealing applying microwave heating.

In chapter 2, physical properties of the liver tissue under the heating were numerically modeled for the development of the numerical simulator to obtain the electromagnetic field and the temperature in the heated tissue.

First, water content ratios, dielectric and thermal constants of liver tissues heated under various conditions were measured, in order to evaluate the relationship between them. As a result, strong dependencies of the dielectric and thermal constants on the water content ratio were observed. Measured results also shows the water content ratio of the heated tissue depends on the heating temperature.

Based on the measured results, the dielectric and thermal constants of the liver tissue were expressed as functions of the water content ratio of the tissue. On the other hand, the water content ratio of the tissue was modeled considering both dehydration mechanisms, the dehydration by the temperature rise below 100°C and the evaporation at 100°C. The stagnation of the temperature rise due to the water evaporation at 100°C was also simulated by considering the evaporation latent heat of water.

In chapter 3, the development of the numerical simulator which analyzes accurate temperature distribution in the biological tissue under the microwave heating was explained.

In the developed simulator, the decrease of the water content ratio of the tissue caused by the heating and the changes of the dielectric and thermal properties of the tissue due to the decrease of the water content ratio were simulated, by employing the tissue model proposed in chapter 2.

As a result, the tissue temperature under the MCT calculated by the developed simulator agreed with the measured value, compared with the simulator which ignored the decrease of the water content ratio, especially in the case that tissue temperature exceeds 100°C.

The developed simulator will provide the valuable information for the setting of the optimum heating conditions (the input power to the antenna and the heating duration) to safely and efficiently treat the region of the tumor, in the MCT.

The method in the developed simulator can also be applied to other treatments applying the microwave thermal effect, such as microwave catheter ablation for cardiac disease, to avoid the postoperative complications cause by the inadequate heating.

In chapter 4, the development of the forceps-type surgical device applying microwave thermal effect was described. The proposed device was designed to be used for the blood vessel sealing. This study mainly focused on the development of the heating antenna which is the most important part of the proposed device.

The coagulating capability of the device was evaluated using the distribution of the temperatures and the water content ratios inside the tissue grasped with the device, which was obtained by using the numerical simulator proposed in chapter 3.

Results of numerical simulations and some experiments indicated that the designed antenna has sufficient heating characteristics to coagulate the biological tissue and stop the blood flow in the blood vessel. These results imply that the proposed device will be realized by attaching the designed antenna and the tissue cutting mechanism.

By using the proposed device and the devices which were developed in the previous studies, various types of surgical treatments using the microwave thermal effect would be provided in the surgical operation.

As above, outcomes of studies in this thesis will promote the medical application of the microwave heating.

The details of the future tasks related to the development of the numerical simulator and the surgical device are described as follows.

In Chapter 4, in the case extremely strong electric fields are generated in the biological tissue, the inaccurate temperatures were calculated. In order to improve the accuracy of the calculation, the modification of the calculation algorithm is required. Moreover, the numerical model of a liver tissue which reproduces the heat-induced changes of the mass density and the blood flow rate of tissue will be developed for more accurate numerical calculation. The mass density of a tissue is expected to depend on the water content ratio, as with the dielectric and thermal constants. In order to reproduce the heat-induced change of the blood flow rate, the investigation about the forming conditions of the blood clot which stems the blood flow is required. In addition, the numerical simulator available for treatments using microwave heating other than microwave coagulation therapy (MCT) of liver cancer such as microwave catheter ablation, will be developed. Therefore, other types of biological tissue except for liver tissue will be numerically modeled by the same

method in this study.

The detailed evaluation of the usefulness of the proposed surgical device is required, by using the prototype of the proposed device available to real clinical use. Moreover, the function to detect the tissue coagulation should be provided to the proposed device, to avoid excessive heating of the tissue, which is capable of causing various postoperative complications. For this purpose, the electrode pair for the measurement of the impedance at several hundred kHz which strongly reflects the tissue coagulation will be attached to the device. In addition to this, by applying a bimetal or a shape memory alloy, whose shape changes according to temperature, the heating antenna with temperature control mechanism will be developed.

# Publication list

## Journals

[J-1]   **Yuta Endo**, Kazuyuki Saito, Soichi Watanabe, Masaharu Takahashi, and Koichi Ito, "Experimental evaluation of SAR around an implanted cardiac pacemaker caused by mobile radio terminal," IEICE Transactions on Communications, vol.E95-B, no.6, pp.2129-2132, June 2012.

[J-2]   **Yuta Endo**, Yoshito Tezuka, Kazuyuki Saito, and Koichi Ito, "Dielectric properties and water contents of coagulated biological tissue by microwave heating," IEICE Communications Express, vol.4, no.4 pp.105-110, Apr. 2015.

[J-3]   **Yuta Endo**, Kazuyuki Saito, and Koichi Ito, "The development of forceps-type microwave tissue coagulator for surgical operation," IEEE Transactions on Microwave Theory and Techniques, vol.63, no.6pp.2041-2049, June 2015.

[J-4]   **Yuta Endo**, Kazuyuki Saito, and Koichi Ito, "Temperature analysis of liver tissue in microwave coagulation therapy considering tissue dehydration by heating," IEICE Transactions on Electronics, vol.E99-C, no.2, pp.257-265, Feb. 2016.

[J-5]   **Yuta Endo**, Kazuyuki Saito, Soichi Watanabe, Masaharu Takahashi, and Koichi ITO, "Study of interference voltage of an implanted pacemaker by mobile terminals," IEEE Transactions on Electromagnetic Compatibility, (accepted).

## Award

The 32nd Annual Meeting of Japanese Society for Thermal Medicine Excellent Paper Presentation Award (September 15, 2015)

## International conferences

[I-1]   Kazuyuki Saito, Ryohei Watanabe, **Yuta Endo**, Soichi Watanabe, Masaharu Takahashi, and Koichi Ito, "Evaluations on SAR around implanted cardiac pacemaker by mobile radio terminal," European Conference on Antennas and

Propagation (EuCAP) 2011, pp.2931-2933, Rome, Italy, Apr. 2011.

[I-2]   Kazuyuki Saito, Soichi Watanabe, **Yuta Endo**, Masaharu Takahashi, and Koichi Ito, "Calculations of SAR around implanted cardiac pacemaker induced by wireless radio terminal -Relation between positions of implanted cardiac pacemaker and wireless radio terminal-," Proceeding of IEEE Region 8 AFRICON, Livingstone, Zambia, Sep. 2011.

[I-3]   **Yuta Endo**, Kazuyuki Saito, Soichi Watanabe, Masaharu Takahashi, and Koichi Ito, "Experimental Evaluation on SAR around the Implanted Cardiac Pacemaker by Mobile Phone," ISABEL2011, Barcelona, Spain, Oct. 2011.

[I-4]   Kazuyuki Saito, **Yuta Endo**, Soichi Watanabe, Masaharu Takahashi, and Koichi Ito, "SAR evaluations around implanted cardiac pacemaker caused by mobile radio terminal," Proceedings of 7th International Workshop on Biological Effects of Electromagnetic Fields, Valletta, Malta, Oct. 2012.

[I-5]   **Yuta Endo**, Kazuyuki Saito, Soichi Watanabe, Masaharu Takahashi, and Koichi Ito, "Evaluation of SAR around an implanted cardiac pacemaker caused by mobile radio terminal," 2012 International Symposium on Antennas and Propagation (ISAP 2012), pp.680-683, Nagoya, Japan, Oct. 2012.

[I-6]   **Yuta Endo**, Kazuyuki Saito, Soichi Watanabe, Masaharu Takahashi, and Koichi Ito, "Evaluation on electromagnetic interference of implanted cardiac pacemaker by mobile phone," 2013 Progress In Electromagnetics Research Symposium (The 33rd PIERS in Taipei), p.166, Taipei, Taiwan, Mar. 2013.

[I-7]   Kazuyuki Saito, **Yuta Endo**, Sota Kojima, Soichi Watanabe, Masaharu Takahashi, and Koichi Ito, "EMI evaluation of implanted cardiac pacemaker using realistic mobile radio terminal model," Bioelectromagnetics Society Annual Meeting, Thessaloniki, Greece, PA-59, Jun. 2013.

[I-8]   **Yuta Endo**, Kazuyuki Saito, Sota Kojima, Soichi Watanabe, Masaharu Takahashi, and Koichi Ito, "Evaluation of electromagnetic interference to implanted cardiac pacemaker due to mobile phone," International Conference on Electromagnetics in Advanced Applications (ICEAA 2013), pp.188-191, Torino, Italy, Sep. 2013.

[I-9]   Kazuyuki Saito, Yoshito Tezuka, **Yuta Endo**, Masaharu Takahashi, and Koichi Ito, "Performance Evaluation of Biological Tissue Coagulation Device by Microwave Energy," Vietnam-Japan International Symposium on Antennas and Propagation, pp.183-186, Hanoi, Vietnam, Jan. 2014.

[I-10] **Yuta Endo**, Yoshito Tezuka, Kazuyuki Saito, and Koichi Ito, "Development of Biological Tissue Coagulation Device by Microwave Energy," 8th European Conference on Antennas and Propagation (EUCAP 2014), pp.367-368, Hague, Netherlands, Apr. 2014.

[I-11] Kenta Suzuki, **Yuta Endo**, Yoshito Tezuka, Kazuyuki Saito, Masaharu Takahashi, and Koichi Ito, "Development on microwave forceps for coagulation of biological tissue," Bioelectromagnetics Society and European BioElectromagnetics Association for the Annual Joint Meeting (BioEM2014), Cape Town, South Africa, PB-12, June 2014.

[I-12] Kazuyuki Saito, Koichi Ito, **Yuta Endo**, and Kenta Suzuki, "Development of Microwave Tissue Coagulator with Cutting Mechanism," 2014 IEEE International Symposium on Antennas and Propagation and USNC-URSI Radio Science Meeting, Memphis, USA, July 2014.

[I-13] **Yuta Endo**, Kenta Suzuki, Yoshito Tezuka, Kazuyuki Saito, Masaharu Takahashi, and Koichi Ito, "Development of forceps type device for biological tissue coagulation by microwave energy," 31st URSI General Assembly and Scientific Symposium, Beijing, China, Aug. 2014.

[I-14] **Yuta Endo**, Yoshito Tezuka, Kenta Suzuki, Kazuyuki Saito, and Koichi Ito, "Numerical evaluation on heating characteristics of microwave forceps with cutting blade," The 6th Asian Congress of Hyperthermic Oncology (ACHO) & The 31st Japanese Congress of Thermal Medicine (JCTM), pp.164, Fukui, Japan, Sep. 2014.

[I-15] Erika Yashima, Kazuyuki Saito, **Yuta Endo**, and Koichi Ito, "Evaluation on heating characteristics of multiple coaxial-slot antenna as a feeding probe of metallic stent for bile duct," The 6th Asian Congress of Hyperthermic Oncology (ACHO) & The 31st Japanese Congress of Thermal Medicine (JCTM), pp.141, Fukui, Japan, Sep. 2014.

[I-16] Kazuyuki Saito, Kenta Suzuki, **Yuta Endo**, and Koichi Ito, "Evaluation on heating performances of microwave forceps for biological tissue coagulation," The 6th Asian Congress of Hyperthermic Oncology (ACHO) & The 31st Japanese Congress of Thermal Medicine (JCTM), pp.165, Fukui, Japan, Sep. 2014.

[I-17] Yoshito Tezuka, **Yuta Endo**, Kazuyuki Saito, and Koichi Ito, "Development of Biological Tissue Coagulation Device Composed of Helical Radiation Element by Microwave Energy,"2014 Asia-Pacific Microwave Conference Proceedings, pp.447-449, Sendai, Japan, Nov. 2014.

[I-18] **Yuta Endo**, Yoshito Tezuka, Kenta Suzuki, Kazuyuki Saito, and Koichi Ito, "Development of Forceps-Type Microwave Coagulation Device for Surgical Operation," 2014 International Symposium on Antennas and Propagation (ISAP 2014), pp.181-182, Kaohsiung, Taiwan, Dec. 2014.

[I-19] Erika Yashima, Kazuyuki Saito, **Yuta Endo**, and Koichi Ito, "Evaluation on Performances of Multiple Coaxial-Slot Antenna for Microwave Heating Compatible with Metallic Stent for Bile Duct Carcinoma," 2014 International Symposium on Antennas and Propagation (ISAP 2014), Kaohsiung, Taiwan, pp.533-534, Dec. 2014.

[I-20] Kazuyuki Saito, **Yuta Endo**, Ryota Akiyama, Soichi Watanabe, and Koichi Ito, "SAR Calculations around Implanted Cardiac Pacemaker Induced by Wireless Radio Terminal in VHF Band," IEEE MTT-S International Microwave Workshop Series on RF and Wireless Technologies For Biomedical and Healthcare Application (IMWS-Bio 2014), London, UK, Dec. 2014.

[I-21] Naoyuki Ogasawara, **Yuta Endo**, Kazuyuki Saito, and Koichi Ito, "Development of Tissue Coagulation Forceps by Microwave Energy," 2015 IEEE International Symposium on Antennas and Propagation and North American Radio Science Meeting, pp.723-724, Vancouver, Canada, July 2015.

[I-22] Sho Suzuki, **Yuta Endo**, Kazuyuki Saito, and Koichi Ito, "Development of Biological Tissue Coagulating and Cutting Device Combining Microwave and Radio Frequency Current," 2015 URSI-Japan Radio Science Meeting (URSI-JRSM), p.98, Tokyo, Japan, Sep. 2015.

[I-23] **Yuta Endo**, Hiroki Kikuchi, Kazuyuki Saito, and Koichi Ito, "Dielectric Properties and Water Contents of Biological Tissue after Microwave Heating," IEEE MTT-S International Microwave Workshop Series on RF and Wireless Technologies for Biomedical and Healthcare Application (IMWS-Bio 2015), pp.272-273, Taipei, Taiwan, Sep. 2015.

[I-24] Kazuyuki Saito, **Yuta Endo**, Sho Suzuki, and Koichi Ito, "Development and Performance Evaluations of Surgical Devices by use of Microwave Energy," Proceedings of the Eighth 2015 Korea-Japan Joint Conference on EMT/EMC/BE (KJJC-2015), pp.35-36, Miyagi, Japan, Nov. 2015.

# Acknowledgements

I would specially like to thank Prof. Kazuyuki Saito for his great assistance through the years of my experience in the laboratory. It has been a great honor to study under his instruction.

I am deeply grateful to Prof. Koichi Ito for his valuable guidance and many helpful discussions regarding my research. I would like to express my gratitude to Prof. Masaharu Takahashi for his valuable guidance and many helpful comments.

I want to thank Prof. Etsuji Yamamoto and Prof. Tatsuo Igarashi for their helpful discussion on my research and dissertation.

I am indebt to Dr. Shimpei Akimoto, Dr. Nozomi Haga, Dr. Chia-Hsien Lin, Dr. Ho-Yu Lin, Dr. Ryotaro Suga, Dr. Hiromasa Nakajima, and Dr. Hiroshi Sato, who are the excellent graduates of Chiba University, for their constructive comments and warm encouragement.

I would also like to express my gratitude to all the other people in Ito and Saito laboratory and Takahashi laboratory.

# Vita

## Yuta Endo

He was born in Tokyo, Japan, in April 1987. He received the B.E. and M.E. degrees from Chiba University, Chiba, Japan, in 2011 and 2013, respectively. He is currently pursuing the D.E. degree at Chiba University.

His main interest is in the area of medical applications of the microwaves. Mr. Endo is a member of the Institute of Electrical, Information and Communication Engineers (IEICE), Japan.

# Appendix 1

# Principle of the microwave heating technique

Generally, biological tissues contain large amount of water in them. For example, the water content ratio of the muscle tissue and the liver tissue are about 80 wt% and 73 wt%, respectively [1]. Under the alternating electrical field, the water molecule causes dielectric polarization (orientation polarization), as shown in Fig. A.1. Here, the dielectric property of the material under the alternating electrical field is represented as a complex dielectric constant $\varepsilon$ [F/m] as follow:

$$\varepsilon = \varepsilon' - j\varepsilon'' \quad \text{(A.1)}$$

where $\varepsilon'$ and $\varepsilon''$ are the real part and the imaginary part of the complex dielectric constants. The imaginary part is the value which indicates the degree of the dielectric loss. The dielectric loss generates heat in the material.

The microwave heating of the biological tissue is mainly based on the dielectric loss occurred in the water molecules contained in the tissue. Therefore, tissues with high water content ratio are efficiently heated by microwave because of the high dielectric loss. In the Ref. [1], the dependencies of the dielectric constants of the biological tissues on the water content ratio in the microwave and millimeter band were observed.

The amount of the heat produced in the tissue by the dielectric loss is

represented by the specific absorption rate (SAR) [W/kg] as follow:

$$\mathrm{SAR} = \frac{\sigma}{\rho} E^2 \quad \text{(A.2)}$$

where $\sigma$, $\rho$, and $E$ are the electrical conductivity [S/m], the mass density [kg/m$^3$], and the root-mean-square electrical field [V/m], respectively. The electrical conductivity is represented by Eq. A.3.

$$\sigma = 2\pi f \, \varepsilon_o \, \varepsilon'' + \sigma_{ion} \quad \text{(A.3)}$$

Here, $f$, $\varepsilon_0$, and $\varepsilon''$ are the frequency [Hz], the dielectric constant of vacuum (= $8.854 \times 10^{-12}$ F/m), and the imaginary part of the complex relative dielectric constant, respectively. The electrical conductivity of the biological tissue also includes the loss due to the ionic conduction $\sigma_{ion}$ [S/m] [2].

Thus, the heat generation in the biological tissue by the microwave is mainly cause by the electrical field component in the microwave. While, the magnetic field component do not generate heat in the biological tissue, because biological tissues are non-magnetic materials.
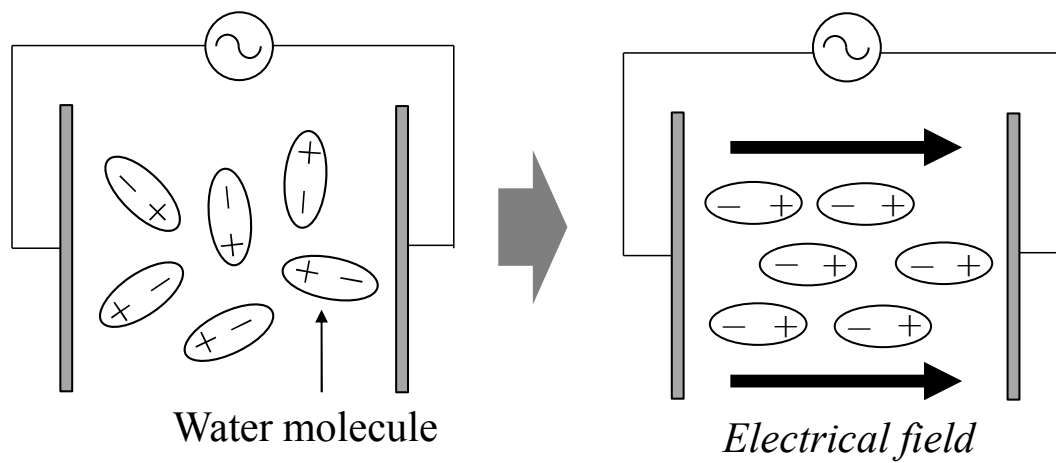
(a) Schematic diagram of polarization.
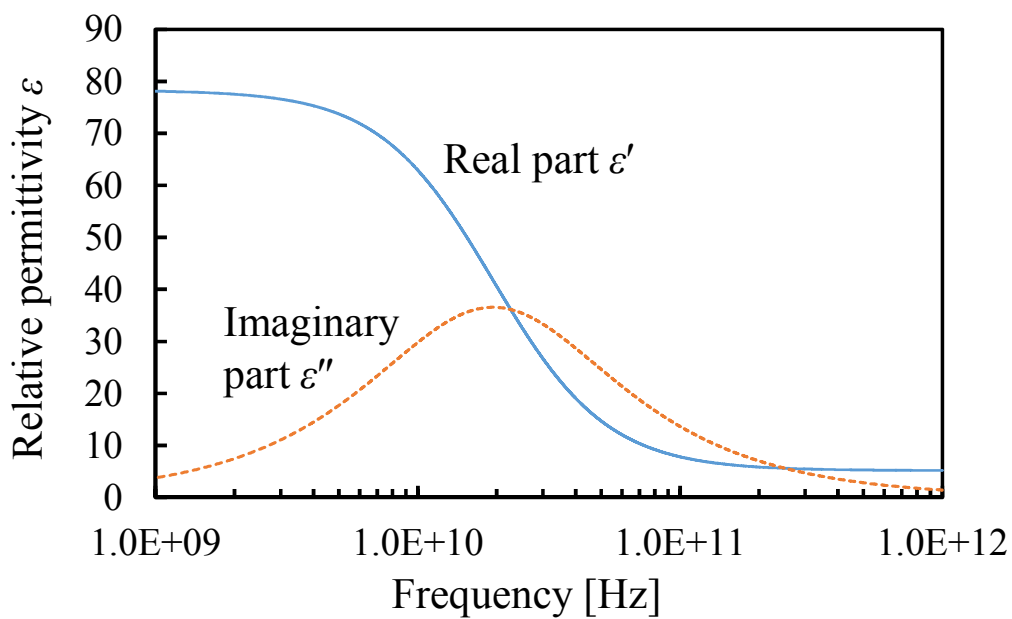


(a) Relative permittivity of the water at 25°C [3].

Fig. A.1. Dielectric polarization (orientation) polarization) of the water molecule.

# Appendix 2

# The influence of the biological tissue due to heating

Biological tissues cause complex reactions by the heating [4]. Here, these reactions are mainly caused by the existence of the various types of proteins inside and outside of the cell [5]. These proteins are roughly divided into two types, functional proteins and structural proteins.

Functional proteins such as vital enzymes included in the cells are heat-denatured and inactivated, even under a low-temperature condition of about 42°C [6]. To heat biological tissues at this temperature range, cell metabolisms are inhibited and necrosis is caused. The high-temperature treatment for BPH and the hyperthermia, treatments which employ low-temperature heating, are based on the necrosis due to the heat-denaturation of functional proteins.

Structural proteins are denatured at the comparatively high temperature of about 60°C [7]-[9]. The denaturation of the functional proteins immediately causes necrosis [10]. Generally, this phenomenon is known as the coagulation of the biological tissue. The MCT and the MEA are treatments based on the necrosis due to the heat-denaturation of the structural proteins.

The denaturation of the structural proteins can be visually discriminated by the discoloration (lighter color) and the shrinking of the tissue. While, denaturation of

the functional proteins are not accompanied with visual changes of the tissue. Moreover, denaturation of the structural proteins causes the decrease in the water contained in the tissue, because the intracellular and extracellular fluid are squeezed out due to the tissue shrinking.

Moreover, it has been known that blood clots is formed inside the blood vessel by heating [11],[12]. It is considered this is the mechanism of the hemostasis by the microwave heating. However, there are not much studies about the relationship between the forming of the blood clots and the heating temperature.

# References

[1]     T. Sakai and S. Watanabe, "Measurement of Pig Tissues for Complex Permittivity and Water Contents in Millimeter Wave Band," IEICE Tech. Rep., vol. 110, no. 17, EMCJ2010-8, pp. 39-43, Apr. 2010 (in Japanese).

[2]     A. Peyman, C. Gabriel, and E. H. Grant, "Complex permittivity of sodium chloride solutions at microwave frequencies," Bioelectromagnetics, vol. 28, no. 4, pp. 264-274, May 2007.

[3]     H. J. Liebe, G. A. Hufford, and T. Manabe. "A model for the complex permittivity of water at frequencies below 1THz," Int. J. of Infrared and Millimeter Waves, vol. 12, no. 7, pp. 659-675, July 1991.

[4]     R. Chopra, "Image-guided thermal therapy (section 31)," in Biomedical Technology and Devices Handbook, eds. J. Moore and G. Zouridakis, CRC Press, Florida, 2003.

[5]     C. Steffer, "Molecular and cellular mechanisms of hyperthermia", in Thermoradiotherapy and Thermochemotherapy, eds. M. H. Seegenschmiedt, P. Fessenden, and C. C. Vernon, Springer-Verlag, Berlin, 1995.

[6]     K. Engin, "Biological rationale and clinical experience with hyperthermia", Controlled Clinical Trials, vol. 17, no. 4, pp. 316-342, Aug. 1996.

[7]     S. J. Graham, L. Chen, M. Leitch, R. D. Peters, M. J. Bronskill, F. S. Foster, R. M. Henkelman, and D. B. Plewes, "Quantifying tissue damage due to focused ultrasound heating observed by MRI," Magn. Reson. Med., vol. 41, no. 2, pp. 321-328, Feb. 1999.

[8]     R. D. Peters, E. Chan, J. Trachtenberg, S. Jothy, L. Kapusta, W. Kucharczyk, and R. M. Henkelman, "Magnetic resonance thermometry for predicting

thermal damage: An application of interstitial laser coagulation in an *in vivo* canine prostate model," Magn. Reson. Med., vol. 44, no. 6, pp. 873-883, Dec. 2000.

[9]    N. J. McDannold, R. L. King, F. A. Jolesz, and K. H. Hynynen, "Usefulness of MR Imaging-Derived Thermometry and Dosimetry in Determining the Threshold for Tissue Damage Induced by Thermal Surgery in Rabbits," Radiology, vol. 216, no. 2, pp. 517-523, 2000.

[10]   M. J. Borrelli, "Time temperature analysis of cell killing of BHK cells heated at temperatures in the range of 43.5 degree C to 57.0 degree C," Int. J. Radiat. Oncol. Biol. Phys., vol. 19, no. 2, pp. 389-399, Aug. 1990.

[11]   M. Ryu, et al. "Clinical experience of microwave tissue coagulator for hepatic surgery," The Japanese journal of gastroenterological surgery, vol. 16, no. 12, pp. 2074-2080, Dec. 1983 (in Japanese).

[12]   K. Tabuse, et al. "Endoscopic microwave-tissue-coagulation method," Gastroenterological Endoscopy, vol. 24, no. 10, pp. 1526-1533, Oct. 1982 (in Japanese).